Single-Particle Photoluminescence and Carrier Dynamics of Cesium Lead Halide Perovskites and Related Materials

A Thesis

Submitted for the Degree of

Doctor of Philosophy

by

Sudipta Seth

School of Chemistry

University of Hyderabad

Hyderabad – 500 046

INDIA

February 2019

Dedicated

To

My Thakuma, Didima,
Maa and Baba

“The measure of intelligence is the ability to change”

– Albert Einstein

“I never lose. I either win or I learn”

– Nelson Mandela

“You are the creator of your own destiny”

– Swami Vivekananda

CONTENTS

STATEMENT

I hereby declare that the matter embodied in the thesis entitled **"*Single-Particle Photoluminescence and Carrier Dynamics of Cesium Lead Halide Perovskites and Related Materials*"** is the result of investigations carried out by me in the School of Chemistry, University of Hyderabad, India under the supervision of **Prof. Anunay Samanta**.

In keeping with the general practice of reporting scientific investigations, the acknowledgements have been made wherever the work described is based on the findings of other investigators. Any omission or error that might have crept in is regretted.

University of Hyderabad

February 2019 **Sudipta Seth**

SCHOOL OF CHEMISTRY

UNIVERSITY OF HYDERABAD

HYDERABAD-500 046, INDIA

Phone: +91-40-2313 4813 (O)
+91-40-2313 0715 (R)
Fax: +91-40-2301 1594
Email: anunay@uohyd.ac.in
anunay.samanta@gmail.com

CERTIFICATE

This is to certify that the thesis entitled "***Single-Particle Photoluminescence and Carrier Dynamics of Cesium Lead Halide Perovskites and Related Materials***" submitted by **Mr. Sudipta Seth** bearing registration number **14CHPH02** in partial fulfilment of the requirements for the award of Doctor of Philosophy (Ph.D.) in the School of Chemistry is a bonafide work carried out by him under my supervision and guidance. This thesis is free from plagiarism and has not been submitted previously in part or full to this or any other University or Institution for any degree or diploma. Further, the student has following publications before submission of the thesis for adjudication and has produced evidences for the same in the form of reprints.

Parts of this thesis have been published in the followings publications:

1. **S. Seth,** N. Mondal, S. Patra and A. Samanta, **J. Phys. Chem. Lett.,** 7 **(2016)** 266-271. **(Chapter 3)**

2. **S. Seth,** T. Ahmed and A. Samanta, **J. Phys. Chem. Lett.,** 9 **(2018)** 7007-7014. **(Chapter 4)**

3. **S. Seth** and A. Samanta, **J. Phys. Chem. Lett.,** 8 **(2017)** 4461-4467. **(Chapter 5)**

The student has made presentations in the following conferences:

1. "Fluorescence Blinking and Photoactivation of All-Inorganic Perovskite Nanocrystals $CsPbBr_3$ and $CsPbBr_2I$", **Recent Advances in Molecular Spectroscopy: Fundamentals and Applications in Materials and Biology (RAMS-2016)**. University of Hyderabad, India, 2-4 March, 2016. **(Poster presentation)**

2. "Photoluminescence of Zero-Dimensional Perovskites", **5th International Conference on Advanced Nanomaterials and Nanotechnology (ICANN 2017)**. Centre for Nanotechnology,

Indian Institute of Technology Guwahati, Assam, India, 18-21 December, 2017. **(Poster presentation)**

3. "Suppressed Auger Recombination in Thiol-Treated $CsPbBr_3$ Perovskite Nanocrystals as Revealed by Single Particle Luminescence Spectroscopy", **Perovskite Solar Cells and Optoelectronics (PSCO-2018)**. Lausanne, Switzerland, 30th September-2nd October, 2018. **(Poster presentation)**

4. "Nucleation and self-assembly of $CsPbX_3$ Perovskite Nanocrystals", **24th Congress and General Assembly of the International Union of Crystallography (IUCr 2017)**. Hyderabad International Convention Centre, Hyderabad, India, 21-28 August, 2017. **(Oral presentation)**

Further, the student has passed the following courses towards the fulfilment of coursework requirement for Ph.D.:

	Course Code	Title	Credits	Pass/Fail
1.	CY-801	Research Proposal	3	Pass
2.	CY-802	Chemistry Pedagogy	3	Pass
3.	CY-805	Instrumental Method A	3	Pass
4.	CY-806	Instrumental Method B	3	Pass

Anunay Samanta
(Thesis Supervisor)

Dean
School of Chemistry
University of Hyderabad

Acknowledgement

It gives me immense pleasure to express my heartfelt gratitude to my research supervisor, Prof. Anunay Samanta, for his valuable guidance, encouragement for exploring new areas of research, management lessons, constant cooperation, patience toward my mistakes, and being an excellent company in many occasions. He is truly my guru both in academic and personal fronts.

I would like to thank former and present Dean(s), School of Chemistry, for their constant support, inspiration and for the available facilities. I am extremely appreciative individually to all the faculty members (especially my doctoral committee members; Prof. M. J. Swamy & Prof. Tushar Jana) of the School for their help, cooperation and encouragement at various stages. Being a master's student of this place, I thank all my teachers for their valuable lessons and love.

I am very thankful to Dr. Moloy Sarkar and Prof. Soma Venugopal Rao for the fruitful research collaboration which enriched my knowledge immensely.

Financial assistance from DST and CSIR, New Delhi is greatly acknowledged. Special thanks are due to CSIR for providing me a research fellowship during this period. I also acknowledge International Travel support scheme of SERB for providing me the financial assistance to attend the PSCO-2018 in Lausanne, Switzerland.

I thank Mr. Durga Prasad for his special care/attention in Transmission Electron Microscope (TEM) measurements at Centre for Nanotechnology, University of Hyderabad and value our close association. I also thank him and Mr. Sunil for their assistance in Field Emissive Scanning Electron Microscope measurements at our School.

I express my heartfelt appreciation to those dedicated teachers that I got at different stages of my life. During school life the teachings of Gopal Mukherjee, Kabul da, Saylen Karmakar, Palash da, Susanta pal have shown me the path towards the persuasion of higher studies. During my B.Sc days I got extremely good teachers like Sukriti da, RP sir, PSS sir, Rizabul sir, Sadhan sir, Palash sir. My passion for Chemistry is the fruit of their advice and lectures,

I still enjoy the happy moments and unforgettable memories that I had with my school mates and friends, specifically my hostel mates of Arambagh high school, kaushik, Partha, Snehasis, Kanai, Dipankar, Abhijit, Souvik, Abhilas. My college and mess friends Subhajit, sourav, Arnab, Soumaya, Anwesha, tushar, jayanta, Madhuri, Sonanki, Aditi, Antu, Kaushik, Ramu, Ditsuman, Sabir, Braja da, Sudipta, Animesh da, Sukanta da are the reason that those days were so colourful. I really cherish my association and time spent with my M.Sc. friends, Suman dana, Suman kuila, Abhoy, Abhisek, Sandeep, harekrishna.

I am very much fortunate that I got friends like Meena, Atindra, Arka, Ranjita, who have always stood by my side in my difficult times, taught me and above all tolerated me. I am really grateful for their contribution in my life.

I value my association with my former lab-mates: Satyen da, Soujanya mam, Prasun da, Moloy da, Tamal da, Aniruddha Da, Ravi anna, Dinesh da whom I met in several occasion like RAMS-2016 (Sir's 60th birth Anniversary), FCS workshop, and Ani's marriage, always encouraged me to pursue good research and reach my goals. I am extremely thankful to my talented seniors Satya da, Ashok anna, Chandu anna, Soumya di, Shalini di, and Navendu da for their help in learning instruments, fruitful scientific discussions in group meeting and various other occasions. Without your love, support and care, it would have been difficult for me to overcome the difficulties during my learning period. I acknowledge my batch mate Sneha and my junior friends Saddam, Apurba, Tasnim, Somnath, Sumanta, Alila and Rajesh for maintaining the friendly and cooperative atmosphere in the lab. All the lab parties and lab trips were full of fun and joy because of the present and former lab members. Thanks to Navendu da for your company in perovskite journey from the very beginning and all the helps in several occasions. Special thanks to Sneha for understanding me and helping me starting from manuscript correction to choosing party venu. I am in debt to Apurba and Saddam for always offering me the warmth of close association and fun times. I am fortunate to have junior like Tasnim who helped me immensely in formulating new ideas, accelerating my works and learning new things. I really enjoyed our thoughtful discussions over several professional and personal topics. I highly appreciate Sumanta for our fruitful scientific discussions and your valueable opinion in several aspects. I must thank Somnath for being such an obedient junior and the reason of happiness and lots of fun in several occasions. I would also like to thank my project students Ravi, Anand, Sumanta, and Rabindranath who helped me in my research projects and with whom I had spent a wonderful time.

I would like to thank Sonali madam, Ani (Anweshan) and boni (Ipsita) for their close association with me.

I thank all the non-teaching staff of the school of chemistry for their time-to-time cooperation. They had all been quite helpful.

I am really lucky for being part of the "the Bengali community" of HCU. I am always in debt to my big brothers and sisters Santanu da, Arpita (Chowdhury) di, Raja da, dinu da, Rishi da, Maity da, Paromita di, Anup Da, Pati da, Nayan da, Arpita (Ghosh) di, Debparna di, Koushik da, Sugata da, Suman da, Rudra da. Your love and care for me is no less than a family member. I will cherish each and every moment spent with you all throughout my life. I am also grateful for the valuable friendship of Mou, Sabari, Arijit, Debika, Sarada, Subham, Soutrik, Sritam, Nilanjan, Suman, Surja, Rabiul, Khokon, golu, Tanmoy, Ram, Puja.I am also thankful to my colleagues Pravakar reddy, Chandrahas,

Subha, Divya, Anil, Surya, Uma Mahesh, Satish, Ankit, Nagamaiyah, Kallol, Mohan anna. I am very much afraid that I have missed some close people.

I am grateful to my hostel party Apurba, Arijit, Bappa, Kuntal with whom I spent the most cherish able time starting from gossiping to drinking to Campus hopping to trekking. I will forever miss your associations.

Though anything said would be less, my parents' love and affection toward me have always been the means of the journey of my life. My mother's endless struggle and effort to keep me in a better ground can never be put to mere words. My father's immense support during my difficult times are the pillars of my present life. My brother's and sister's selfless love and care is unparalleled. I am fortunate to have two wonderful and powerful women of my life, my thakuma and didima. I owe all my success and achievements to them. I value the close association with all my relatives.

Sudipta

List of Publications

1. Sivalingam Soumya, **Sudipta Seth**, Sneha Paul and Anunay Samanta, Contrasting Response of Two Dipolar Fluorescence Probes in a Leucine-Based Organogel and Its Implications. *ChemPhysChem*, **2015**, *16*, 2440-2446.

2. Satyajit Patra, **Sudipta Seth** and Anunay Samanta, Effect of Controlled Deposition of ZnS Shell on the Photostability of CdTe Quantum Dots as Studied by Conventional Fluorescence and FCS Techniques. *ChemPhysChem*, **2015**, *16*, 3871-3876.

3. **Sudipta Seth**, Navendu Mondal, Satyajit Patra, and Anunay Samanta, Fluorescence Blinking and Photoactivation of All-Inorganic Perovskite Nanocrystals $CsPbBr_3$ and $CsPbBr_2I$. *J. Phys. Chem. Lett.*, **2016**, *7*, 266–271. **(Chapter 3)**

4. **Sudipta Seth** and Anunay Samanta, A Facile Methodology for Engineering the Morphology of $CsPbX_3$ Perovskite Nanocrystals under Ambient Condition. *Scientific Reports*, **2016**, *6*, 37693.

5. Debashis Majhi, Prabhat Kumar Sahu, **Sudipta Seth**, and Moloy Sarkar, Probing the interactions of structurally similar but chemically distinguishable organic solutes with 1-ethyl-3-methylimidazolium alkyl sulfate (alkyl= ethyl, hexyl and octyl) ionic liquids through fluorescence, NMR and fluorescence correlation spectroscopy (FCS) studies. *Phys. Chem. Chem. Phys.* **2016,** *18*, 22343-22354.

6. Prabhat Kumar Sahu, Raju Nanda, **Sudipta Seth**, Arindam Ghosh and Moloy Sarkar, Nuclear magnetic resonance, fluorescence correlation spectroscopy and time-resolved fluorescence anisotropy studies of intermolecular interactions in bis (1-methyl-1H-imidazol-3-ium-3-yl) dihydroborate bis (trifluoromethylsulfonyl) amide and its mixtures with various cosolvents. *Chem. Phys. Lett.*, **2016**, *661*, 100-106.

7. **Sudipta Seth** and Anunay Samanta, Fluorescent Phase-Pure Zero-Dimensional Perovskite-Related Cs_4PbBr_6 Microdisks: Synthesis and Single-Particle Imaging Study. *J. Phys. Chem. Lett.*, **2017**, *8*, 4461–4467. **(Chapter 5)**

8. Debashis Majhi, **Sudipta Seth**, and Moloy Sarkar, Differences in the behavior of dicationic and monocationic ionic liquids as revealed by time resolved-

fluorescence, NMR and fluorescence correlation spectroscopy. *Phys. Chem. Chem. Phys.*, **2018**, *20*, 7844-7856.

9. **Sudipta Seth** and Anunay Samanta, Photoluminescence of zero-dimensional perovskites and perovskite-related materials. *J. Phys. Chem. Lett.*, **2018**, *9*, 176–183.
10. Katturi Naga Krishnakanth, **Sudipta Seth**, Anunay Samanta, and Soma Venugopal Rao, Broadband femtosecond nonlinear optical properties of $CsPbBr_3$ perovskite nanocrystals. *Optics Letters*, **2018**, 43, 603-606.
11. Subhasis Roy, Naupada Preeyanka, Debashis Majhi, **Sudipta Seth**, and Moloy Sarkar, Striking Similarities in the Fluorescence Behavior between Carbon Dots and Ionic Liquids: Toward Understanding the Fluorescence Behavior of Carbon Dots. *J. Phys. Chem. C,* **2018**, 122, 12384–12394.
12. Tasnim Ahmed, **Sudipta Seth**, and Anunay Samanta, Boosting the Photoluminescence of $CsPbX_3$ (X = Cl, Br, I) Perovskite Nanocrystals Covering a Wide Wavelength Range by Postsynthetic Treatment with Tetrafluoroborate Salts. *Chem. Mater.*, **2018**, *30*, 3633–3637.
13. **Sudipta Seth**, Tasnim Ahmed and Anunay Samanta, Photoluminescence Flickering and Blinking of Single $CsPbBr_3$ Perovskite Nanocrystals: Revealing Explicit Carrier Recombination Dynamics. *J. Phys. Chem. Lett.* **2018**, *9*, 7007–7014. **(Chapter 4)**
14. K.N. Krishnakanth, **Sudipta Seth**, Anunay Samanta, S. Venugopal Rao, Broadband Ultrafast Nonlinear Optical Studies Revealing Exciting Multi-photon Absorption Coefficients in Phase Pure Zero-dimensional Cs_4PbBr_6 Perovskite Films. *Nanoscale*, **2019**, *11*, 945-954.
15. Aman Kumar Agrawal, Prabhat Kumar Sahu, **Sudipta Seth**, and Moloy Sarkar, Electrostatically Driven Förster Resonance Energy Transfer between a Fluorescent Metal Nanoparticle and J-Aggregate in an Inorganic–Organic Nanohybrid Material. *J. Phys. Chem. C*, Article ASAP.

Google scholar Citations

Cited by

	All	Since 2014
Citations	187	186
h-index	6	6
i10-index	5	5

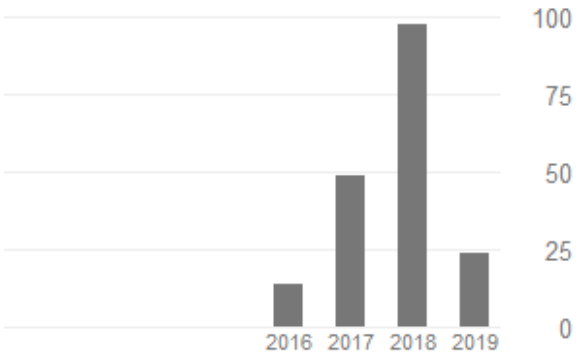

Presentations

Oral Presentations

1. "Nucleation and self-assembly of $CsPbX_3$ Perovskite Nanocrystals", **24th Congress and General Assembly of the International Union of Crystallography (IUCr 2017)**. Hyderabad International Convention Centre, Hyderabad, India, 21-28 August, **2017.**
2. "Fluorescent Phase-Pure Zero-Dimensional Perovskite-Related Cs_4PbBr_6 Microdisks: Synthesis and Single-Particle Imaging Study", **workshop during Indo-Japan cooperative Science Program**, Kanagawa university, Hiratsuka city, Japan, 6th December, **2017**.
3. "Are the Zero-Dimensional Perovskites Fluorescent? Fabrication and Imaging of Phase-pure Cs_4PbBr_6 Microdisks", **ACS on Campus event**, University of Hyderabad, Hyderabad, December 23, **2017**.

Poster Presentations

1. "Fluorescence Blinking and Photoactivation of All-Inorganic Perovskite Nanocrystals $CsPbBr_3$ and $CsPbBr_2I$", **Recent Advances in Molecular Spectroscopy: Fundamentals and Applications in Materials and Biology (RAMS-2016)**. University of Hyderabad, India, 2-4 March, **2016**.
2. "Post-synthetic Modification of $CsPbBr_3$ Perovskite Nanocrystals: Luminescence Enhancement and Blinking Suppression**",** **21st CRSI National Symposium in Chemistry-2017**. CSIR-Indian Institute of Chemical Technology, Hyderabad, India, 14-16 July, **2017**.
3. "Photoluminescence of Zero-Dimensional Perovskites", **5th International Conference on Advanced Nanomaterials and Nanotechnology (ICANN 2017)**. Centre for Nanotechnology, Indian Institute of Technology Guwahati, Assam, India, 18-21 December, 2017. (**Best Poster Award**)
4. "Insight into the Photoluminescence of Zero-Dimensional Perovskite Related Cs_4PbBr_6 Microdisks", **Trombay Symposium on Radiation & Photochemistry (TSRP- 2018)**. Bhabha Atomic Research Centre, Mumbai, India, 3-7 January, **2018**.

5. “Suppressed Auger Recombination in Thiol-Treated $CsPbBr_3$ Perovskite Nanocrystals as Revealed by Single Particle Luminescence Spectroscopy”, **Perovskite Solar Cells and Optoelectronics (PSCO-2018)**. Lausanne, Switzerland, 30th September-2nd October, **2018**.

Chapter 1

Introduction

This chapter provides an overview of the basic properties of bulk semiconductor materials and modulation of their optical and electronic properties when size is reduced to nanocrystals (NCs) level. A brief discussion on quantum confinement and surface chemistry of the NCs is provided. Then the inspiring journey of the lead halide perovskites as a promising photovoltaic material is traced. Specific attention is given to the perovskite NCs of all-inorganic category ($CsPbX_3$, X = Cl, Br, I) highlighting their promise towards high efficiency optoelectronic devices. Zero-dimensional perovskite related materials are introduced (Cs_4PbBr_6) and controversy over its photoluminescence (PL) is discussed elaborately. A detailed discussion on PL blinking of single semiconductor NCs including their types and mechanisms are presented. Finally the motivation behind the thesis and its chapter-wise organization are presented.

1.1 Semiconductors: Bulk to nanocrystals.

Semiconductors are one of the most celebrated solids of modern times. This class of materials possess electrical properties in between those of metal and insulator. In general, the band gap of the semiconductors lie between 0.5–3 eV and they have very less free carriers in their crystal lattice. Charge carriers can be generated by promoting one electron to the conduction band leaving behind a hole in the valence band. This is achieved by providing external energy equal or more than the band gap in the form of heat or photons. Due to Columbic interaction theses opposite charges are attracted to each other and form a bound pair which is termed as exciton. Often this bound pair moves together and is considered as a quasi-particle. Electronic properties of the semiconductor are highly dependent on the binding energy and mobility of the excitons.

In general, excitons are two types, Frenkel and Wannier-Mott. Excitons which have higher binding energies are known as Frenkel excitons and mostly observed in the materials where atoms interact weakly with each other. Semiconductor crystals having periodic array of atoms mostly feature weakly bound Wannier-Mott excitons. In our discussion, we will consider only the Wannier-Mott excitons as these are most commonly found in metal chalcogenide quantum dots (QDs) or perovskite nanocrystals (NCs), which are the subject matter of this thesis. Being one electron system an exciton in a crystal can be approximated as a Hydrogen atom system and the energy of it can be expressed as[1]

$$E_{ex} = E_g - \frac{R_y}{n^2} + \frac{\hbar^2 k^2}{2(m_e^* + m_h^*)} \qquad (1.1)$$

Where, E_g is the band gap, n is the principal quantum number with values 1,2,3…, R_y is the exciton binding energy given by $\frac{m_r}{\epsilon^2} \times 13.6$ eV (ϵ and m_r are the dielectric constant and reduced mass of electron and hole, respectively).[1] Even though, exciton is a hydrogen like system it cannot move freely and has to encounter dielectric environment imparted by other constituting atoms of the crystal. The most probable distance between the electron and hole is the exciton Bohr radius, which can be expressed as

$$a_B^{ex} = a_H^B \times \frac{\epsilon}{m_r} \qquad (1.2)$$

Where, a_H^B is the hydrogen Bohr radius.

Versatile and ubiquitous use of semiconductor is realized when optical and electronic properties are modulated by various methods. One of the most convenient approach is by reducing its dimensionality. Bulk materials possess a high density of electronic states providing continuity in the valence band (VB) and conduction band (CB). When size of the particle decreases, density of states decreases and as a consequence the energy levels become discreet with an increased band gap. While doing so when the size of the particle becomes comparable or less than exciton Bohr radius, it becomes quantum confined. As shown in Figure 1.1, depending on the extent of confinement in different spatial directions, particle of desired dimensionalities can be prepared. When the size of the particle becomes less than the Bohr radius only in one dimension it becomes a 2D quantum well (confined in 1D). Likewise other dimensionalities (quantum wire and quantum dots) can be achieved as demonstrated below having a typical size of few nanometers (nm).

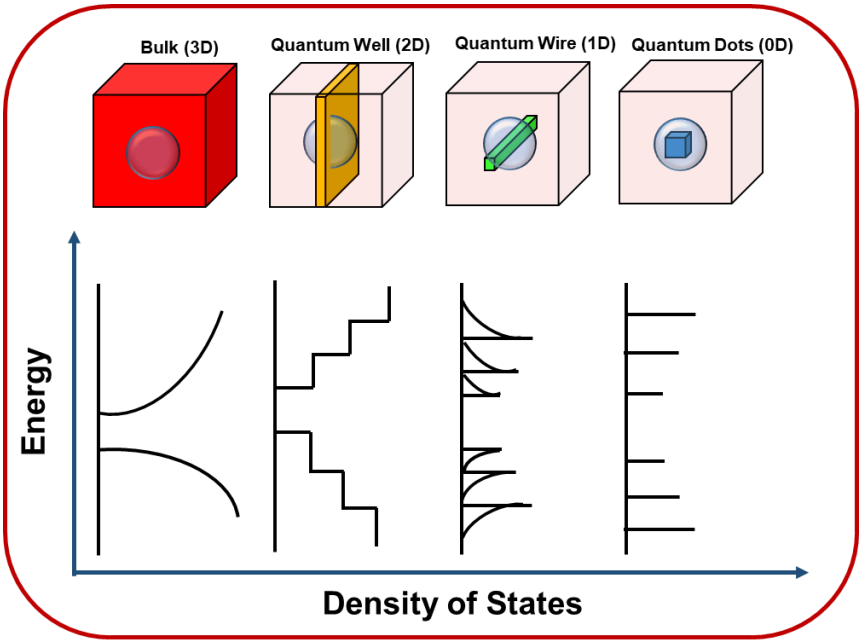

Figure 1.1. Demonstration of quantum confinement by decreasing dimensionality and its effect on density of states and band gap.

These confined materials are pseudo-atomic systems consisting of hundreds to thousands of atoms bridging between molecular and bulk materials. Due to the confinement effect band gap of the smaller particle is higher as compared to the bulk (Eg) and can be expressed as[2,3]

$$E_{QD} = E_{Bulk} + \frac{\hbar^2 \pi^2}{2m_e^* R^2} + \frac{\hbar^2 \pi^2}{2m_h^* R^2} - \frac{1.786e^2}{\epsilon R} - 0.248E_{Ry}^* \quad (1.3)$$

Where, 2nd and 3rd terms are confinement energy of electrons and holes, respectively. Fourth term is the coulomb interaction energy and the final one represents exciton Rydberg energy. The Rydberg energy is generally very small and can be neglected but becomes important when the dielectric constant of the material is very low.[4] Since, in the confinement regime, oscillator strength of transition is high, it leads to efficient radiative recombination rate thus making quantum materials exciting light emitters. Due to smaller size, high PL efficiency, tunable band gap and discrete energy levels, quantum confined materials are highly promising candidates for several applications like light emitting diodes (LEDs), low threshold lasers, biological imaging, and nonlinear photonic devices.[5-9]

1.2. Surface chemistry of the nanocrystals.

As the size of the semiconductors decreases to nanoscale, their surface to volume ratio and surface free energy also increases. Atoms inside the crystals are fully bonded in all three dimensions but those on the surface, where crystalline periodicity breaks, become under-coordinated (Figure 1.2).[10] These outermost atoms with unpassivated orbitals form an energy band that could lie within the VB and CB or at higher energy. If the energy level falls within the band gap it acts as a trapping center for the photogenerated charge carriers. These surface generated trapping centers (surface traps) open up recombination channel apart from the band to band carrier recombination. In majority of the cases, this recombination is nonradiative and is a matter of serious concern in optoelectronic applications.[11] In some cases, emission may arise from these trap states but is red shifted with a large full width at half maximum (FWHM) and low quantum efficiency (Figure

1.2). Depending on the position of the trap states and nature of the carriers being trapped these traps can be classified into shallow or deep and electron or hole traps, respectively.

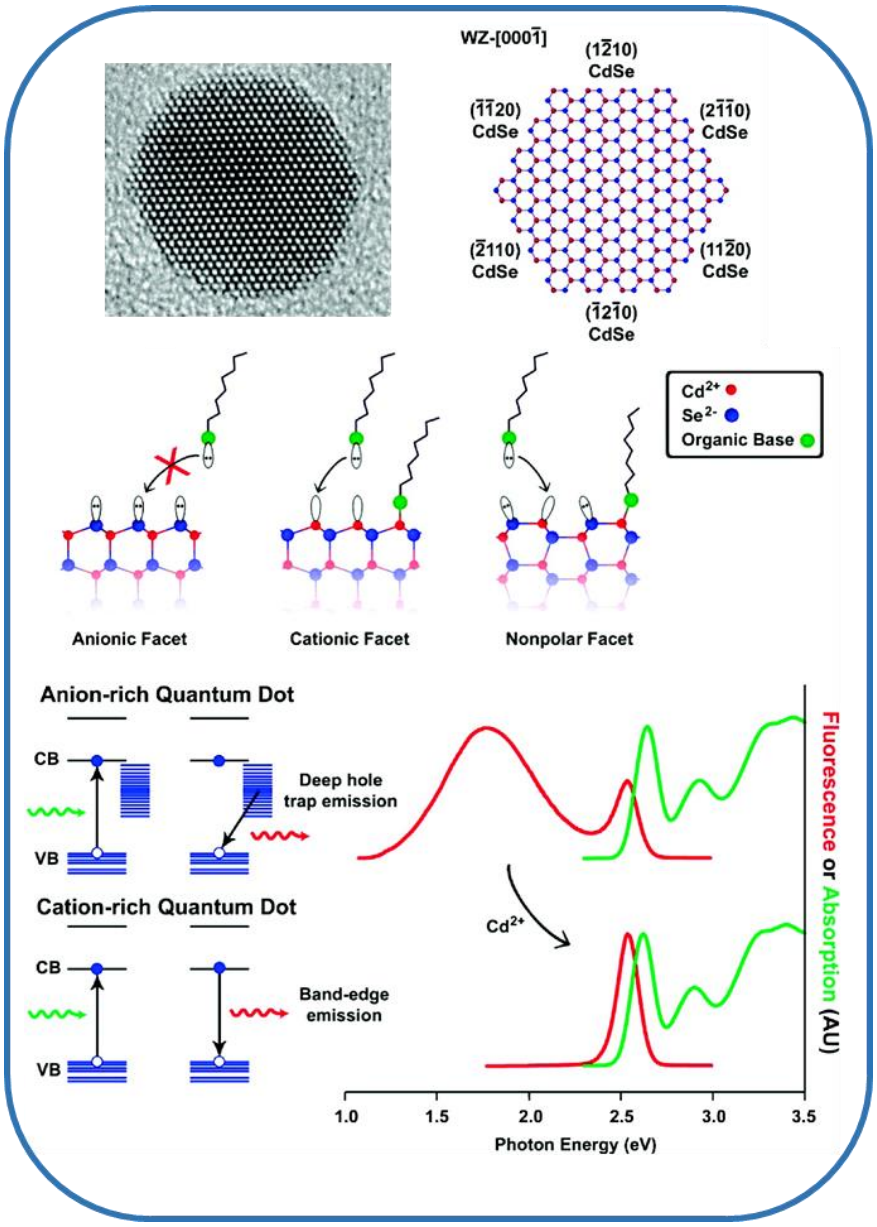

Figure 1.2. Demonstrating origin of the surface trap states, their effect on optical properties of the NCs (with CdSe QDs as example) and suppression of these states by ligand capping (adapted from reference 10).

One of the simple approaches to eliminate these trap states is by passivating the under-coordinated surface atoms by suitable capping ligands, as shown in figure 1.2. Depending on the crystal facets, surface atoms could be electron rich or deficient and a judicious choice of the capping ligands may reduce the trap state density.[11,12] Capping ligands are generally amphiphilic in nature with a polar head group and a long hydrocarbon chain as tail. Commonly used polar groups in the capping ligands are carboxylate, amine, thiol and phosphine, which are Lewis bases and cap cationic species on the NC surface.[13] Hence, by enriching the surface with metal cations or anions one can eliminate trap assisted nonradiative recombination, as shown for CdSe QDs in Figure 1.2. Capping ligands not only passivate the surface but also play a crucial role in the synthesis of nanoparticle. Generally amphiphilic ligands form a miceller structure in the reaction medium where nucleation leads to formation of seed crystals which then grow to become NCs of different morphologies. The ligands control the growth of the NCs and provide stability to the colloidal particles in different media.

Capping ligands are generally labile and cannot provide ideal capping due to the weak interaction in the organic-inorganic interface.[12,13] Another approach to improve the surface quality of a NC is by epitaxially growing a protective layer of another semiconductor material.[10,14-16]

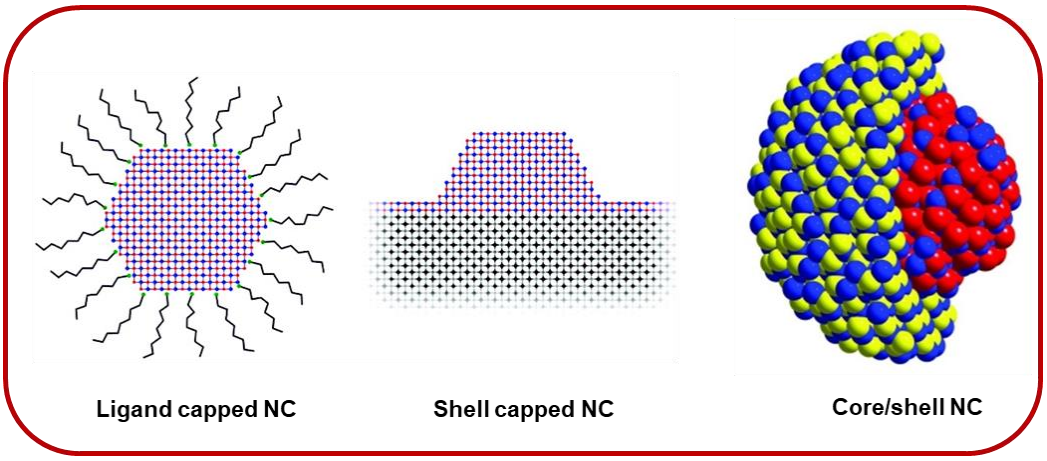

Figure 1.3. Ligand capped NC, island of epitaxially grown core/shell NC, and 3D representation of core/ shell NCs. (adapted from reference 10, and https://cen.acs.org/articles/89/web/2011/12/Quantum-Dots-Blink.html)

As shown in figure 1.3, shelling materials with less lattice mismatch can passivate the cationic and anionic surface defects simultaneously and reduce the mid-band gap surface traps. Several types of core/shell NCs can be synthesized depending on the band gap and relative band alignment of the core and shell materials.[16] Though shell provides better protection with a rigid structure, it often produces some defect states at the core/shell interface that can act as a mid-band state and facilitate nonradiative recombination. Several novel ideas (like engineering core-shell interface, giant core shell QDs etc.) have been developed over the years to eliminate the activity of these detrimental trap states.[17,18]

1.3. Perovskites.

Journey of the perovskite started with calcium titanium oxide ($CaTiO_3$) when Gustav Rose first discovered this mineral in 1939 from the Mountains of Ural and named after Russian mineralogist, Count Lev Alekseevich Perovski. It has a cubic crystal structure containing inter-connected $[TiO_6]^{4-}$ octahedral units and Ca^{2+} ions residing outside filling the voids. Any material having similar cubic crystal structure and generic ABX_3 formulation belongs to the perovskite community (Figure 1.4). Versatility of this structure is reflected from the large number of compositions available in this crystal phase. However, a perovskite structure is stable only when its tolerance factor (t) as proposed by Goldsmith and defined in equation 1.4 lies well within the range of 0.75 to 1.0.[19]

$$Tolerance\ factor\ (t) = \frac{r_A + r_X}{\sqrt{2}(r_B + r_X)} \qquad (1.4)$$

Oxide perovskites are well known for their multidimensional applications in magnetism, piezo- and ferro-electricity, capacitors, superconductivity to name a few.[20]

Apart from the oxide perovskites a major portion of the perovskite field is occupied by the halide perovskites. Here, oxides (X) are replaced by anionic halides (Cl^-, Br^-, I^-) and central metal ion (B) is a bivalent cation (Pb^{2+}, Sn^{2+}) and monovalent cations (A^+) reside in the voids between the $[BX_6]^{4-}$ octahedral network. Lead halide perovskites are the most stable and popular amongst the halide perovskites. Depending on the identity of the monovalent cation, halide perovskites can be classified into hybrid organic-

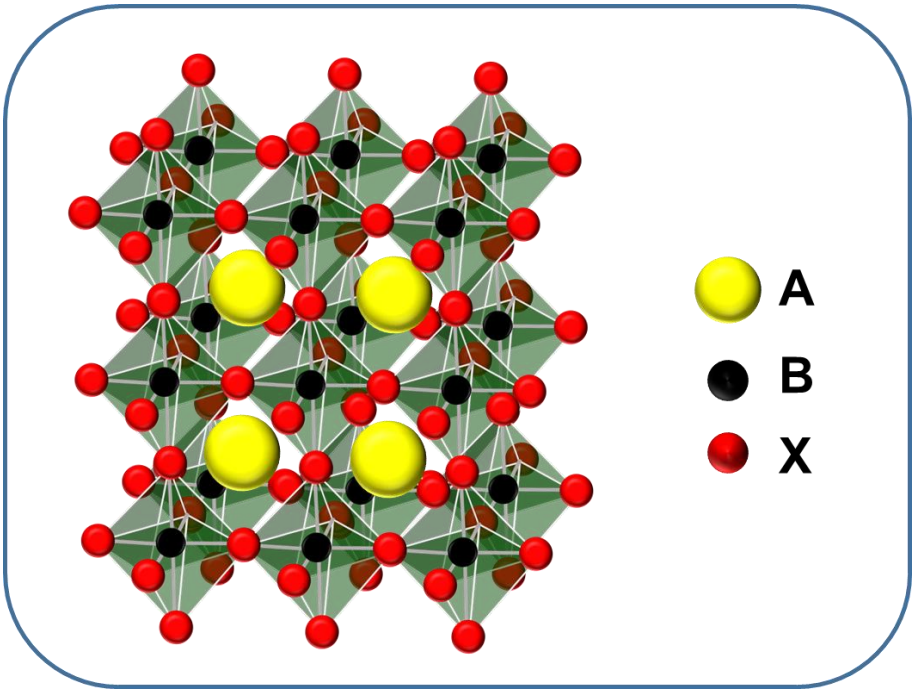

Figure 1.4. Schematic representation of the generic ABX_3 perovskite crystal structure.

inorganic or all-inorganic subsection. When A is a small organic cation such as methyl ammonium (MA) or Formamidinium (FA), the perovskites are called hybrid organic-inorganic metal halide perovskite but when A is replaced by an inorganic cation such as cesium (Cs) or rubidium (Rb) they fall in the all-inorganic category.

Lead halide perovskites were first reported by H. L. Wells in 1893 and the structure was first deduced by C. K. Moller in 1959 for cesium plumbo iodide ($CsPbI_3$).[21,22] Late last century both hybrid and all-inorganic materials of different dimensionalities were synthesized but the development was limited to understanding the optoelectronic properties.[23-25] Popularity of these materials started since Miyasaka's group first introduced it in photovoltaic technology in 2009.[26] They used $MAPbI_3$ as a photosensitizer in a similar architecture like dye sensitized solar cells (DSSC) and reported an efficiency of 3.8%. Since then several modifications have been made on the solar cell architecture by changing the thickness and morphology of the perovskite layer or employing a solid state

electrolyte and these pushed the efficiency up to 15%.[27-29] Because of the steep growth in efficiency and potential in solar cells, this class of material has opened up a new research field as perovskite sensitized solar cells (PSSC). Continuous development in this field has made it possible to achieve an efficiency exceeding 22% (http://www.nrel.gov/ncpv).

1.3.1. All-inorganic perovskite NCs.

Research on perovskite opened up a new dimension when Kovalenko and coworkers introduced Cs-based all-inorganic perovskite NCs with enticing optical properties in 2015.[30] PL of these NCs is tunable throughout the entire visible spectrum just by changing the halogen identity (Figure 1.5).[30-32] Optical properties can also be tuned by changing the size of the NCs in the quantum confinement regime.[33,34]All-inorganic perovskites are nominally different from their hybrid counterpart in terms of electronic properties as monovalent cations do not play much role in contributing to the frontier orbitals, which mostly determine the band gap and optical properties.[30] However they do exert some influence on the structure as the size and hydrogen bonding interaction of the organic cation may lead to minute structural changes (B-X bond length and B-X-B bond angle) even though similar lead halide octahedral units are present in both cases.[35-37]

Major difference between hybrid and all-inorganic NCs appears in terms of their environmental stability. Due to the hygroscopic nature of the organic cations, the hybrid materials are prone to degradation whereas all-inorganics are more robust against photon or moisture induced degradation.[38-40] More importantly all-inorganic $CsPbX_3$ NCs are highly luminescent and defect tolerant.[30,37] Dimensionality, morphology and consequent optical properties of these $CsPbX_3$ NCs can be tuned easily by changing the ligand concentration, chain length, reaction temperature and time.[41-43] Change in dimensionality leads to modulation of the quantum confinement and better the confinement higher is the radiative recombination. Owing to these advantageous properties, all inorganic NCs have come out to be a highly promising material for photon emitting applications such as low threshold lasers, LEDs, single photon emitters, etc.[44-46] However, with decrease in size, surface to volume ratio of the crystals increases, which leads to generation of more surface defects and enhancement of the nonradiative recombination exerted by these surface defects.

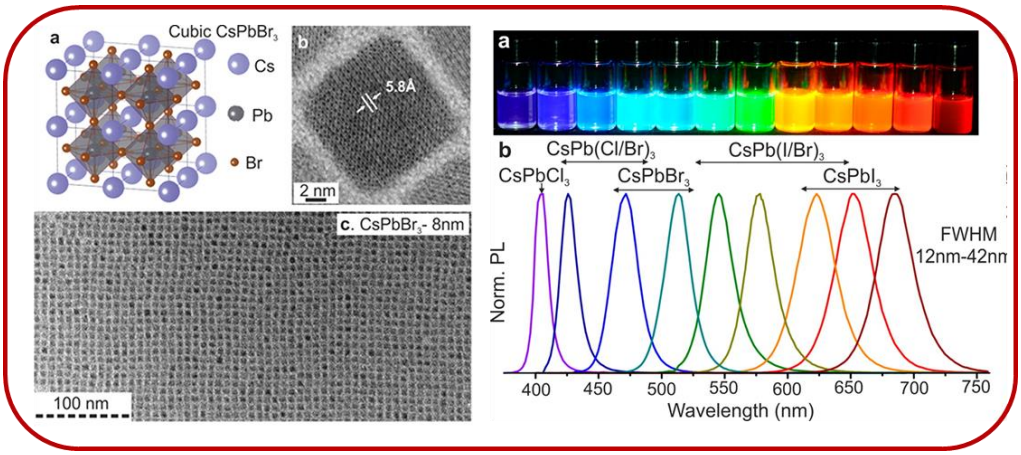

Figure 1.5. All-inorganic cesium lead halide perovskite NCs and their halogen dependent PL properties. (Adapted from ref 31)

Hence, the surface of the NCs plays a crucial role in determining the optical properties of the material. Despite being defect tolerant, presence of a few structural or intrinsic defects can lead to effective quenching of PL because of very high charge carrier mobility.[47] Mostly halogen vacancies, under-coordinated lead atoms and lead nanoparticles are considered to be the potential defects at work to quench the PL of these NCs.[48-54] Of late several strategies have been developed to eliminate the surface as well as intrinsic defects to obtain near-unity PLQY with improved lifetime. Using capping ligands of softer Lewis base functionalities, doping of metal halide salts, and surface treatment with thiocyanate or tetrafluoroborate salts are some of the most efficient methods to achieve this goal.[48-54]

1.3.2. Zero-dimensional perovskite-related materials.

A low-dimensional semiconductor can be realized by confining the excitons within a volume of radius comparable or less than the Bohr radius. This can be achieved by two means. First, because the excitons created in the BX_6 octahedra are connected to each other in ABX_3-type perovskites, a 0-D perovskite material is obtained when the particle size is below its exciton diameter, as illustrated in Figure 1.6. Considering $CsPbBr_3$ as a representative 3-D perovskite with an exciton diameter of ~7 nm, a 0-D perovskite will form when the size of the particle is comparable to or less than 7 nm.[30] Because of

similarity with the metal chalcogenide QDs, such 0-D perovskites are termed perovskite QDs. Second, a 0-D perovskite can also be realized when the BX_6 octahedral units are isolated by introduction of a structural barrier inside a bulk crystal lattice. Such a 0-D structure is best demonstrated in a rhombohedral Cs_4PbBr_6 crystal, where the $PbBr_6$ octahedral units are spatially isolated by the intervening Cs atoms (Figure 1.6).[55-57] This kind of 0-D materials can have a physical dimension of several millimeters or larger, similar to a bulk material, but because of their intrinsic confined nature, they act as a bulk quantum material. Such low-dimensional bulk material is difficult to design but can be easily obtained for perovskite material using an appropriate synthetic methodology. Unlike the 3-D perovskites, these are commonly termed 0-D perovskite-related materials (0-D PRMs) as these bulk quantum materials do not have corner-sharing connectivity. The beauty of the 0-D PRMs is that these can have diverse morphologies and sizes, but properties similar to a single-constituent octahedral unit.

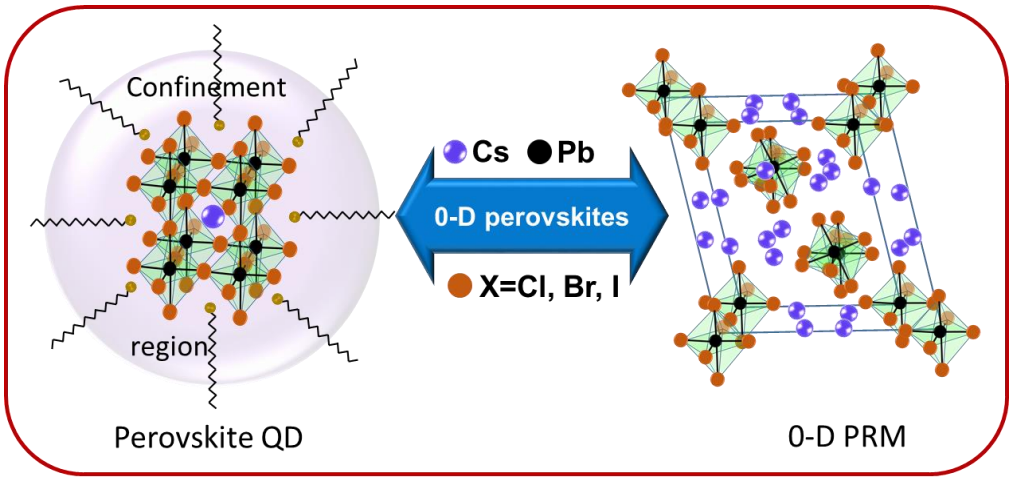

Figure 1.6. Schematic representation of two types of 0-D perovskites. Perovskite QDs with general formulas of ABX_3 and size less than the exciton Bohr diameter (represented by the diameter of the circle) and 0-D PRM with spatially isolated octahedra in a bulk crystal lattice. (Adapted from reference 58).

1.3.3. PL of Zero-dimensional perovskite-related materials and contriversy

Of late, the 0-D PRMs, in particular, Cs_4PbBr_6, have received considerable attention because of their intriguing structure-associated optical properties. Generally, a decrease in dimensionality of the material leads to an increase in the band gap. As the BX_6 octahedra are electronically decoupled in 0-D PRMs, one expects a larger band gap in these materials as compared to their higher-dimensional counterparts. This is indeed demonstrated by Manna and co-workers in a recent report, where they have shown that Cs_4PbBr_6 NCs exhibit a sharp absorption peak at 314 nm corresponding to a band gap of 3.95 eV.[56] According to this report, such a high-band-gap material cannot show PL in the visible region for band to band pure excitonic transitions. Similar nonluminescent Cs_4PbBr_6 NCs were also observed by Alivisatos and co-workers while studying ligand-mediated postsynthetic transformation of green-emitting $CsPbBr_3$ NCs.[58] The NCs reported in these works vary in size, but all of them show the first absorption onset at ~315 nm, indicating that the optical properties of these materials are determined by the individual $PbBr_6$ octahedral units. A few other studies dealing with transformation of crystal structure and composition between $CsPbBr_3$ and Cs_4PbBr_6 also indicate that Cs_4PbBr_6 is a PL-inactive material.[59-61]

On the contrary, several other reports indicate intense green emission of Cs_4PbBr_6 with particle size ranging from NCs to single crystals.[55,57,62-67] PL of the powder form of Cs_4PbBr_6 with a λ_{max} of 520 nm and QY of ~45% is shown.[55] Another report indicates a high PL QY (~65%) of Cs_4PbBr_6 NCs in colloidal form.[63] An interesting point to note in this context is that unlike the other perovskite NCs it is observed that Cs_4PbBr_6 thin films retain a high PL QY (~54%) when prepared from colloidal dispersions.[63] Few other reports on Cs_4PbBr_6 single crystals confirm the PL of these 0-D PRMs.[62,64,66] Irrespective of their shapes and sizes, these crystals exhibit PL in the green region (515–524 nm) with an average FWHM of ~22 nm and QY of 38% or higher. Observed PL in this material is attributed to the mid band gap trap state mediated radiative recombination and these trap states arise most probably from the halogen vacancies.[68,69]

1.4. PL blinking.

PL emission from a fluorophore is often not steady and produce large fluctuations with time. When this fluctuation results in reversible and rapid transition between highly emitting (ON) and non-emitting or less emitting (OFF) states of a fluorophore under constant excitation, it is generally termed as PL blinking. It is essentially a single molecule or single particle phenomena and often gets masked by an average signal when an ensemble of emitting particles is considered. PL blinking has been observed in many molecular single photon emitters prior to its appealing appearance in semiconductor QDs.[70,71] It is universally accepted that blinking in semiconductor NCs is a direct consequence of charge carrier trapping.

In semiconductor NCs, lattice defects or unsaturated bonds on the surface can trap the photogenerated charge carriers and hence decrease band to band radiative recombination (due to decrease in overlap of the valence and conduction band wave functions). Depending on the energetic location and density, charge carriers in these defect states reside for a range of times (ns to ms) and introduce non-emitting states causing PL blinking. It is observed over the years that blinking rate in NCs or QDs is diverse and can properly be expressed with a power law function.[70,72-74] This is because charge carrier trapping and detrapping rates are highly distributed and can vary as a function of time. Statistical and time-resolved analysis of the ON and OFF states of a blinking trace provides kinetic and dynamic information about the charge carrier recombination in a single NC. Hence, studying PL blinking has become an important experimental method to find out the nature of the trap states and trapping kinetics in a single particle.

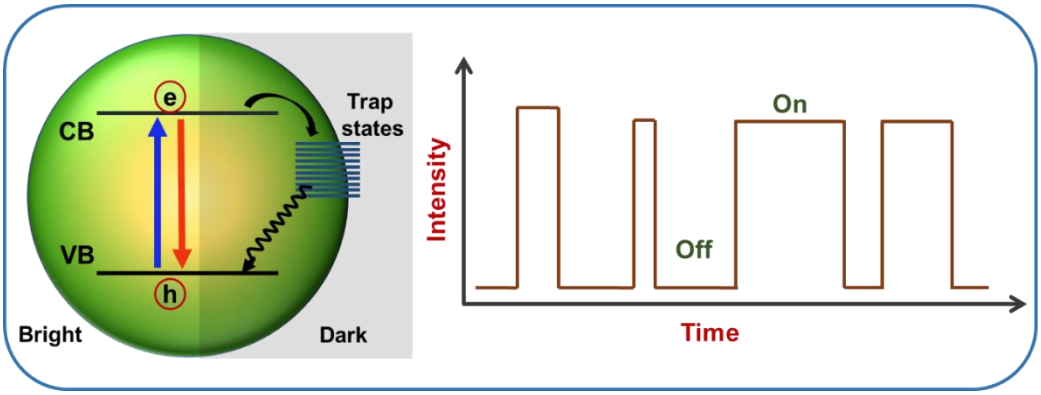

Figure 1.7. Schematic representation of competitive recombination processes and PL blinking in a single semiconductor NC.

Even though charge carrier trapping is considered as the only reason for PL blinking, the underlying mechanism is highly intriguing and debatable even after two decades of research. Two different approaches accepted widely as the reason behind PL blinking are charging model and multiple recombination center (MRC) model.[74,75] Early interpretation for the blinking was charging model i.e. photoionization and neutralization of the NCs. In this model, first a photogenerated charge gets trapped in a long-lived trap state on the surface leaving an unpaired charge in the core thus charging the NC. Subsequent generation of another electron-hole pair and transfer of the recombination energy to the third carrier leads to effective quenching of the emission. As long as the charge remains trapped this Auger process goes on and the particle remains dark. NC becomes bright again when radiative recombination prevails over the carrier trapping (Figure 1.8). Later this charging model is proved by performing PL intensity-lifetime scaling (η, as discussed below) on different intensity regions (ON, OFF) of the blinking timetrace.[76,77]

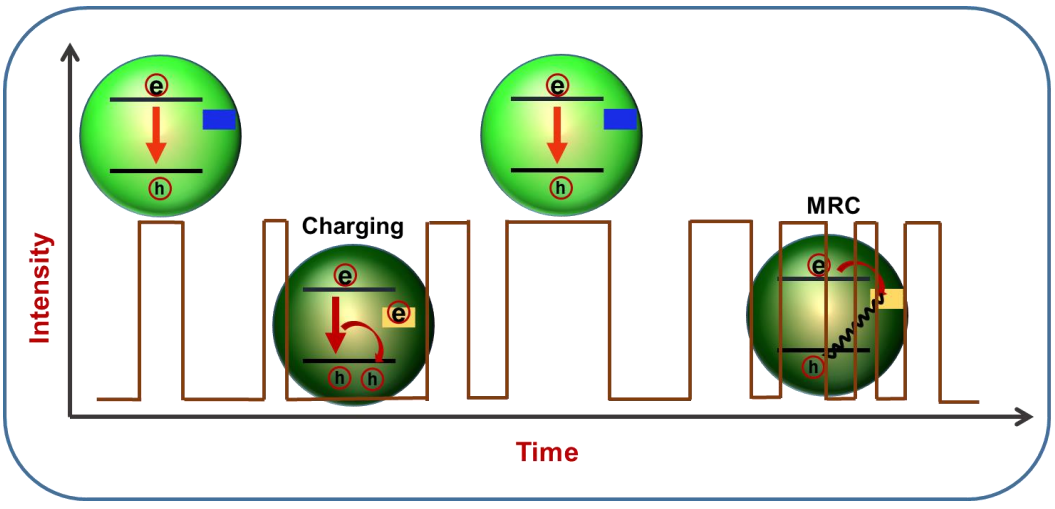

Figure 1.8. Schematic depiction of the models explaining the blinking mechanism.

Intensity-lifetime scaling (η) or the ratio of radiative rates of two different intensity levels (OFF to ON) is defined as

$$\eta = \frac{\tau_{OFF}}{I_{OFF}} \times \frac{I_{ON}}{\tau_{ON}} \quad (1.5)$$

Where τ and I are the PL lifetime and intensity of the corresponding ON or OFF states.

In charged NC, continuous photo-excitation leads to formation of trion, which recombines twice faster than a single electron-hole pair as additional charge exerts double Coulombic interaction. Hence, an η value of 2 for the given set of OFF and ON states suggests trion recombination to be responsible for the OFF states. Once a NC is charged it restricts further trapping of the charge carriers due to Coulomb blockade.

While an exponential distribution of the ON and OFF states are predicted from the charging model, practically it is found to be power law distributed. Over the years several modifications have been invoked to explain the power law behavior. Initially electron tunneling to the static traps were considered to explain the power law OFF state behavior, but it predicts a single ON to OFF switching rate.[72] To rationalize this anomaly time dependent fluctuation of the electron tunneling barrier to the trap states was introduced.[78] Blinking behavior is explained more successfully when trapping centers are considered to be dynamic.[79-82] Here, diffusion of the trap state energies or relative distribution of the trap state and NC energies provide a dynamic resonance condition with the charge carrier in the valence or conduction band.

At several instances it is observed that only charging model is not sufficient to explain the behavior of the OFF events. A lower PL QY of the OFF state than what is predicted from the Auger quenching suggests that there could be another nonradiative process which does not require charging.[83-85] Blinking traces often consist of several intensity levels and intensity-lifetime scaling of these levels yields a value near unity. This suggests that radiative recombination rates of these states are same, only the nonradiative rates vary.[73,85] Here the trap states are rather short lived (≤1μs) and trapped charge carrier undergoes a quick recombination with the counter-charge in the core of the NC.[73] Variation in the recombination rates and power law distribution of the ON-OFF events can be explained well considering the MRC model proposed by Frantsuzov et.al.[74] According to this model, nonradiative recombination centers switch between active and inactive form

providing a dynamic nature to the trap sites. Practically, both types of blinking can coexist in a single NC and yield an η value between 1 and 2.[86]

For perovskite NCs, PL blinking is found to be very fast i.e. NC switches between ON and OFF states very rapidly. In many cases, it is really hard to differentiate between clear ON and OFF states and a continuous distribution of states with different emissivity are often observed. This PL fluctuation pattern is sometimes termed as PL flickering. A few reports available on perovskite PL blinking do not provide a consistent picture of the process. Initially charging was considered as the only reason for blinking,[46,87,88] but later it is shown that blinking may arise because of pure nonradiative recombination via shallow traps in accordance with the MRC model.[89,90]

Recent studies on hybrid halide perovskites have shown, however, that PL blinking is not restricted to particles in nanoscale dimension, but can also be observed in larger size crystals (up to micrometers).[91-94] This finding is quite interesting because large-size conventional semiconductors do not exhibit this kind of behavior. This interesting PL blinking is attributed to fluctuating nonradiative relaxation due to some metastable but efficient defect states.

1.5. Motivation of the work done.

Declining level of the fossil fuels and its detrimental effects on environment have enforced the quest of the renewable energy research all over the globe. Solar energy being the most promising renewable source has received enormous attention in last few decades. Among several solar cell materials, lead halide perovskites have become the rising star because of their low cost, high efficiency and easy process ability. From the point of view of reduction of energy consumption by developing highly efficient LEDs, lasers and other optoelectronic devices also, all inorganic lead halide perovskite ($CsPbX_3$) NCs are promising because of their high defect tolerance, superior optical properties and environmental stability.

Performance of a photovoltaic or optoelectronic device largely depends on the activity of the defects of the used photosensitizer as it introduces losses via fast nonradiative recombination. Generally, these devices work under continuous illumination, higher photon fluence, high temperature and open atmosphere. These harsh conditions can

generate new charge trapping centers. Hence, in-depth understanding of the defect properties is an integral part of the material development. More specifically, knowledge on location, density, lifetime and efficiency of the charge trapping centers are very crucial to control its activity. These considerations led me to take up the following projects focusing on the PL fluctuation and carrier dynamics of single $CsPbX_3$ (X=Br, I) perovskite NCs with different time resolution.

Generally, PL fluctuation or blinking occurs in a range of time scales from μs to several tens of ms (or even longer) and no single particle experimental technique can cover the entire time window. Hence, we have considered two different experimental techniques to probe the blinking dynamics. Fluorescence correlation spectroscopy is the only technique which can provide better resolution up to few μs and is limited by the diffusion time of the particle (few ms) as freely diffusing single particles are considered in this experiment. Variation of the excitation power reveals the fate of multicarrier processes and information on the brightness of the particles. As halides largely controls the optical and electronic properties of these NCs, a comparative study of two different composition, $CsPbBr_3$ and $CsPbBr_2I$ can highlight the effect of halides on the carrier dynamics.

Investigating PL blinking over a longer time-window by immobilizing the particle is a very useful trait. By looking at the blinking pattern one can get the first impression of the NC quality. Analysis of different intensity levels using time-tagged-time-resolved method reveals types of radiative and nonradiative recombination processes and their corresponding timescales. Probability density of the ON and OFF events sheds light on the kinetics of the PL blinking. Hence, we chose the most stable, luminescent and widely used among all the NCs, $CsPbBr_3$ to study the influence of the trap states and their manifestation in the recombination dynamics.

Low dimensional materials are highly desirable for applications towards light emission, imaging and optical communication as these materials possess very high exciton binding energy which, facilitates radiative recombination of the excitons. It becomes far more important when dimensionality does not depend on the particle size. Cs_4PbBr_6 is such a zero-dimensional perovskite related material possessing very high exciton binding energy (≥170 MeV) irrespective of its size and shape. But PL of this material is highly

intriguing. While some reports explain it as a nonluminescent, insulating band gap material, some others consider it as highly luminescent quantum material. Detailed structural analysis and PL imaging study only can resolve the long standing controversy and provide a reasonable explanation about the origin of the PL. Hence, we have undertaken a project of imaging this material (microcrystals) in single particle level using a confocal fluorescence microscope which represents the first single particle study on this material.

1.6. Chapter-wise organization of the thesis.

The thesis has been classified into nine chapters. ***Chapter 1*** starts with a brief introduction on semiconductor NCs, their size dependent optical and surface properties. This chapter introduces a new class of an emerging photovoltaic and optoelectronic materials, perovskites along with their composition dependent optical and electronic properties. We have briefly discussed structural and optical properties of zero-dimensional perovskite related materials. An overview of PL blinking and the processes influencing the phenomenon are presented. Motivation behind the work done in the thesis is presented at the end. ***Chapter 2*** contains details of the materials, synthetic methodologies of different nanocrystals, and techniques for composition, morphology and structural characterization of these nanomaterials. Major focus is given to the instrumentation of confocal fluorescence microscope and data acquisition processes. Details of different single particle spectroscopic techniques based on this instrument are introduced. ***Chapter 3*** describes the PL blinking and photoactivation behavior of all-inorganic perovskite nanocrystals ($CsPbX_3$) of two different halide compositions employing FCS technique. ***Chapter 4*** presents the complete charge carrier dynamics of single $CsPbX_3$ NCs by analyzing the PL blinking behavior before and after post-synthetic treatment with alkylthiol ligands. ***Chapter 5*** deals with the controversy over the PL behavior of Zero-dimensional perovskite related material, Cs4PbBr6 materials. A new method has been developed for the synthesis of the microdisks of this kind and the controversy over the PL is also resolved by employing single particle PL imaging. ***Chapter 6*** summarizes the findings of the present investigations and highlights the possible directions for further studies based on the present work.

References.

(1) Knox, R. S. "Theory of Excitons," *Academic Press, New York* **1963**.

(2) Brus, L. E. *J. Chem. Phys.* **1983**, *79*, 5566.

(3) Brus, L. E. *J. Chem. Phys.* **1984**, *80*, 4403.

(4) Wang, Y.; Herron, N. *J. Phys. Chem.* **1991**, *95*, 525.

(5) Kelly, M. J. Low-Dimensional Semiconductors: Materials, Physics, Technology, Devices (Series on Semiconductor Science and Technology). *Clarendon Press, Oxford University Press, Oxford, New York* **1995**.

(6) Peaker, A. R.; Grimmeiss, H. G. Low-Dimensional Structures in Semiconductors. *Plenum Press, New York* **1991**.

(7) Jaiswal, J. K.; Mattoussi, H.; Mauro, J. M.; Simon, S. M. *Nature Biotechnology* **2003**, *21*, 47.

(8) Gao, X. H.; Chan, W. C. W.; Nie, S. M. *J. Biomed. Opt.* **2002**, *7*, 532.

(9) Pelton, M.; Yamamoto, Y. *Phys. Rev. A* **1999**, *59*, 2418.

(10) Smith, A. M.; Nie, S. *Acc. Chem. Res.* **2010**, *43*, 190.

(11) Alivisatos, A. P. *J. Phys. Chem.* **1996**, *100*, 13226.

(12) Kalyuzhny, G.; Murray, R. W. *J. Phys. Chem. B* **2005**, *109*, 7012.

(13) Groeneveld, E.; Donegá, C. d. M. *Nanoparticles* **2014**, 145.

(14) Dabbousi, B. O.; Rodriguez-Viejo, J.; Mikulec, F. V.; Heine, J. R.; Mattoussi, H.; Ober, R.; Jensen, K. F.; Bawendi, M. G. *J. Phys. Chem. B* **1997**, *101*, 9463.

(15) Peng, X.; Schlamp, M. C.; Kadavanich, A. V.; Alivisatos, A. P. *J. Am. Chem. Soc.* **1997**, *119*, 7019.

(16) Reiss, P.; Protiere, M.; Li, L. *Small* **2009**, *5*, 154.

(17) Chen, Y.; Vela, J.; Htoon, H.; Casson, J. L.; Werder, D. J.; Bussian, D. A.; Klimov, V. I.; Hollingsworth, J. A. *J. Am. Chem. Soc.* **2008**, *130*, 5026.

(18) Ratchford, D.; Dziatkowski, K.; Hartsfield, T.; Li, X.; Gao, Y.; Tang, Z. *J. Appl. Phys.* **2011**, *109*, 103509.

(19) Peña, M. A.; Fierro, J. L. G. *Chem. Rev.* **2001**, *101*, 1981.

(20) Bednorz, J. G.; Muller, K. A. *Z. Phys. B: Condens Matter* **1986**, *64*, 189.

(21) Wells, H. L. *Zeitschrift für Anorganische Chemie* **1893**, *3*, 195.

(22) Moller, C. K. *Matematisk-Fysike Meddelelser* **1959**, *32*, 1.

(23) Weber, D. Z. *Naturforsch* **1978**, *33*, 1443.

(24) Mitzi, D. B.; Field, C. A.; Harrison, W. T. A.; Guloy, A. M. *Nature* **1994**, *369*, 467.

(25) Kagan, C. R.; Mitzi, D. B.; Dimitrakopoulos, C. D. *Science* **1999**, *286*, 945.

(26) Kojima, A.; Teshima, K.; Shirai, Y.; Miyasaka, T. *J. Am. Chem. Soc.* **2009**, *131*, 6050.

(27) Burschka, J.; Pellet, N.; Moon, S.-J.; Humphry-Baker, R.; Gao, P.; Nazeeruddin, M. K.; Grätzel, M. *Nature* **2013**, *499*, 316.

(28) Kim, H.-S.; Lee, C.-R.; Im, J.-H.; Lee, K.-B.; Moehl, T.; Marchioro, A.; Moon, S.-J.; Humphry-Baker, R.; Yum, J.-H.; Moser, J. E.; Grätzel, M.; Park, N.-G. *Sci. Rep.* **2012**, *2*, 591.

(29) Liu, M.; Johnston, M. B.; Snaith, H. J. *Nature* **2013**, *501*, 395.

(30) Protesescu, L.; Yakunin, S.; Bodnarchuk, M. I.; Krieg, F.; Caputo, R.; Hendon, C. H.; Yang, R. X.; Walsh, A.; Kovalenko, M. V. *Nano Lett.* **2015**, *15*, 3692.

(31) Nedelcu, G.; Protesescu, L.; Yakunin, S.; Bodnarchuk, M. I.; Grotevent, M. J.; Kovalenko, M. V. *Nano Lett.* **2015**, *15*, 5635.

(32) Akkerman, Q. A.; D'Innocenzo, V.; Accornero, S.; Scarpellini, A.; Petrozza, A.; Prato, M.; Manna, L. *J. Am. Chem. Soc.* **2015**, *137*, 10276.

(33) Dong, Y.; Qiao, T.; Kim, D.; Parobek, D.; Rossi, D.; Son, D. H. *Nano Lett.* **2018**, *18*, 3716.

(34) Butkus, J.; Vashishtha, P.; Chen, K.; Gallaher, J. K.; Prasad, S. K. K.; Metin, D. Z.; Laufersky, G.; Gaston, N.; Halpert, J. E.; Hodgkiss, J. M. *Chem. Mater.* **2017**, *29*, 3644.

(35) Protesescu, L.; Yakunin, S.; Kumar, S.; Bar, J.; Bertolotti, F.; Masciocchi, N.; Guagliardi, A.; Grotevent, M.; Shorubalko, I.; Bodnarchuk, M. I.; Shih, C.-J.; Kovalenko, M. V. *ACS Nano* **2017**, *11*, 3119.

(36) Imran, M.; Caligiuri, V.; Wang, M.; Goldoni, L.; Prato, M.; Krahne, R.; De Trizio, L.; Manna, L. *J. Am. Chem. Soc.* **2018**, *140*, 2656.

(37) Kang, J.; Wang, L.-W. *J. Phys. Chem. Lett.* **2017**, *8*, 489.

(38) Kulbak, M.; Gupta, S.; Kedem, N.; Levine, I.; Bendikov, T.; Hodes, G.; Cahen, D. *J. Phys. Chem. Lett.* **2016**, *7*, 167.

(39) Christians, J. A.; Miranda Herrera, P. A.; Kamat, P. V. *J. Am. Chem. Soc.* **2015**, *137*, 1530.

(40) Leyden, M. R.; Lee, M. V.; Raga, S. R.; Qi, Y. *J. Mater. Chem. A* **2015**, *3*, 16097.

(41) Akkerman, Q. A.; Motti, S. G.; Srimath Kandada, A. R.; Mosconi, E.; DInnocenzo, V.; Bertoni, G.; Marras, S.; Kamino, B. A.; Miranda, L.; De Angelis, F.; Petrozza, A.; Prato, M.; Manna, L. *J. Am. Chem. Soc.* **2016**, *138*, 1010.

(42) Sun, S.; Yuan, D.; Xu, Y.; Wang, A.; Deng, Z. *ACS Nano* **2016**, *10*, 3648.

(43) Pan, A.; He, B.; Fan, X.; Liu, Z.; Urban, J. J.; Alivisatos, A. P.; He, L.; Liu, Y. *ACS Nano* **2016**, *10*, 7943.

(44) Yakunin, S.; Protesescu, L.; Krieg, F.; Bodnarchuk, M. I.; Nedelcu, G.; Humer, M.; De Luca, G.; Fiebig, M.; Heiss, W.; Kovalenko, M. V. *Nat. Commun.* **2015**, *6*, 8056.

(45) Song, J.; Li, J.; Li, X.; Xu, L.; Dong, Y.; Zeng, H. *Adv. Mater.* **2015**, *27*, 7162.

(46) Park, Y.-S.; Guo, S.; Makarov, N. S.; Klimov, V. I. *ACS Nano* **2015**, *9*, 10386.

(47) Yettapu, G. R.; Talukdar, D.; Sarkar, S.; Swarnkar, A.; Nag, A.; Ghosh, P.; Mandal, P. *Nano Lett.* **2016**, *16*, 4838.

(48) Pan, J.; Shang, Y.; Yin, J.; De Bastiani, M.; Peng, W.; Dursun, I.; Sinatra, L.; El-Zohry, A. M.; Hedhili, M. N.; Emwas, A.-H.; Mohammed, O. F.; Ning, Z.; Bakr, O. M. *J. Am. Chem. Soc.* **2018**, *140*, 562.

(49) Liu, F.; Zhang, Y.; Ding, C.; Kobayashi, S.; Izuishi, T.; Nakazawa, N.; Toyoda, T.; Ohta, T.; Hayase, S.; Minemoto, T.; Yoshino, K.; Dai, S.; Shen, Q. *ACS Nano* **2017**, *11*, 10373.

(50) Koscher, B. A.; Swabeck, J. K.; Bronstein, N. D.; Alivisatos, A. P. *J. Am. Chem. Soc.* **2017**, *139*, 6566.

(51) Di Stasio, F.; Christodoulou, S.; Huo, N.; Konstantatos, G. *Chem. Mater.* **2017**, *29*, 7663.

(52) Nenon, D. P.; Pressler, K.; Kang, J.; Koscher, B. A.; Olshansky, J. H.; Osowiecki, W. T.; Koc, M. A.; Wang, L.-W.; Alivisatos, A. P. *J. Am. Chem. Soc.* **2018**, *140*, 17760.

(53) Mondal, N.; De, A.; Samanta, A. *ACS Energy Lett.* **2018**, *4*, 32.

(54) Ahmed, T.; Seth, S.; Samanta, A. *Chem. Mater.* **2018**, *30*, 3633.

(55) Saidaminov, M. I.; Almutlaq, J.; Sarmah, S.; Dursun, I.; Zhumekenov, A. A.; Begum, R.; Pan, J.; Cho, N.; Mohammed, O. F.; Bakr, O. M. *ACS Energy Lett.* **2016**, *1*, 840.

(56) Akkerman, Q. A.; Park, S.; Radicchi, E.; Nunzi, F.; Mosconi, E.; Angelis, F. D.; Bresci, R.; Rastogi, P.; Prato, M.; Manna, L. *Nano Lett.* **2017**, *17*, 1924.

(57) Seth, S.; Samanta, A. *J. Phys. Chem. Lett.* **2018**, *9*, 176.

(58) Liu, Z.; Bekenstein, Y.; Ye, X.; Nguyen, S. C.; Swabeck, J.; Zhang, D.; Lee, S.-T.; Yang, P.; Ma, W.; Alivisatos, A. P. *J. Am. Chem. Soc* **2017**, *139*, 5309−5312.

(59) Wu, L.; Hu, H.; Xu, Y.; Jiang, S.; Chen, M.; Zhong, Q.; Yang, D.; Liu, Q.; Zhao, Y.; Sun, B.; al, e. *Nano Lett.* **2017**, *17*, 5799−5804.

(60) Palazon, F.; Almeida, G.; Akkerman, Q. A.; Trizio, L. D.; Dang, Z.; Prato, M.; Manna, L. *Chem. Mater.* **2017**, *29*, 4167−4171.

(61) Palazon, F.; Urso, C.; Trizio, L. D.; Akkerman, Q.; Marras, S.; Locardi, F.; Nelli, I.; Ferretti, M.; Prato, M.; Manna, L. *ACS Energy Lett.* **2017**, *2*, 2445.

(62) Bastiani, M. D.; Dursun, I.; Zhang, Y.; Alshankiti, B. A.; Miao, X.-H.; Yin, J.; Yengel, E.; Alarousu, E.; Turedi, B.; Almutlaq, J. M.; al., e. *Chem. Mater.* **2017**, *29*, 7108.

(63) Zhang, Y.; Saidaminov, M. I.; Dursun, I.; Yang, H.; Murali, B.; Alarousu, E.; Yengel, E.; Alshankiti, B. A.; Bakr, O. M.; Mohammed, O. F. *J. Phys. Chem. Lett.* **2017**, *8*, 961.

(64) Cha, J.-H.; Han, J. H.; Yin, W.; Park, C.; Park, Y.; Ahn, T. K.; Cho, J. H.; Jung, D.-Y. *J. Phys. Chem. Lett.* **2017**, *8*, 565−570.

(65) Chen, D.; Wan, Z.; Chen, X.; Yuan, Y.; Zhong, J. *J. Mater. Chem. C* **2016**, *4*, 10646.

(66) Rakita, Y.; Kedem, N.; Gupta, S.; Sadhanala, A.; Kalchenko, V.; Böhm, M. L.; Kulbak, M.; Friend, R. H.; Cahen, D.; Hodes, G. *Cryst. Growth Des.* **2016**, *16*, 5717−5725.

(67) Yang, H.; Zhang, Y.; Pan, J.; Yin, J.; Bakr, O. M.; Mohammed, O. F. *Chem. Mater.* **2017**, DOI: 10.1021/acs.chemmater.7b04161.

(68) Yin, J.; Zhang, Y.; Bruno, A.; Soci, C.; Bakr, O. M.; Bredas, J.-L.; Mohammed, O. F. *ACS Energy Lett.* **2017**, *2*, 2805.

(69) Yin, J.; Yang, H.; Song, K.; El-Zohry, A. M.; Han, Y.; Bakr, O. M.; Bredas, J.-L.; Mohammed, O. F. *J. Phys. Chem. Lett.* **2018**, *9*, 5490.

(70) Cichos, F.; von Borczyskowski, C.; Orrit, M. *Curr. Opin. in Colloid & Interface Sci.* **2007**, *12*, 272.

(71) Zondervan, R.; Kulzer, F.; Orlinskii, S. B.; Orrit, M. *J. Phys. Chem. A* **2003**, *107*, 6770.

(72) Verberk, R.; van Oijen, A. M.; Orrit, M. *Physical Review B* **2002**, *66*, 233202.
(73) Frantsuzov, P. A.; Marcus, R. A. *Phys. Rev. B* **2005**, *72*, 155321.
(74) Frantsuzov, P. A.; Volkan-Kacso, S.; Janko, B. *Phys. Rev. Lett.* **2009**, *103*, 207402.
(75) Nirmal, M.; Dabbousi, B. O.; Bawendi, M. G.; Macklin, J. J.; Trautman, J. K.; Harris, T. D.; Brus, L. E. *Nature* **1996**, *383*, 802.
(76) Jha, P. P.; Guyot-Sionnest, P. *ACS Nano* **2009**, *3*, 1011.
(77) Wang, L.-W.; Califano, M.; Zunger, A.; Franceschetti, A. *Phys. Rev. Lett.* **2003**, *91*, 056404.
(78) Kuno, M.; Fromm, D. P.; Hamann, H. F.; Gallagher, A.; Nesbitt, D. J. *J. Chem. Phys.* **2001**, *115*, 1028.
(79) Jau, T.; Marcus, R. A. *J. Chem. Phys.* **2005**, *123*, 054704.
(80) Shimizu, K. T.; Neuhauser, R. G.; Leatherdale, C. A.; Empedocles, S. A.; Woo, W. K.; Bawendi, M. G. *Phys. Rev. B* **2001**, *63*, 205316.
(81) Tang, J.; Marcus, R. A. *Phys. Rev. Lett.* **2005**, *95*, 107401.
(82) Kuno, M.; Fromm, D. P.; Johnson, S. T.; Gallagher, A.; Nesbitt, D. J. *Phys. Rev. B* **2003**, *67*, 125304.
(83) Zhao, J.; Nair, G.; Fisher, B. R.; Bawendi, M. G. *Phys. Rev. Lett.* **2010**, *104*, 157403.
(84) Rosen, S.; Schwartz, O.; Oron, D. *Phys. Rev. Lett.* **2010**, *104*, 157404.
(85) Zhang, K.; Chang, H.; Fu, A.; Alivisatos, A. P.; Yang, H. *Nano Lett.* **2006**, *6*, 843.
(86) Yuan, G.; Gomez, D. E.; Kirkwood, N.; Boldt, K.; Mulvaney, P. *ACS Nano* **2018**, *12*, 3397.
(87) Hu, F.; Yin, C.; Zhang, H.; Sun, C.; Yu, W. W.; Zhang, C.; Wang, X.; Zhang, Y.; Xiao, M. *Nano Lett.* **2016**, *16*, 6425.
(88) Yarita, N.; Tahara, H.; Ihara, T.; Kawawaki, T.; Sato, R.; Saruyama, M.; Teranishi, T.; Kanemitsu, Y. *J. Phys. Chem. Lett.* **2017**, *8*, 1413.
(89) Li, B.; Huang, H.; Zhang, G.; Yang, C.; Guo, W.; Chen, R.; Qin, C.; Gao, Y.; Biju, V. P.; Rogach, A. L.; Xiao, L.; Jia, S. *J. Phys. Chem. Lett.* **2018**, *9*, 6934.
(90) Yuan, G.; Ritchie, C.; Ritter, M.; Murphy, S.; Gomez, D. E.; Mulvaney, P. *J. Phys. Chem. C* **2018**, *122*, 13407.
(91) Halder, A.; Pathoor, N.; Chowdhury, A.; Sarkar, S. K. *J. Phys. Chem. C* **2018**, *122*, 15133.
(92) Merdasa, A.; Tian, Y.; Camacho, R.; Dobrovolsky, A.; Debroye, E.; Unger, E. L.; Hofkens, J.; Sundstrom, V.; Scheblykin, I. G. *ACS Nano* **2017**, *11*, 5391.
(93) Yuan, H.; Debroye, E.; Caliandro, G.; Janssen, K. P. F.; van Loon, J.; Kirschhock, C. E. A.; Martens, J. A.; Hofkens, J.; Roeffaers, M. B. J. *ACS Omega* **2016**, *1*, 148.
(94) Pathoor, N.; Halder, A.; Mukherjee, A.; Mahato, J.; Sarkar, S. K.; Chowdhury, A. *Angew. Chem. Int. Ed.* **2018**, *57*, 11603.

Chapter 2

Materials, Instrumentation and Methods

This chapter mainly presents the details of preparation and characterization of the various materials, experimental setups and various methodologies. Briefly, sources of the chemicals used, synthesis procedure and purification of different materials, specifically the perovskites and perovskite-related nano- and microcrystals are detailed. Methods of sample preparation for spectral measurements and experiments involving the microscopy techniques have been described. The instrumentation details, especially time-correlated single photon counting setup and time-resolved confocal fluorescence microscope setup have been discussed in detail. Theory and methods of data analysis of different single particle spectroscopic techniques are explained. Information on various other instruments and methodologies used for structural and optical characterization such as electron microscopy, X-ray diffraction, fluorescence quantum yield measurements are also provided.

2.1 Materials.

Laser grade organic dyes like Coumarin 153 (C153) and Rhodamine 6G were purchased from Estman Kodak and Loba Chemie, respectively. Lead chloride (99.9%, trace metal basis), lead bromide (>98%), lead iodide (99.9% trace metals basis), cesium carbonate (99.9%, trace metal basis), cesium bromide (99.999%, trace metals basis), oleic acid (OA), oleylamine (OLA) and octadecene (ODE, 90%, technical grade) were purchased from Sigma-Aldrich. Cetyltrimethylammonium bromide (CTAB) was purchased from Aldrich Chemicals. Dimethyl formamide (DMF), dimethyl sulfoxide (DMSO) were purchase from Merck. All these chemical were used as received. Ethyl acetate, chloroform, toluene, hexane, acetonitrile, acetone of analytical grade were purchased from Finar and redistilled prior to use. Drying agents such as calcium chloride, calcium hydride, metallic sodium were used for solvent purification.

2.2 Synthesis of perovskite and perovskite-related materials.

2.2.1. $CsPbX_3$ nanocrystals.

2.2.1.1. Hot-injection method.

$CsPbX_3$ (X= Cl, Br, I) perovskite nanocrystals were synthesized at high temperatures (150-200 °C) in inert condition following a reported procedure.[1] Briefly, the injecting precursor, Cs-oleate, was prepared separately by mixing 0.10175 g Cs_2CO_3, 0.3125 mL OA and 5 mL ODE in a 50 mL double-necked round-bottom (RB) flux and keeping it in vacuum for 1 hour at 120°C. Then the temperature was raised to 160 °C for complete solubilisation of the solid material to form a clear solution of Cesium oleate (Cs-oleate). Before injection, Cs-oleate solution was heated to 100 °C under N_2 atmosphere to avoid precipitation at room temperature.

In another 50 mL double-necked RB flask, 0.188 mmol PbX_2 and 5 mL ODE were dried for 1 hour at 120 °C. Previously dried OA and OLA (0.5 mL each) were injected into the flask under N_2 atmosphere at 120 °C. Temperature was raised to 150-180 °C after complete solubilisation of the PbX_2 salts. Later 0.4 mL of heated Cs-oleate solution was quickly injected into the flask and the reaction mixture was cooled by ice-water bath after 5 seconds of the reaction. Reaction mixture was centrifuged for 6 minutes at 6000 rpm to

discard unreacted precursors as supernatant. Precipitated NCs were dispersed in ODE, hexane or toluene after washing twice with the same solvent.

2.2.1.2. Anti-solvent precipitation method.

Principle of this method is poor solvent (anti-solvent) induced nucleation of the precursors dissolved in good solvent. Unlike the hot injection method, this is a room temperature and open atmosphere process. Suitable ligands and anti-solvent determines the shape, size and optical properties of the NC. In the first step, a mixture of $PbBr_2$ and CsBr in 1:1 molar ratio were dissolved in polar DMF (4 mL) or a mixture of DMF and DMSO. Typically, 200 µL of the precursor solution was added into a vigorously stirred reaction media containing OLA (20–70 µL), OA (0.2–0.5 mL) and a larger amount (4 mL) of a less polar solvent (anti-solvent). Nucleation of the $CsPbBr_3$ NCs happened immediately after the addition. One can control the morphologies by varying the anti-solvent (e.g. ethyl acetate, toluene, and chloroform), quantity of the capping ligands (OLA and OA) and reaction time. This method is very facile for $CsPbBr_3$ NCs and can be used efficiently for gram scale synthesis. NCs constituting other halogens can easily be prepared by employing halide exchange technique.[2]

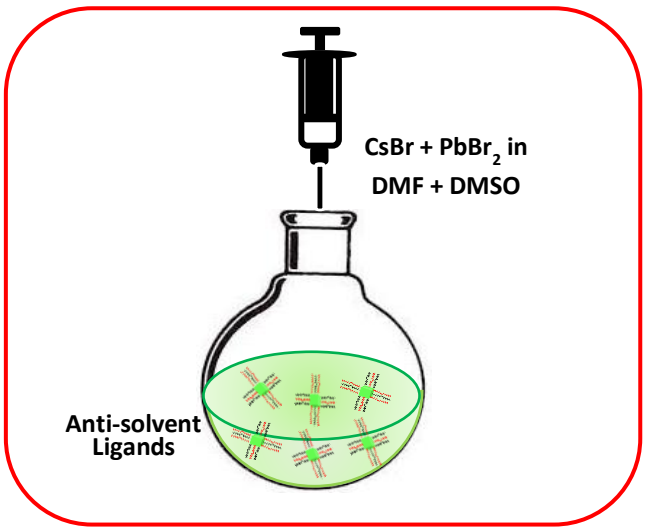

Figure 2.1. Schematic representation of NC synthesis by anti-solvent precipitation method.

2.2.2. Perovskite-related material, Cs_4PbBr_6.

2.2.2.1. Nonluminescent Cs_4PbBr_6 NCs.

NCs of this kind were synthesized following a reported procedure.[3] 0.0367 gm $PbBr_2$, 5 mL ODE, 0.2 mL oleic acid and 1.5 mL oleylamine were mixed in a 100 mL double-necked flask and heated to 130 °C under vacuum until the solution became clear. Temperature of the solution was then decreased to 80 °C and 0.36 mL of Cs-oleate solution was added quickly. After 30 seconds, the solution became turbid indicating the formation of NCs. Solution was quickly cooled down under water stream and centrifuged to separate the NCs. The solid was washed repeatedly and finally dissolved in toluene for measurements.

2.2.2.2. Luminescent Cs_4PbBr_6 NCs.

Cs_4PbBr_6 NCs were prepared following anti-solvent precipitation method.[4] Firstly, 0.011 gm $PbBr_2$ was dissolved in 1 mL of DMF followed by addition of 20 µL of HBr, 0.1 mL of oleic acid and 0.05 mL of oleylamine. In a 50 mL round-bottom flask, 10 mL hexane, 5 mL oleic acid and 0.2 mL of as-prepared Cs-oleate solution were added. Previously prepared $PbBr_2$ solution was then quickly added into the RB in vigorous stirring condition. The solution immediately turned greenish white. Then it was centrifuged and washed for spectroscopic studies.

2.2.2.3. Luminescent Cs_4PbBr_6 microdisks.

Microdisks of Cs_4PbBr_6 were synthesized following anti-solvent precipitation method at room temperature and open atmosphere by replacing the conventional capping ligands with CTAB. In a typical synthesis, $PbBr_2$ (0.1 mM) and CsBr (0.1 mM) were dissolved in 3 mL of DMF. CTAB of desired amount (0.05-0.2 mM) was dissolved into the solution by sonication. This precursor solution was transferred to a 50 mL round bottom flask and 0.75 mL of toluene was added into it under vigorously stirring condition. After 5-10 minutes, when the solution changed its color to greenish yellow, the resulting solution was centrifuged at 7000 rpm for 5 minutes. Supernatant containing unreacted precursors is discarded. Precipitated microcrystals were washed thrice with toluene. The film of Cs_4PbBr_6 microdisks was prepared by drop casting the toluene dispersion.

2.3. Instrumentation.

2.3.1. Time-correlated single photon counting fluorimeter.

2.3.1.1. Experimental setup.

Time-resolved PL measurements were performed using a time-correlated single photon counting (TCSPC) fluorimeter (Horiba Jobin Yvon IBH). The schematic diagram of the experimental setup is shown in Figure 2.2. The experiment starts with simultaneous excitation of the sample and sending a signal to the electronics (Scheme 2.4). Constant fraction discriminator (CFD) receives the excitation signal and accurately measures the arrival time of the photon and then diverts the signal towards the time to amplitude convertor (TAC) to start the voltage ramp. The second channel (CFD) which accurately measures the arrival time of the emitted photon makes TAC to stop the voltage ramp. The voltage ramp developed by TAC is proportional to the time difference between the excitation and emission signals. Programmable gain amplifier (PGA) amplifies the resultant voltage, which is converted later to a numerical value by analog-to-digital convertor (ADC). This numerical value representing the photon detection time is stored as a single event. The above process is repeated several times to construct the histogram of fluorescence intensity over time.

In the presented studies, PicoBrite (405 nm, 1 MHz repetition rate, and 60 ps FWHM) was used as the excitation source and an MCP photomultiplier tube (PMT, Hamamatsu R3809U-50) as the detector. The instrument response function (IRF) was recorded by placing a dilute scatterer solution (Ludox) inside the sample chamber.

2.3.1.2. Data analysis.

The lifetimes of the samples were estimated from the PL decay profiles and the instrument response function using a nonlinear least-square iterative fitting procedure (decay analysis software IBH DAS6, Version 2.2). In general, the PL decay of the excited molecules can be expressed as

$$I(t) = I_0 e^{-t/\tau} \qquad (2.1)$$

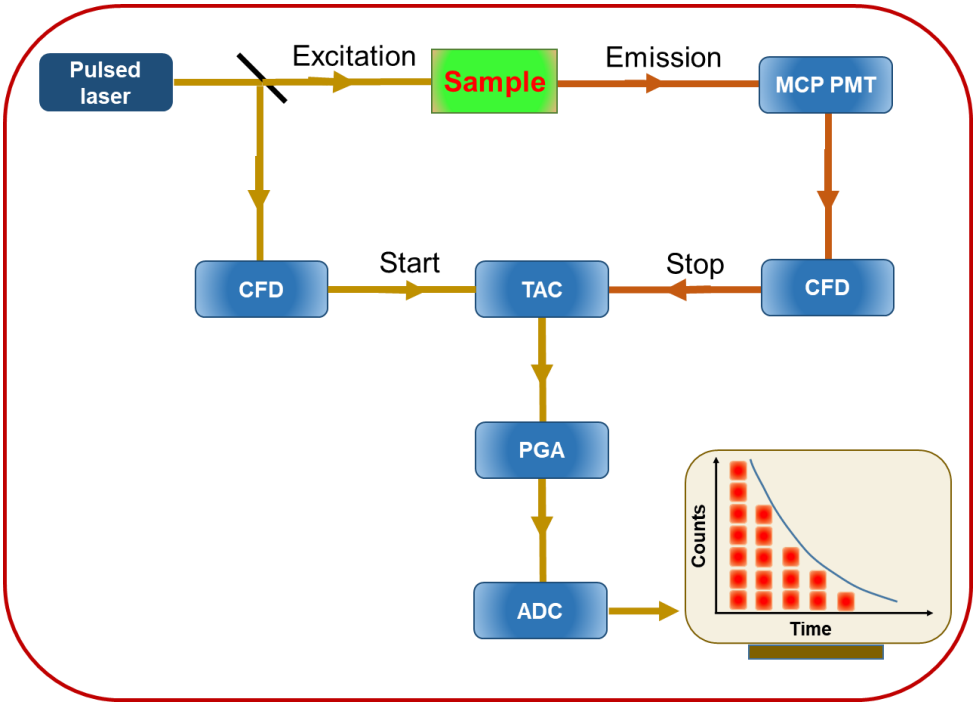

Figure 2.2. Schematic representation of the TCSPC setup.

Where, I_0 is the intensity at t = 0 and τ is the lifetime and is expressed as $\tau = 1/(k_r + k_{nr})$ with k_r and k_{nr} are the radiative and non-radiative decay rate constants, respectively. In case of multi-exponential decay, I(t) is expressed as

$$I(t) = \sum_{i=1}^{n} a_i e^{-t/\tau} \qquad (2.2)$$

Where, a_i and τ_i represent the amplitude and lifetime of the i^{th} component, respectively. The quality of the fit was judged by careful examination of the plot of residuals versus time and ensuring a chi-square value of ≤ 1.2.

2.3.2. Time-resolved confocal fluorescence facility.

2.3.2.1. Experimental setup.

Optical microscopes, being a tool to magnify the images of micro objects, are in constant development to enhance the resolution and contrast. Overall resolution is determined by the excitation wavelength and numerical aperture of the objective and it cannot be better than the half of the excitation wavelength. Time resolution of optical

microscopy can be modulated depending on the excitation source and configuration of the microscope. A confocal fluorescence microscope (CFM) is particularly important when higher temporal resolution (upto few ns) is required with high signal to noise ratio (SNR). Basic difference of a CFM with a wide field microscope is that the former employs multiple pinholes in the detection path and allow only the tightly focused light which results in aberration free images. A schematic diagram of the confocal fluorescence microscope is shown in Figure 2.3.

For our measurements, we have used MicroTime 200 (PicoQuant) model of time-resolved CFM. Pulsed picosecond diode lasers of excitation wavelength of 405 nm, 485 nm and 640 nm (mostly used 405 nm) with tunable repetition rates from 1-80 MHz were used in this setup as the excitation source. The output of the laser beam was guided to the sample placed on a movable stage of an inverted microscope (Olympus IX71) through polarization maintained optical fiber, dichroic mirror, and water immersion objective (UPlanSApo, NA =1.2, 60X) as the main optical components. A charged coupled device (CCD) detector was used to monitor the position of the focal point on the sample. Part of the emitted isotropic PL will pass through the dichroic mirror and a long pass filter eliminates any interfering excitation photon. A 50 μm pinhole assures collection of only tightly focused photons which were collected in single photon avalanche photodiode (SPAD). Depending on the measurement technique single or multiple SPAD detectors can be used. A piezo scanning stage is mounted in the microscope body to control the sample position. Micro-meter screws for manual positioning or software controlled piezo-scanner can be used for precise and repeatable XY scanning and Z –positioning of the sample. At a time 100 μm × 100 μm area can be imaged employing raster scanning method. An important component of this CFM is the standalone TCSPC module, PicoHarp 300 which offers advanced and versatile Time-Tagged-Time-Resolved (TTTR) data acquisition mode.

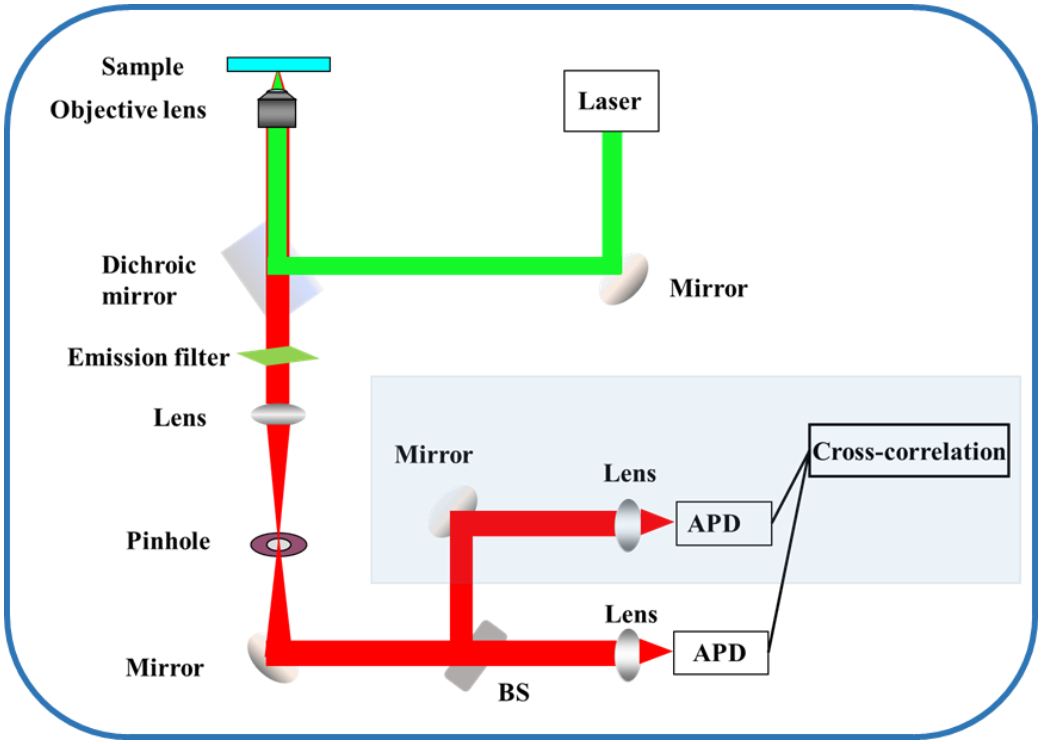

Figure 2.3. Basic configuration of the confocal fluorescence microscope.

2.3.2.2. Data acquisition techniques, theory and analysis.

When single fluorophore species are the topic of research, not only the fast PL lifetime (ps - ns) but also the slower PL dynamics (μs – ms) is of major interest. Short lifetimes were measured using TCSPC technique, as discussed in the earlier section. However, slower intensity dynamics cannot be obtained from the conventional histograms of the TCSPC and requires time-tag method. When both the processes run in parallel, it is called time-tagged-time-resolved or TTTR method.[9] A schematic representation of the concept of TTTR mode is shown below (Figure 2.4). In principle, faster time as in TCSPC is obtained by recording the time difference between the laser pulse and arrival of the fluorescence photons. In addition a parallel timing is done on each photon with respect to the beginning (time-tag) of the measurement to get the slower dynamics.

State of the art CFM with TTTR data acquisition mode is used to design or employ several spectroscopic techniques having single molecule/particle resolution. As for

example, fluorescence correlation spectroscopy (FCS), single-fluorophore PL intermittency, PL imaging, single-molecule Forster resonance energy transfer, single-molecule anisotropy are of major interest. In this dissertation, we have employed the first three techniques to reveal the PL properties and carrier dynamics of the perovskite materials.

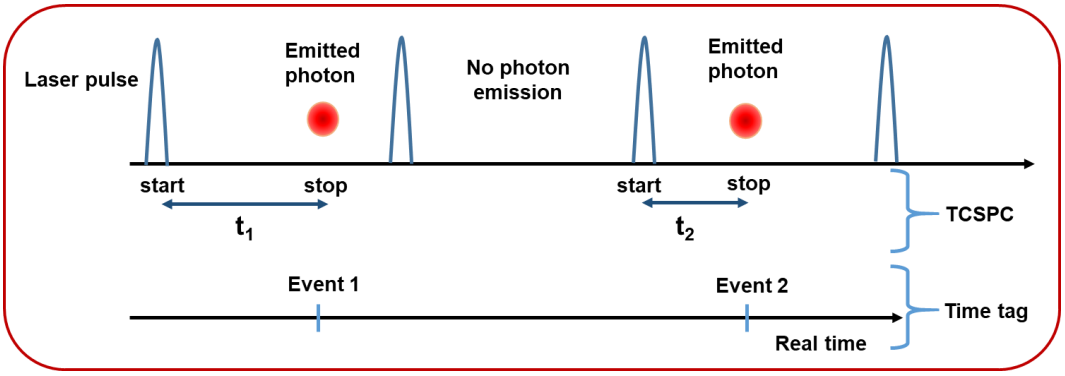

Figure 2.4. Concept of the TTTR mode data acquisition.

2.3.2.2.1. Fluorescence correlation spectroscopy (FCS).

FCS is a noninvasive PL-fluctuation based technique used to obtain information on the dynamic processes responsible for the fluctuation.[5-7] It is a solution-based technique, where fluorophores diffuse freely through the detection volume and generate signal fluctuations due to diffusion and other processes which are faster than diffusion. To generate sharp fluctuation, the number of species has to be small as concentrated sample produces nearly constant average signal throughout the measurement time. Generally, few nanomolar solution is used for the measurement, which gives nearly single molecule sensitivity depending on the size of the observation volume. Signals are then correlated to obtain the correlation curves. Since, FCS is based on diffusion which is a random process, the occupancy of the fluorescent species in the observation volume is described by Poisson statistics. Experimental setup for this technique is same as shown in Figure 2.3. To increase SNR and achieve better temporal resolution signals are generally cross-correlated.

Figure 2.5 shows the diffusion of the fluorophore through the ellipsoidal observation volume and PL intensity fluctuation. The autocorrelation function is defined

as the product of the fluctuation of PL intensity at time t, $\delta F(t)$ and t+τ, $\delta F(t+\tau)$ and averaged over a large number of measurements. The autocorrelation function, $G(\tau)$ normalized by the square of average fluorescence intensity ($\langle F(t)\rangle$) is given by the following Equation,

$$G(\tau)=\frac{\langle \delta F(t)\delta F(t+\tau)\rangle}{\langle F(t)\rangle^2} \tag{2.3}$$

Here, $\delta F(t)$ and $\delta F(t+\tau)$ are defined as

$$\delta F(t)=F(t)-\langle F(t)\rangle \text{ and } \delta F(t+\tau)=F(t+\tau)-\langle F(t)\rangle \tag{2.4}$$

Autocorrelation function for pure diffusion in three dimension can be written as

$$G(\tau)=\frac{1}{N}\left(1+\frac{\tau}{\tau_D}\right)^{-1}\left(1+\frac{\tau}{\kappa^2\tau_D}\right)^{-\frac{1}{2}} \tag{2.5}$$

Where, <N> is the average number of fluorophore in the observation volume, τ_D is the diffusion time, κ (= ω_{xy}^2/ω_z^2) is the structure parameter of the observation volume. Details of the derivation of this equation (2.5) can be found elsewhere.[7, 8] From equation 2.5 diffusion coefficient (D) of the fluorescent species can be derived as

$$D=\frac{\omega_{xy}^2}{4\tau_D} \tag{2.6}$$

The correlation function G(τ), in equation 2.5 is based on the fact that only diffusion contributes to the fluorescence fluctuation. However, this may not be the scenario always. Fluorophores may undergo reversible fluorescence ON and OFF transitions during their stay in the observation volume.

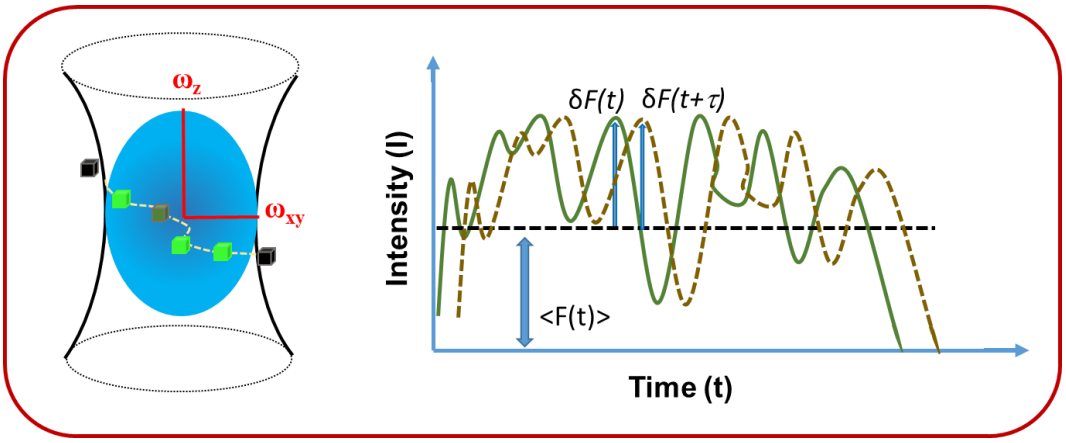

Figure 2.5. Diffusion of fluorophores through the effective observation volume of the CFM and the fluctuating PL signal.

There are several factors which can contribute to such fast fluctuation. For example, intersystem crossing in the excited dye molecules, charge carrier trapping in the defects of semiconductors, conformational change in the biomolecules, etc. In these cases, correlation function can be expressed as

$$G_{total}(\tau) = G_{diffusion}(\tau)G_{faster\ process}(\tau) \qquad (2.7)$$

Depending on the nature of the processes and factors controlling the fluctuation $G_{faster\ process}(\tau)$ can have different forms, which will be discussed in relevant portions of the subsequent chapters. As for example, autocorrelation curve that includes several faster processes responsible for PL fluctuation at their characteristic time scales are shown in Figure 2.6.

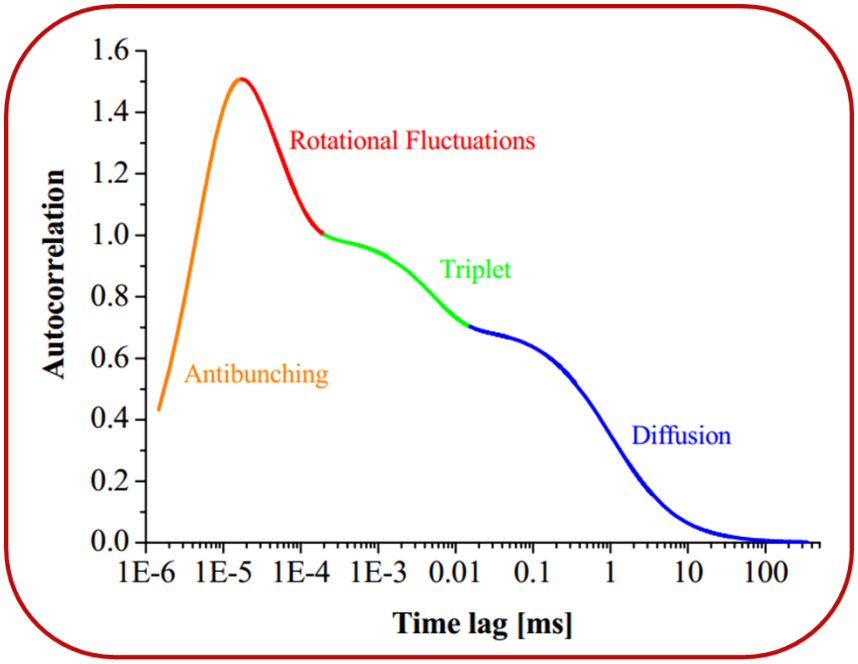

Figure 2.6. Typical autocorrelation curve showing several faster process indicating their timescales. (Adapted from reference 8)

2.3.2.2.2. Determination of observation volume.

The knowledge of exact size and shape of the observation volume is very crucial for the measurements as absolute diffusion coefficients and concentration depend on the structure parameters. The diffusion time (τ_D) depends on the transverse radius (ω_{xy}) of the observation volume (Equation 2.6). Size and elongation of the observation volume are determined by calibration measurement on a system with known diffusion coefficient. In the present study, calibration was done using aqueous solution of rhodamine 6G with known diffusion coefficients of 426 µm2/s.[10] The estimated observation volume was found to ~0.43 fL for 405 nm excitation.

2.3.2.2.3. PL intensity time-trace.

PL characteristics of a single molecule or particle can be studied by continuous excitation of the fluorophore which generates PL trajectory as a function of real time. In general, almost all fluorophores show random fluctuation in their PL with time as demonstrated in Figure 2.7. This behavior is commonly termed as PL intermittency or blinking and can occur over a wide range of time starting from few milliseconds to hundreds of seconds. To increase the SNR, photon arrival times are averaged in time bins which generally varies from 1-100 ms. Statistical and dynamical analysis and interpretation of this time-trace provides essential information about all the pertaining radiative and nonradiative processes in excited fluorophore.

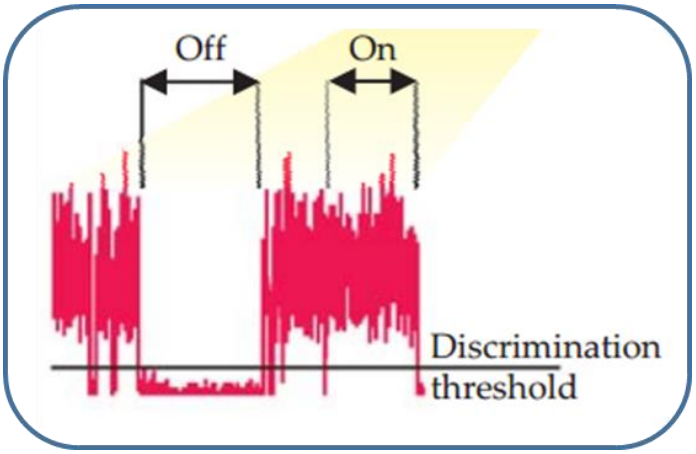

Figure 2.7. PL trajectory of a single fluorophore (Adapted from reference 11)

A very dilute solution (picomolar) of the fluorophores is drop-casted on a clean coverslip and dried to form the sample film. Sometimes, to obtain a better film with clear spatial separation of individual fluorophores, sample solution is prepared by adding some amount of non-interacting polymers. In this dissertation, we will limit ourselves to discussing the PL intermittency of the semiconductor NCs. To obtain kinetic information of the charge recombination in a NC, PL trajectory is classified into two segments i.e. higher intensity ON state and lower intensity OFF state, by setting a discrimination threshold (Figure 2.7). the probability distribution ($P(t)$) of these two states can be obtained from equation

$$P_i(t) = \frac{N_i(t)}{N_{total}} \times \frac{1}{\Delta t_{avg}} \qquad \text{(i = on } or \text{ off)} \qquad (2.8)$$

Where, N(t) is the number of ON and OFF events, N_{total} is the total number of ON and OFF events and Δt_{avg} is the average time between the nearest neighbor event bins. Plot of probability distribution versus ON or OFF time provides the information about the kinetics of the charge carrier recombination.

On the other hand, TCSPC lifetime of different ON and OFF events can be used to get the dynamic information of the carriers. This method becomes very informative when intensity levels are not clearly separable by setting a threshold or there are several intensity levels. Intensity and lifetime correlation of the trajectory provides information on the possible recombination process and their timescales. Details of this analysis are presented while discussing the results.

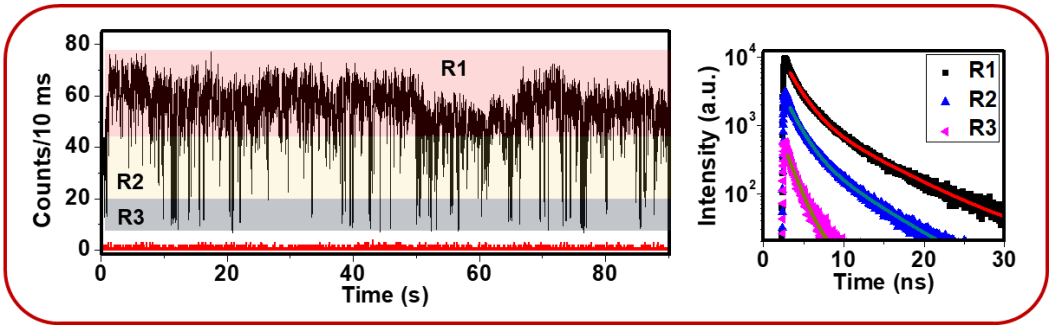

Figure 2.8. PL trajectory of a single fluorophore and decay behavior of the different intensity regions marked.

2.3.2.2.4. PL lifetime imaging (FLIM).

Simple fluorescence intensity imaging microscopy can be extended to fluorescence lifetime imaging by taking advantage of the TTTR mode. A piezo scanner is used for capturing a 2D image of the sample by scanning in the XY direction with certain speed. Here, spatial distribution of the photons is also recorded along with the TCSPC data by incorporating additional line and frame markers in the TTTR mode (Figure 2.4). Lifetimes obtained from the arrived photons in each pixel is used to construct the PL lifetime image. This imaging technique has become very important in the field of material

science. A direct correlation between structure or morphology, PL intensity and lifetime can be drawn from the images, which in effect provide information about the carrier dynamics and influence of the nonradiative recombination.

2.3.3. Other experimental techniques for materials characterization.

For measuring the shape, size and selected area electron diffraction pattern of the synthesized nano- and micro-crystals, Tecnai G2 FE1 F12 transmission electron microscope (TEM) operating at an accelerating voltage of 200 kV were used. High resolution TEM (HRTEM) images were also obtained from the same instrument. Lattice spacing and fast Fourier transform pattern of the perovskite and perovskite related crystals were estimated from the HRTEM images using the Gatan Digital Micrograph software. Field emission-scanning electron microscope (FESEM, Ultra 55 Carl Zeiss instrument) was used to get the structure and surface morphology of the synthesized materials. Elemental composition analysis and mapping were done using energy-dispersive X-ray spectrometer (EDX) coupled with the same FESEM instrument. Powder X-ray diffraction (PXRD) patterns of the synthesized crystals were recorded on a Bruker D8 X-ray diffractometer [λ (Cu-Kα) = 1.54 Å]. All the steady-state absorption and PL spectra were recorded in a UV-vis spectrophotometer (Cary 100, Varian) and (FluoroLog-3, Horiba Jobin Yvon) spectrofluorimeter respectively.

2.3.4. Measurement of PL quantum yield (QY).

The PL QYs of the synthesized perovskite NCs and perovskite related microcrystals were estimated using the following equation.

$$QY(S) = QY_R \times (I_S/I_R) \times (OD_R/OD_S) \times (n_S^2/n_R^2)$$

Where I represent the integrated area under the curve of the PL spectrum, OD is the optical density at the excitation wavelength and n is the refractive index of the medium. The subscript S and R refer to sample and reference, respectively. Coumarin 153 in acetonitrile (PLQY = 0.56)[12] and rhodamine 6G in ethanol (0.95)[13] were used as a reference.

References

1. Protesescu, L.; Yakunin, S.; Bodnarchuk, M. I.; Krieg, F.; Caputo, R.; Hendon, C. H.; Yang, R. X.; Walsh, A.; Kovalenko, M. V., *Nano Lett.* **2015**, *15*, 3692-3696.
2. Akkerman, Q. A.; D'Innocenzo, V.; Accornero, S.; Scarpellini, A.; Petrozza, A.; Prato, M.; Manna, L. *J. Am. Chem. Soc.* **2015**, **137**, 10276−10281.
3. Akkerman Q. A.; Park, S.; Eros, R.; Nunzi, F.; Mosconi, E.; Angelis, F. D.; Brescia, R.; Rastogi, P.; Prato, M.; Manna, L. *Nano Lett.* **2017**, *17*, 1924–1930.
4. Zhang, Y.; Saidaminov, M. I.; Dursun, I.; Yang, H.; Murali, B.; Alarousu, E.; Yengel, E.; Alshankiti, B. A.; Bakr, O.M.; Mohammed, O.F. *J. Phys. Chem. Lett.*, **2017**, *8*, 961–965.
5. Magde, D.; Eison, E.; Webb, W. W. *Phys. Rev. Lett.* **1972**, *29*, 705.
6. Magde, D.; Eison, E.; Webb, W. W. *Bioplymers* **1974**, *13*, 29.
7. Schwille, P.; Haustein, E.; Fluorescence Correlation Spectroscopy: An introduction to its concepts and applications, *Biophysical text books online* **2004**, 1-33.
8. Lackowicz, J. R. Principles of Fluorescence Spectroscopy, *Third Edition, Springer, New York* **2006**.
9. Wahl, M.; Erdmann,R.; Lauritsen,K.; Rahn, H.J. *Proc.SPIE*, **1998**, *3259*,173-178
10. Kapusta, P. *Absolute Diffusion Coefficients: Compilation of Reference Data for FCS Calibration, PicoQuant GmbH* **2010**, *Rev 1*.
11. Stefani, F. D.; Hoogenboom, J. P.; Barkai, E. *Physics Today*, **2009**, *62*, 34.
12. Jones-II, G.; Jackson, W. R.; Choi, C.-Y.; Bergmerk, W. R. *J. Phys. Chem*. **1985**, *89*, 294.
13. Kubin, R. F. and A. N. Fletcher. *J. Luminescence* **1982**, 27, 455-462.

Chapter 3

Fluorescence Blinking and Photoactivation of All-Inorganic Perovskite Nanocrystals $CsPbBr_3$ and $CsPbBr_2I$

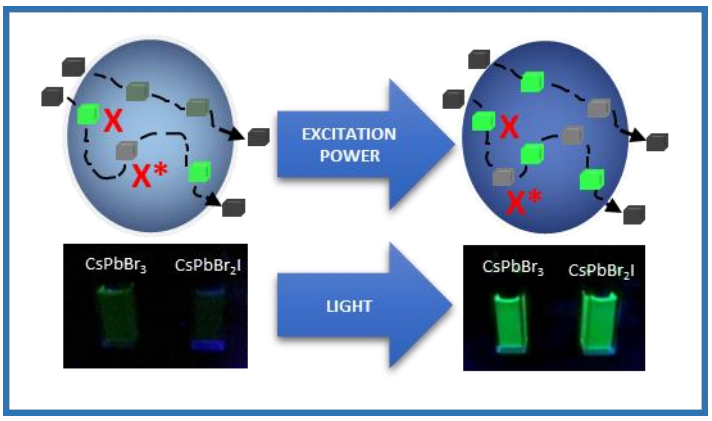

Abstract.

Study of the emission behavior of all-inorganic perovskite nanocrystals $CsPbBr_3$ and $CsPbBr_2I$ as a function of the excitation power employing fluorescence correlation spectroscopy and conventional techniques reveals fluorescence blinking in the microsecond time scale and photoinduced emission enhancement. The observation provides insight into the radiative and nonradiative deactivation pathways of these promising substances. Because both blinking and photoactivation processes are intimately linked to the charge separation efficiency and dynamics of the nanocrystals, these key findings are likely to be helpful in realizing the true potential of these substances in photovoltaic and optoelectronic applications.

3.1. Introduction

Metal halide perovskites are currently under intense investigations because of their potential application in solar cells and as light emitting diodes, photodetectors and lasers.[1-14] Even though the organo-metal halide perovskites (OMHP) are the ones currently being considered for these applications, all-inorganic cesium lead halide ($CsPbX_3$, X = Cl, Br, I or their mixtures) perovskite nanocrystals (NCs) are also rapidly emerging as promising alternatives in optoelectronic to multicolor biological imaging applications because of their broad absorption spectrum and narrow, tunable and intense emission (quantum yield, QY ~ 10-90%).[15-24]

The emission QY of the perovskite NCs depends highly on the synthetic condition and QY values ranging from 10% to 90% are reported.[15-17] Even though the $CsPbX_3$ NCs reported by Kovalenko and coworkers are highly fluorescent and are largely free from the mid band gap surface trap states,[17-19] a significant contribution of the trap states is expected in the case of less fluorescent NCs. The trap states can arise from intrinsic point defects in less emissive perovskite NCs[20-22] and/or surface defects.[23] These trap states, in particular, the mid-band ones, can act as nonradiative relaxation channels and reduce the luminescence efficiency.[23] In order to realize the potential of these all-inorganic $CsPbX_3$ NCs in photovoltaic[24-26] and optoelectronic devices,[16,19,27] an understanding of how the trap states and external factors such as illumination, temperature, electric field, etc. affect the electronic properties and excited state charge carrier dynamics of these NCs is essential. Herein, we report the first fluorescence correlation spectroscopy (FCS) study of all-inorganic $CsPbX_3$ NCs that sheds light into some of the above issues.

FCS is a non-invasive single molecule based sensitive technique, in which fluctuations of the fluorescence intensity in a small volume (~ 1 fL) is monitored to obtain information relating to the process responsible for fluctuation. This technique has recently been applied to understand the fluorescence intensity fluctuation of metal-chalcogenide quantum dots (QDs) in the microsecond time domain.[28-31] The present FCS study on $CsPbBr_3$ and $CsPbBr_2I$ in a nonpolar and non-interacting medium, 1-octadecene (ODE),[32] is undertaken considering that the fluorescence correlation curves can provide valuable information relating to the charge separation and recombination processes. Conventional steady state and time-resolved fluorescence measurements have also been performed to

supplement the FCS results. To the best of our knowledge, this FCS study reveals for the first time photoactivation and blinking kinetics of freely diffusing all-inorganic perovskite NCs in the ms-μs time-scale.

3.2. Results and Discussion

Colloidal $CsPbBr_3$ and $CsPbBr_2I$ NCs with oleic acid and oleylamine as capping ligands were synthesized following a reported procedure[17,19] with slight modification of the synthetic conditions (see Appendix I for details). The size of the as-synthesized NCs (10 – 12 nm, Figure AI.1, Appendix 1) was estimated from the TEM images and the individual constituents of the NCs were confirmed by energy dispersive X-ray (EDX) spectroscopic measurements (Figure AI.2, Appendix 1). A cubic crystal structure of $CsPbBr_3$ with 10 ± 2 nm edge length and a distorted structure of $CsPbBr_2I$ with 12 ± 3 nm edge length (Figure 3.1) was observed. Optical absorption and emission spectra of the two types of NCs are shown in Figure 3.1. The emission maximum (λ_{max}^{em}) appears at 509 and 528 nm for $CsPbBr_3$ and $CsPbBr_2I$, respectively. A higher λ_{max}^{em} value for $CsPbBr_2I$ is consistent with the literature.[15,17,18] Fluorescence QY of $CsPbBr_3$ and $CsPbBr_2I$ are measured to be ~40% and ~10%, respectively. A lower QY of $CsPbBr_2I$, which is

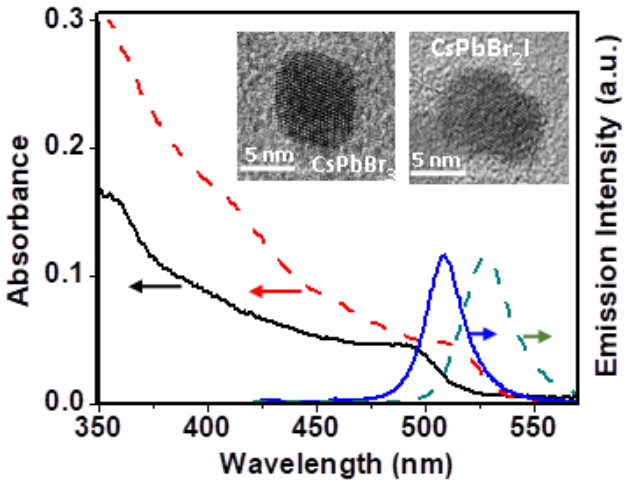

Figure 3.1: Optical absorption and emission spectra of $CsPbBr_3$ (continuous lines) and $CsPbBr_2I$ (dashed lines) in ODE. Inset depicts the TEM images of the single NCs.

consistent with the pioneering work of Kovalenko and coworkers,[17] is due to the trap states resulting from (large) iodine-induced distortion of the corner sharing [Pb(Br/I)$_6$] octahedra of the cubic CsPb(Br/I)$_3$ NCs and consequent distortion of the cubic crystal structure.

3.2.1. FCS theory and measurements

Figure 3.2 depicts the time dependence of fluorescence correlation data of 1.3 nM $CsPbBr_3$ and 0.5 nM $CsPbBr_2I$ NCs solutions[33] for different excitation power. The amplitude of correlation at time τ, G(τ), is given by[34]

$$G(\tau) = \frac{\langle \delta F(t) \delta F(t+\tau) \rangle}{\langle F(t) \rangle^2} \tag{3.1}$$

Where, $\langle F(t) \rangle$ is the average fluorescence intensity. $\delta F(t)$ and $\delta F(t+\tau)$ are the fluctuations in fluorescence intensity from the mean value at time t and t+τ respectively, and are expressed as

$$\delta F(t) = F(t) - \langle F(t) \rangle \text{ and } \delta F(t+\tau) = F(t+\tau) - \langle F(t) \rangle \tag{3.2}$$

The FCS data is fitted to a model [equn. (3.3)], which involves a diffusion component and a stretched exponential decay component. This widely accepted fitting model has been used previously for metal-chalcogenide quantum dots (QDs)[28-31,35] The fit quality to equn. (3.3) and a few other attempted models are provided as supporting information (Figure AI.3–AI.5, Appendix 1).

$$G(\tau) = \left[1 + \frac{T}{1-T}\exp\left(-\frac{\tau}{\tau_T}\right)^{\beta}\right] \frac{1}{N}\left(1+\frac{\tau}{\tau_D}\right)^{-1}\left(1+\frac{\tau}{\kappa^2\tau_D}\right)^{-\frac{1}{2}} \tag{3.3}$$

Where, N is the average number of NCs in the observation volume undergoing reversible fluorescence off-on transition, T is the off-state fraction, τ_T is the off-state relaxation or blinking time, τ_D is the time taken by the particle to diffuse through the observation

volume, β (0<β<1) is the stretching exponent representing the distribution of τ_T, and κ is the structure parameter of the observation volume.

Figure 3.2, which depicts the time dependent G(τ) values of the solutions of two perovskite NCs for various laser excitation power and the fits to equn. (3.3), reveals a sharp drop of the amplitude of correlation at zero time delay, G(0) with increasing power. The decrease in G(0) value is more drastic for $CsPbBr_2I$ compared to $CsPbBr_3$. For example, the G(0) value drops by a factor of 3.6 in the case of $CsPbBr_3$, whereas it decreases by a factor of 6.7 for $CsPbBr_2I$ for a change of excitation power from 2.5 to 30.0 μW (Table 3.1). In addition, a change in shape of the correlation curves is also observed with variation of excitation power. This is evident from the normalized fitted correlation curves shown in Figure 3.3. This change in shape of the correlation curves, which is most pronounced in the μs time scale, is found to be due to a variation of the off-state fraction (T) and blinking time (τ_T) with change in the excitation power, as evident from the parameters collected in Table 3.1.

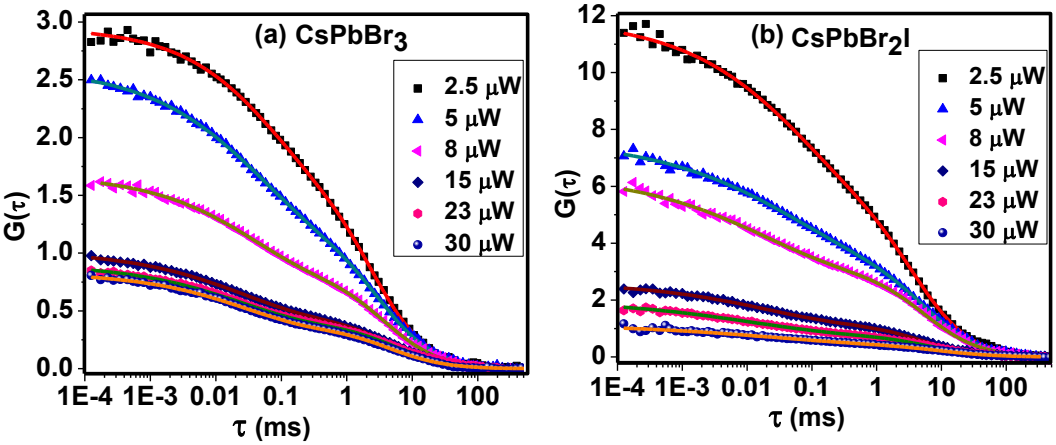

Figure 3.2: Amplitude of fluorescence correlation of (a) 1.3 nM $CsPbBr_3$ (b) 0.5 nM $CsPbBr_2I$ in ODE as a function of time for different excitation power. The data points are represented by symbols and the solid lines represent fits to equn. (3.3). Excitation wavelength is 405 nm.

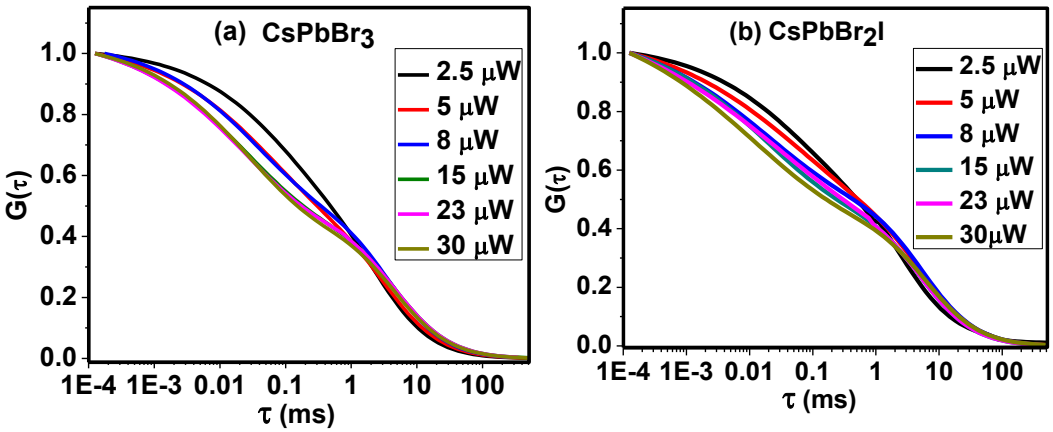

Figure 3.3: Normalized fitted correlation curves of (a) $CsPbBr_3$ and (b) $CsPbBr_2I$ in ODE for different excitation powers.

Table 3.1: Estimated values of G(0), off-state fraction (T) and blinking time (τ_T) for $CsPbBr_3$ and $CsPbBr_2I$ NCs at different excitation powers.

Sample	Excitation power (μW)	G(0)	T	τ_T (μs)
$CsPbBr_3$	2.5	2.80 ± 0.11	0.41 ± 0.008	62 ± 6
	5	2.61 ± 0.10	0.5 ± 0.006	39 ± 5
	8	1.65 ± 0.05	0.51 ±0.074	32 ± 2
	15	0.96 ± 0.02	0.55 ± 0.08	25 ± 2
	23	0.80 ± 0.04	0.57 ± 0.03	23 ± 4
	30	0.77 ± 0.02	0.64 ± 0.09	10 ± 1
$CsPbBr_2I$	2.5	10.0 ± 0.80	0.45 ± 0.09	45 ± 6
	5	6.75 ± 0.23	0.54 ± 0.10	33 ± 6
	8	4.90 ± 0.24	0.57 ± 0.11	21 ± 5
	15	2.75 ± 0.22	0.61 ± 0.11	16 ± 3
	23	1.90 ±0.05	0.615 ± 0.08	11 ± 2
	30	1.50 ± 0.18	0.63 ± 0.10	10.5 ± 5

The observation that the correlation data is better represented by a stretched exponential rather than a simple exponential suggests that charge carrier trapping and relaxation processes in perovskite NCs occur with a distribution of rate constants rather than a single rate constant. This implies that photo-generated charge carriers in $CsPbBr_3$ and $CsPbBr_2I$ perovskite NCs are trapped by a number of states with a distribution of energies. This conclusion is consistent with the power law and truncated power law behavior of the off-time and on-time probabilities observed by Park et al. in their study of blinking (in ms time scale) of $CsPbBr_3$ in immobilized state[16] and also in other studies involving metal-chalcogenide based QDs.[36-38] A decrease of the β value (Figure AI.6, Appendix 1) with increasing excitation power suggests a more dispersive blinking kinetics at higher power regime due to generation of additional relaxation pathways, which lead to an increase in the value of T. Table 3.1 also indicates an acceleration of the blinking rate at higher excitation power. As the average number of excitons (<N>) generated per pulse at an excitation power of 5 μW (81 μJ cm^{-2}) is 1.6,[39] the role of Auger-like nonradiative processes, which is recently found on similar materials of comparable absorption cross-section and laser intensity,[16,27] is evident from the T and τ_T values. As the contribution of Auger recombination increases with increase in excitation power a decrease in τ_T and increase in T values are observed (Table 3.1).

3.2.2. Controlled experiments to substantiate photoactivation

As *G(0) = 1/N (1-T)*, an increase in T with increase in excitation power (Table 3.1) should lead to an increase of the G(0) value for a constant value of N. However, the observed behavior is quite opposite. Considering that a number of factors[40-43] can influence the G(0) value, several control experiments have been performed (as stated below) to determine the origin of its excitation power dependence.

An increase in background noise at higher excitation power can affect the G(0) value. However, this factor is not responsible for large reduction of the G(0) value is evident form the fact that an identical variation of the excitation power led to a small increase of the G(0) value for a solution of coumarin dye, C153 in the same medium (Figure AI.7, Appendix 1). That optical trapping and/or broadening of the observation volume due to excitation saturation are not responsible for large drop of the G(0) value is

evident from the fact that saturation occurs only at a higher laser power of 30-50 μW and a very small change of the diffusion time with excitation power is observed in the experimental power regime (Figure AI.8, Appendix 1).

Thus the decrease of G(0) value can only be explained by considering an increase in the value of N at higher laser power. This implies photon-induced conversion of the dim or dark NCs to bright NCs, a process commonly termed as photoactivation,[44] which increases the number of particles undergoing reversible transition between fluorescence on- and off-state in the observation volume.

3.2.3. Light irradiation effect on steady-state and time-resolved data

The photoactivation of these NCs is further substantiated by conventional steady-state and time-resolved fluorescence measurements as a function of light irradiation time. Figure 3.4 depicts the effect of light illumination for different periods on the emission behavior of the two samples and Figure 3.5 plots the quantitative data on relative emission intensity (I/I_0) and λ_{max}^{em} values with irradiation time. It is evident that the emission intensity of $CsPbBr_3$ and $CsPbBr_2I$ increases by factors of 2 and 4.5, respectively, in about 5-7 hours. During the early stages of irradiation a sharp blue shift of λ_{max}^{em} is also observed for $CsPbBr_2I$ (Figure 3.5). Interestingly, prolonged exposure leads to a slow decrease in emission intensity accompanied by a steady red shift of λ_{max}^{em} for both NCs.

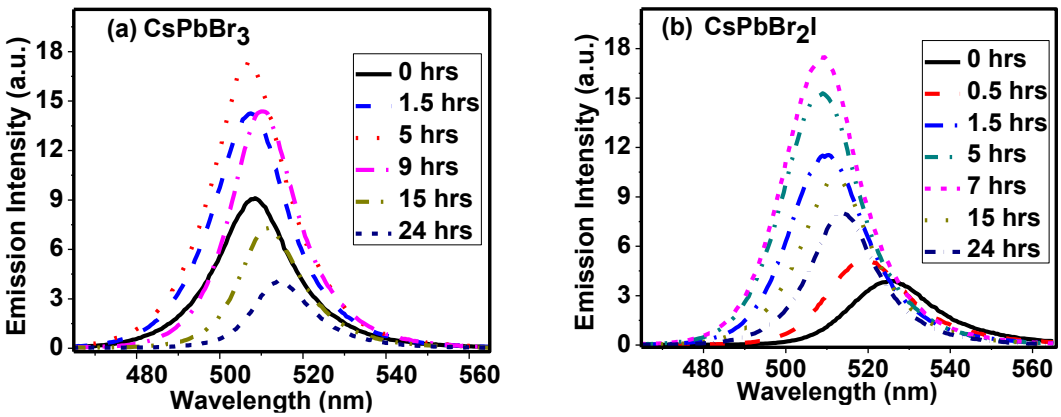

Figure 3.4: Emission spectra of (a) $CsPbBr_3$ and (b) $CsPbBr_2I$ recorded following irradiation of samples for different periods.

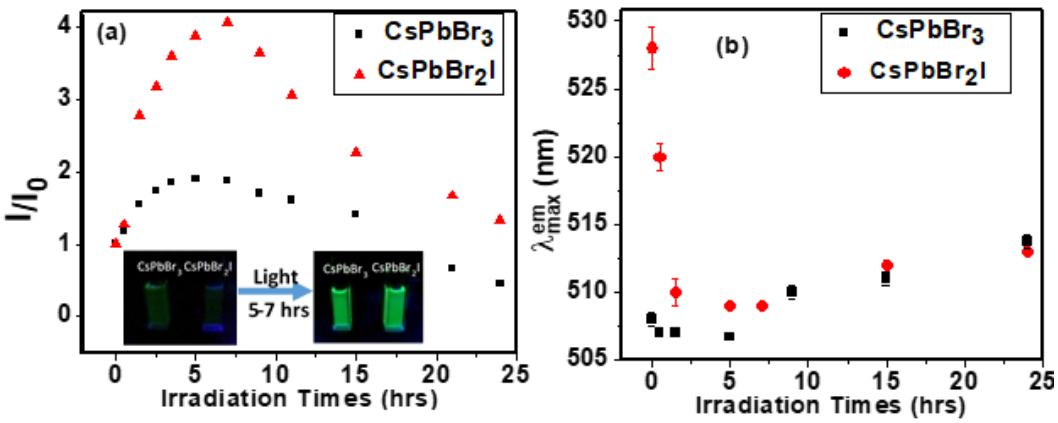

Figure 3.5: Plot of (a) relative emission intensity (I/I_0) and (b) emission peak wavelength of the NCs as a function of light irradiation time. Inset of (a) shows the photographs of emission enhancement on photoactivation.

Fluorescence decay profiles were also measured following light irradiation of these NCs for different periods to find out the effect of photo-exposure on the fluorescence lifetime (Figure AI.11, Appendix 1). The emission decay profiles were characterized by tri-exponential function (as determined from the fit residuals and χ^2 values) of the form, $I(t) = \alpha_1 \exp(-t/\tau_1) + \alpha_2 \exp(-t/\tau_2) + \alpha_3 \exp(-t/\tau_3)$. The individual lifetime components, associated amplitudes and average lifetimes of the systems after irradiation for different periods are provided as supporting information (Table AI.1, Appendix 1). It is observed that for both NCs the average fluorescence lifetime, $\langle\tau\rangle$ increases initially upon exposure to light up to a certain period (~5-7 hrs) and then decreases, a behavior similar to that observed for the steady state emission intensity (I_{em}).

As in the light irradiation experiment constant intensity light is used, the nature of the fluorescence blinking of the perovskite NCs will not change significantly. Only conversion of dark or dim NCs into bright NCs in the presence of light leads to enhancement in emission intensity. That the origin of the drop of the G(0) value with increasing excitation power and enhancement of steady state luminescence intensity is the same photoactivation phenomenon is evident from the fact that when the FCS experiments are carried out on light-exposed perovskite samples a much smaller drop of the G(0) value (by factors of 1.75 and 2.1 for $CsPbBr_3$ and $CsPbBr_2I$, respectively, Figure AI.12,

Appendix 1) with increase in excitation power when compared with the enhancement of 3.6 and 6.7 observed for the unexposed samples. Literature reports on semiconductor quantum dots suggest that photoactivation can be due to passivation of the surface trap states by photo-adsorbed molecules,[29,30,45] photo-induced rearrangement of the surface stabilizing agents,[46] smoothing of the surface during photocorrosion,[45] photo-induced neutralization of the local charged centers both inside and outside of the QDs[47] and reorganization of the crystal framework.[23,48] As ODE is a noninteracting solvent,[32] surface passivation by photo-adsorbed solvent molecules leading to photoactivation can be neglected. That oxygen dissolved in the solvent does not contribute to the photoactivation of the perovskite NCs by passivating the surface is evident from the fact that no emission enhancement on exposure to light could be observed in toluene (Figure AI.13, Appendix 1), in which the oxygen solubility is significantly higher than that in ODE.[49] As photoactivation is more prominent in the case of $CsPbBr_2I$, which has a distorted crystal structure compared to $CsPbBr_3$, we conjecture that photoactivation of the NCs is the result of light induced structural reorganization. In the case of $CsPbBr_2I$, the removal of iodine-induced trap states of the distorted cubic crystals is a distinct possibility, as evident from the changes in the $\lambda_{max}^{exciton}$ and λ_{max}^{em} values (Figure 3.5 & AI.10, Appendix 1). This mechanism is in agreement with the hypothesis of Gottesman et al, according to which the photo-induced structure of the perovskite crystals is more ordered than the dark structure.[48] As discussed in some recent reports[13,50] photoactivation of the perovskite NCs could be a result of filling of some of the mid-band gap trap states (quenchers) by photogenerated charge carriers with increasing excitation power or illumination time thus, converting completely dark NCs into bright NCs. The decrease of I_{em} and $\langle\tau\rangle$ values accompanied by a red shift of $\lambda_{max}^{exciton}$ and λ_{max}^{em} at longer irradiation time is unclear to us at the moment. Even though aggregation of the NCs (as indicated by an increase in diffusion time of the photo-exposed particles compared to the unexposed ones, Figure AI.14, Appendix 1) is a distinct possibility, we shall refrain from emphasizing this point at this stage.

3.3. Conclusion

In conclusion, this first FCS study on all-inorganic perovskite NCs, $CsPbBr_3$ and $CsPbBr_2I$, reveals fluorescence blinking in the microsecond time scale. The dispersive

nature of the blinking kinetics suggests the existence of a distribution of trap states in these NCs. A faster blinking at higher excitation power is attributed to an enhancement of the contribution of nonradiative Auger recombination process. The photoactivation phenomenon, which is found to be more prominent in the case of $CsPbBr_2I$, appears to be due to structural reorganization as well as filling of the trap states of the NCs. These key findings are expected to be useful in improving the potential of these substances in various applications.

References:

(1) Green, M. A.; Ho-Baillie, A.; Snaith, H. J. *Nat. Photonics* **2014**, *8*, 506-514.

(2) Zhou, H.; Chen, Q.; Li, G.; Luo, S.; Song, T.-b.; Duan, H.-S.; Hong, Z.; You, J.; Liu, Y.; Yang, Y. *Science* **2014**, *345*, 542-546.

(3) Christians, J. A.; Manser, J. S.; Kamat, P. V. *J. Phys. Chem. Lett.* **2015**, *6*, 2086-2095.

(4) Christians, J. A.; Fung, R. C. M.; Kamat, P. V. *J. Am. Chem. Soc.* **2014**, *136*, 758-764.

(5) Tan, Z.-K.; Moghaddam, R. S.; Lai, M. L.; Docampo, P.; Higler, R.; Deschler, F.; Price, M.; Sadhanala, A.; Pazos, L. M.; Credgington, D.; Hanusch, F.; Bein, T.; Snaith, H. J.; Friend, R. H. *Nat.Nanotechnol.* **2014**, *9*, 687-692.

(6) Li, G.; Tan, Z.-K.; Di, D.; Jiang, M. L. L.; Lim, J. H.-W.; Friend, R. H.; Greenham, N. C. *Nano Lett.* **2015**, *15*, 2640-2644.

(7) YH, K.; H, C.; JH, H.; TS, K.; N, M.; CL, L.; SH, I.; TW, L. *Adv. Mater.* **2015**, *27*, 1248-1254.

(8) Dou, L.; Yang, Y. M.; You, J.; Hong, Z.; Chang, W.-H.; Li, G.; Yang, Y. *Nat. Commun.* **2014**, *5*, 5404.

(9) Guo, Y.; Liu, C.; Tanaka, H.; Nakamura, E. *J. Phys. Chem. Lett.* **2015**, *6*, 535-539.

(10) Sutherland, B. R.; Hoogland, S.; Adachi, M. M.; Wong, C. T. O.; Sargent, E. H. *ACS Nano* **2014**, *8*, 10947-10952.

(11) Zhang, Q.; Ha, S. T.; Liu, X.; Xiong, T. C. S. *Nano Lett.* **2014**, *14*, 5995-6001.

(12) Xing, G.; Mathews, N.; Lim, S. S.; Yantara, N.; Liu, X.; Sabba, D.; Grätzel, M.; Mhaisalkar, S.; Sum, T. C. *Nature Mater.* **2014**, *13*, 476-480.

(13) Deschler, F.; Price, M.; Pathak, S.; Klintberg, L. E.; Jarausch, D.-D.; Higler, R.; Hüttner, S.; Leijtens, T.; Stranks, S. D.; Snaith, H. J.; etal *J. Phys. Chem. Lett.* **2014**, *5*, 1421-1426.

(14) Zhu, H.; Fu, Y.; Meng, F.; Wu, X.; Gong, Z.; Ding, Q.; Gustafsson, M. V.; Trinh, M. T.; Jin, S.; Zhu, X.-Y. *Nature Mater.* **2015**, *14*, 636-642.

(15) Wang, Y.; Li, X.; Song, J.; Xiao, L.; Zeng, H.; Sun, H. *Adv. Mater.* **2015**, *27*, 7101-7108.

(16) Kulbak, M.; Cahen, D.; Hodes, G. *J. Phys. Chem. Lett.* **2015**, *6*, 2452-2456.

(17) Eperon, G. E.; Paterno, G. M.; Sutton, R. J.; Zampetti, A.; Haghighirad, A. A.; Caciallibc, F.; Snaith, H. J. *J. Mater. Chem. A* **2015**, *3*, 19688-19695.

(18) Park, Y.-S.; Guo, S.; Makarov, N. S.; Klimov, V. I. *ACS Nano* **2015**, *9*, 10386-10393.

(19) Yakunin, S.; Protesescu, L.; Krieg, F.; Bodnarchuk, M. I.; Nedelcu, G.; Humer, M.; Luca, G. D.; Fiebig, M.; Heiss, W.; Kovalenko, M. V. *Nat. Commun.* **2015**, *6*, 8515.

(20) Yantara, N.; Bhaumik, S.; Yan, F.; Sabba, D.; Dewi, H. A.; Mathews, N.; Boix, P. P.; Demir, H. V.; Mhaisalkar, S. *J. Phys. Chem. Lett.* **2015**, DOI: 10.1021/acs.jpclett.5b02011.

(21) Wu, K.; Liang, G.; Shang, Q.; Ren, Y.; Kong, D.; Lian, T. *J. Am. Chem. Soc.* **2015**, *137*, 12792−12795.

(22) Protesescu, L.; Yakunin, S.; Bodnarchuk, M. I.; Krieg, F.; Caputo, R.; Hendon, C. H.; Yang, R. X.; Walsh, A.; Kovalenko, M. V. *Nano Lett.* **2015**, *15*, 3692-3696.

(23) Akkerman, Q. A.; Innocenzo, V. D.; Accornero, S.; Scarpellini, A.; Petrozza, A.; Prato, M.; Manna, L. *J. Am. Chem. Soc.* **2015**, *137*, 10276-10281.

(24) Nedelcu, G.; Protesescu, L.; Yakunin, S.; Bodnarchuk, M. I.; Grotevent, M. J.; Kovalenko, M. V. *Nano Lett.* **2015**, *15*, 5635-5640.

(25) Smyth, D. M. *Ann. Rev. Mater. Sci.* **1985**, *15*, 329-57.

(26) Kim, J.; Lee, S.-H.; Lee, J. H.; Hong, K.-H. *J. Phys. Chem. Lett.* **2014**, *5*, 1312-1317.

(27) Xiao, Z.; Zhou, Y.; Hosonoab, H.; Kamiya, T. *Phys. Chem. Chem. Phys.* **2015**, *17*, 18900-18903.

(28) Tachikawa, T.; Karimata, I.; Kobori, Y. *J. Phys. Chem. Lett.* **2015**, *6*, 3195-3201.

(29) Ito, S.; Toitani, N.; Pan, L.; Tamai, N.; Miyasaka, H. *J. Phys.: Condens. Matter* **2007**, *19*, 486208 (1-10).

(30) Patra, S.; Samanta, A. *J. Phys. Chem. C* **2013**, *117*, 23313 −23321.

(31) Patra, S.; Samanta, A. *J. Phys. Chem. C* **2014**, *118*, 18187 −18196.

(32) Patra, S.; Seth, S.; Samanta, A. *ChemPhysChem* **2015**, *16*, 3871-3876.

(33) Farkhani, S. M.; Valizadeh, A. *IET Nanobiotechnol.* **2014**, *8*, 59-76.

(34) Tian, Y.; Peter, M.; Unger, E.; Abdellah, M.; Zheng, K.; Pullerits, T.; Yartsev, A.; Sundström, V.; Scheblykin, I. G. *Phys. Chem. Chem. Phys.* **2015**, *17*, 24978-24987.

(35) Tian, Y.; Merdasa, A.; Unger, E.; Abdellah, M.; Zheng, K.; McKibbin, S.; Mikkelsen, A.; Pullerits, T.; Yartsev, A.; Sundström, V.; Scheblykin, I. G. *J. Phys. Chem. Lett.* **2015**, *6*, 4171-4177.

(36)

(37) Lackowicz, J. R. *Springer: New York, 2006; Chapter 24.*

(38) Heuff, R. F.; Swift, J. L.; Cramb, D. T. *Phys. Chem. Chem. Phys.* **2007**, *9*, 1870-1880.

(39) Kuno, M.; Fromm, D. P.; Johnson, S. T.; Gallagher, A.; Nesbitt, D. J. *Phys. Rev. B* **2003**, *67*, 125304.

(40) Peterson, J. J.; Nesbitt, D. J. *Nano Lett.* **2009**, *9*, 338-345.

(41) Shimizu, K. T.; Neuhauser, R. G.; Leatherdale, C. A.; Empedocles, S. A.; Woo, W. K.; Bawendi, M. G. *Phys. Rev. B* **2001**, *63*, 205316.

(42)

(43) Hess, S. T.; Webb, W. W. *Biophys. J.* **2002**, *83*, 2300-2317.

(44) Gregor, I.; Patra, D.; Enderlein, J. *ChemPhysChem* **2005**, *6*, 164-170.

(45) Doose, S.; Tsay, J. M.; Pinaud, F.; Weiss, S. *Anal. Chem.* **2005**, *77*, 2235-2242.

(46) Murthy, A. V. R.; Patil, P.; Datta, S.; Patil, S. *J. Phys. Chem. C* **2013**, *117*, 13268-13275.

(47) Carrillo-Carrión, C.; Cárdenas, S.; Simonet, B. M.; Valcárcel, M. *Chem. commun.* **2009**, 5214-5226.

(48) Jones, M.; Nedeljkovic, J.; Ellingson, R. J.; Nozik, A. J.; Rumbles, G. *J. Phys. Chem. B* **2003**, *107*, 11346-11352.

(49) Oda, M.; Hasegawa, A.; Iwami, N.; Nishiura, K.; Ando, N.; Nishiyama, A.; Horiuchi, H.; Tani, T. *Colloids Surf. B* **2007**, *56*, 241-245.

(50) Gottesman, R.; Gouda, L.; Kalanoor, B. S.; Haltzi, E.; Tirosh, S.; Rosh-Hodesh, E.; Tischler, Y.; Zaban, A.; Quarti, C.; Mosconi, E.; Angelis, F. D. *J. Phys. Chem. Lett.* **2015**, *6*, 2332-2338.

Chapter 4

Photoluminescence Flickering and Blinking of Single $CsPbBr_3$ Perovskite Nanocrystals: Revealing Explicit Carrier Recombination Dynamics

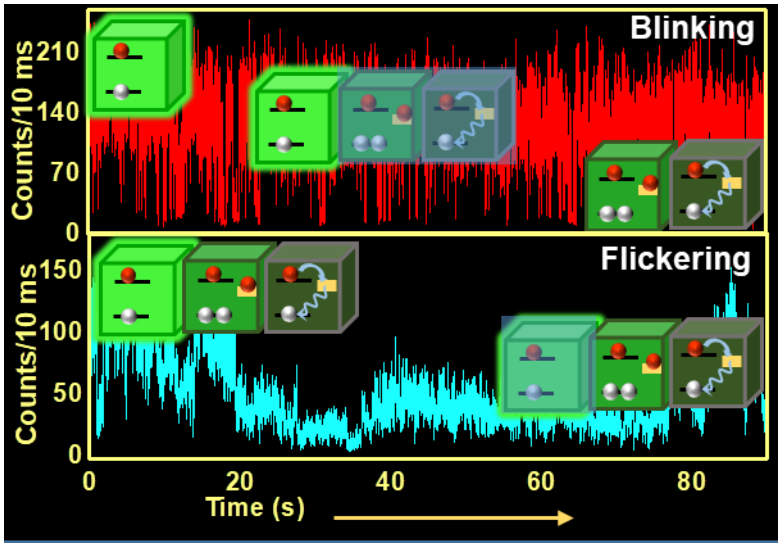

Abstract.

In order to obtain an in-depth understanding of the carrier recombination dynamics of $CsPbBr_3$ nanocrystals (NCs), a comprehensive picture of all possible recombination processes and to provide remedy for the undesired recombination, we have investigated the photoluminescence (PL) of this material at the single particle level using time-tagged-time-resolved method. Our study reveals two distinct types of PL fluctuations of the NCs, which we have assigned to flickering and blinking. We found the flickering to be due to the excess surface trap of the NCs and show that post-synthetic surface treatment can convert the flickering NCs into the blinking ones with significant enhancement of PL and stability. Intensity correlated lifetime analysis of the PL time-trace reveals both trap-mediated nonradiative band edge carrier recombination and positive trion recombination in single NCs. Dynamical and statistical analysis suggests a diffusive nature of the trap states, which is responsible for the PL intermittency in these systems. These findings throw light on the nature of the trap states, show the manifestation of these trap states in PL fluctuation and provide an effective way to control the dynamics in these systems.

4.1. Introduction

Semiconductor nanocrystals (NCs) are the most important candidates driving the recent progress in the field of photovoltaic and optoelectronics.[1] As the photogenerated charge carriers in these NCs are confined to a small volume, a strong Coulomb interaction between these carriers is often the driving force for many interesting multicarrier processes such as multiexciton generation,[2, 3] Auger recombination,[4, 5] efficient intraband relaxation[6] and spectral diffusion.[7] Among these, Auger recombination, in which electron - hole recombination energy is transferred to a third carrier instead of being released in the form of a photon is an undesired process for optoelectronic applications.[4, 5] The Auger process in small size NCs is faster than radiative lifetime of a single electron-hole (e-h) pair and generally occurs at subnanosecond time scale.[4] This process assumes significance when multiexcitons are generated (simultaneously) in a single NC or when the NCs are charged by direct trapping of one of the charge carriers in long lived defect state.[8] In charged NCs, photoluminescence (PL) quenching due to nonradiative Auger recombination introduces intermittency in the single NC PL trajectory, which is undesirable in photon emission applications such as light emitting diodes, lasers and single photon emitters.[9-11] The simplest form of the charged NC is trion having one extra charge in addition to one exciton.[12] Positive (2h-e) and negative (h-2e) trions are considered to be responsible for non-emissive or less-emissive off-states of single NC PL intermittency or blinking.[12, 13] For Auger recombination to happen the NCs need to be charged, but blinking can also happen even when the NCs are not charged.[14-16] Shallow trap states with short lifetime can facilitate rapid nonradiative relaxation of the photogenerated carrier before another exciton is generated. This process, termed in our discussion as nonradiative band edge carrier (NBC) recombination, does not involve the long-lived traps.[17] The NBC and trion recombination rates fluctuate with time depending on the position and density of the defect states on the NCs. Unlike blinking when the single NC does not show clear on- and off-states rather a continuous and random distribution of several intensity levels are observed, such behavior is often termed as flickering.[18-20] It is observed that excess trapped charge is one of the main reason for PL flickering in the NCs.[18, 19]

Recently it is observed that PL blinking is not restricted in the nanoscale regime rather it can be observed in larger size crystals (up to μm).[20-23] This interesting fact is

observed in case of hybrid halide perovskite materials contrary to conventional semiconductors. Fluctuating nonradiative relaxation via some metastable but efficient defect states are considered to be responsible for PL fluctuation than the well accepted charging mechanism in nanoscale QDs.

The all-inorganic perovskite NCs have emerged in recent years as a highly promising material for photovoltaic, optoelectronic and photonic applications because of their enticing optical properties such as broad absorption, narrow tunable emission, high PL quantum yield (QY), large multi-photon absorption cross-section, high charge carrier mobility and tolerance to intrinsic defects.[24-34] Despite the absence of intrinsic deep trap states (high formation energy)[34-37], recent reports show that $CsPbX_3$ (X=Br, I) NCs are not completely devoid of charge trapping centers and vulnerable towards photocharging forming trions and dark excitons.[30, 31, 38-41] Trion decay in these NCs is found to be dominated by nonradiative Auger recombination.[40, 41] Despite being defect tolerant, origin of the shallow traps causing nonradiative deactivation of the carriers in these NCs is not well understood at the moment.

One of the approaches to probe the fate of the charge carriers of a semiconductor is by assessing their PL properties in the single NC level as interaction of the charge carriers with any internal or external defects leads to fluctuation in their PL with time. Scarcely populated literature on single particle PL study of $CsPbX_3$ NCs reveals a collection of patterns of PL fluctuation rather than a unifying trend.[16, 30, 32, 33, 40, 42-44] Very few studies present a consistent picture for explaining the mechanism of observed PL fluctuation.[16, 30, 39, 40, 42, 43] Some reports attribute blinking in these materials to random charging/ discharging and the OFF state to trion recombination without providing any concrete information on the type.[30, 39, 40] While another report consider NBC recombination as the major reason for PL intermittency where trion plays a minor role.[16] Biexponential PL kinetics of the bright states and variation of the fluorescence intensity lifetime distribution (FLID) lack clear interpretation. At this instance a clear correlation among these observed fluctuation patterns and factors responsible for such behavior is urgently required. Here we attempt to provide a comprehensive picture of the charge carrier dynamics in single $CsPbBr_3$ NC taking into consideration all possible radiative and nonradiative recombination pathways.

In order to understand the nature of charge trapping defects and their manifestation in PL properties of $CsPbBr_3$ NCs, we have studied single particle PL behavior by combining intensity correlated lifetime analysis and statistical analysis of the ON and OFF states. Signature of random fluctuation of PL with discrete or continuous distribution of intensity is observed. Excess surface traps play a crucial role in the fast ON-OFF cycle. NBC recombination and trion Auger recombination are shown to dictate the course of the PL time-trace.

4.2 Result and discussion.

$CsPbBr_3$ NCs are synthesized following room temperature anti-solvent precipitation method adapted from a recent report[45] and detailed procedure is provided in the method section. Figure 4.1a shows transmission electron microscopy (TEM) images of the $CsPbBr_3$ nanocubes indicating an average size of 12 ± 1 nm. As evident from Figure 4.1b, first absorption onset and PL peak of these NCs appear at 505 nm and 512 nm, respectively. Confocal PL microscopic image of a film containing well-separated NCs are shown in Figure 4.1c. The sample preparation methodology and instrumentation are detailed in the method section. Individual NCs were excited with a 405 nm pulsed picosecond diode laser with repetition rate of 5 MHz and PL signals were detected through time-tagged-time-resolved mode. Laser intensity used was 0.04 μW. Number of excitons generated per pulse was calculated using the formulae, $\langle N \rangle = J_p \times \sigma = \sim 0.09$, where J_p is per pulse photon fluence and $\sigma = 2.0 \times 10^{-14}$ cm^2 is the absorption cross section.[30, 41, 42] Measurements were performed on nearly ~60 individual single particles of as-synthesized and ethanethiol-treated NCs.

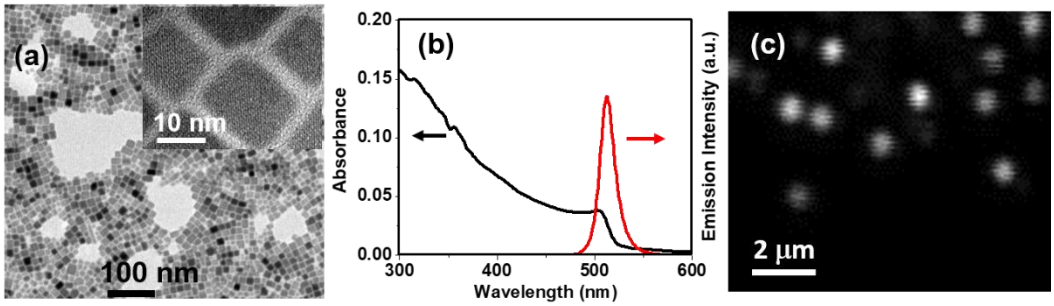

Figure 4.1. (a) TEM and high resolution TEM images of $CsPbBr_3$ NCs, (b) optical absorption and PL spectra of the NCs dispersed in toluene and (c) PL intensity image of a very low density NC film obtained using confocal microscope.

4.2.1. PL blinking.

Literature reports show that temporal fluctuation of PL intensity of single $CsPbBr_3$ NC is of two types.[18, 32, 33, 40, 42, 44] Few reports show that NCs undergo rapid transition between high intensity ON and low intensity OFF state (i.e. PL blinking)[32, 33, 40, 44] whereas, some other reports indicate that the NCs do not show clear ON–OFF transitions, instead they exhibit a PL trajectory with continuous distribution of intensity as a function of time, which sometimes termed as PL flickering.[18, 42, 44] In this work, we find that the as-synthesized NCs show both types of PL behavior; 30% of the studied NCs show blinking behavior (Figure 4.2 and AII.1, Appendix II) for which the distribution of PL intensity time-trace shows two distinct intensity regions corresponding to ON and OFF states and some intermediate intensity states (GREY states) as well. The OFF states are not completely non-emissive for these NCs as the intensity corresponding to this state is quite above the background level (red line in Figure 4.2a). Blinking pattern of this nature is reported previously for $CsPbBr_3$ as well as for the CdSe/CdS quantum dot systems.[5, 40, 43] Time-resolved PL (TRPL) intensity profiles corresponding to different intensity regions of the blinking time-trace (marked by R1, R2, R3 and R4) are shown in Figure 4.2b. The highest intensity region R1 mostly shows a single long lifetime component of 8.9±0.8 ns. Rest of the intensity regions (R2, R3 and R4) are characterized by a biexponential decay,

except for 40% cases where lowest intensity OFF state (R4) shows a single lifetime component of 1.3 ±0.3 ns. Table 4.1 summarizes the individual lifetime components and their relative amplitudes corresponding to different intensity regions, averaged over all studied NCs which exhibit this blinking pattern. As evident from the table, each intensity level (R2/R3/R4) except R1 is associated with a long and a short lifetime component, representing two different recombination processes. Under our experimental condition, multiple exciton formation in a NC is ruled out. As trions are short-lived compared to the single exciton and mostly undergo nonradiative Auger recombination, the longer lifetime component (8.9±0.8 ns) associated with the highest intensity state is assigned to the single exciton and the shorter one most likely due to the trion recombination.

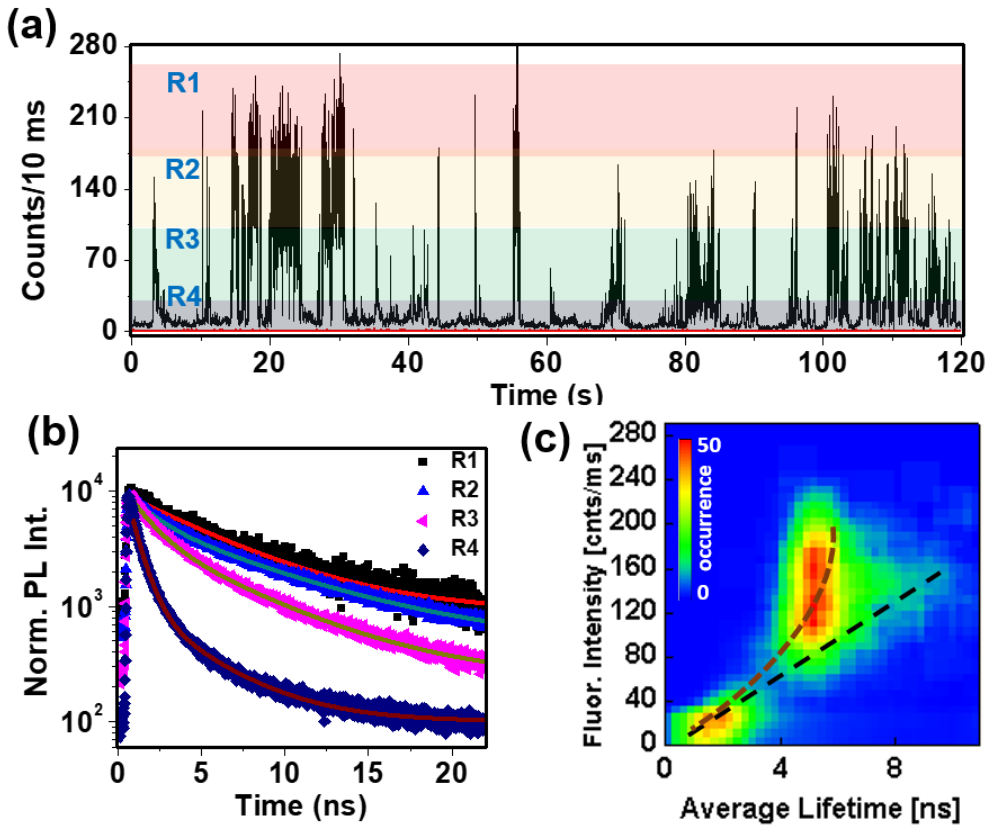

Figure 4.2. (a) PL intensity time trace of a blinking NC with a binning time of 10 ms. (b) PL decay dynamics of different intensity levels marked (R1, R2, R3, R4) and (c) FLID with false color representation of single $CsPbBr_3$ NC when <N> = ~0.09.

Table 4.1. Average lifetime components and their relative amplitudes corresponding to different intensity regions of the blinking time-trace.

Region	τ_1 (α_1)	τ_2 (α_2)
R1	8.9 ± 0.8	
R2	9.2 ± 0.4 (0.43)	1.6 ± 0.4 (0.57)
R3	8.1 ± 0.6 (0.28)	1.3 ± 0.4 (0.72)
R4	6.7 ± 0.6 (0.13)	1.0 ± 0.2 (0.87)
		1.3 ± 0.3

The FLID (Figure 4.2c) appears to be quite interesting. The correlation points at higher intensities and longer lifetimes are broad and scattered. The FLID data neither follows a pure linear nor a pure curvature relationship, rather it carries a combined signature of both. The dashed lines in Figure 4.2c present a guide to the eye. A linear FLID implies the ratio of the radiative rates of two different intensity levels (defined hereafter as intensity-lifetime scaling (η), Appendix II for details) is nearly unity and only the nonradiative rates differ in the two levels. This process happens when band edge carriers undergo nonradiative relaxation via shallow trap states without charging the NC.[14, 15] If the trion recombination was only responsible for the lower intensity states then FLID should have been curved and intensity-lifetime scaling value would have been nearly 2, as trion recombination rate is twice faster than that of neutral exciton.[18, 30] Hence, the nonradiative band edge carrier (NBC) recombination and trion recombination concomitantly contributes to the blinking of single $CsPbBr_3$ NCs. To substantiate this claim we have done intensity-lifetime scaling over two small regions of the ON and OFF states in the blinking trace (Figure AII.2, Appendix II). Obtained η value of ~1.22 implies that both NBC recombination and trion recombination are responsible for the observed PL blinking. Hence, the short lifetime component (τ_2) that contributes to the different intensity levels of the blinking trace is evidently due to the trion recombination influenced by the NBC recombination.

Even though the measurements have been performed on the single isolated NCs (Figure 4.1c), considering the fact that different intensity states contain two lifetime

components, one may doubt that the observed blinking pattern arises from a cluster of NCs instead of single NCs. This however can be ruled out considering the following: Assuming the cluster to consist of two NCs, (a) if the NCs are of similar type then one expects both the lifetimes (τ_1 and τ_2) to be very close, which however, is not the case (Table 4.1); (b) If the NCs are somewhat different, then the decay of even the highest intensity level should have been biexponential as two NCs are contributing to this level however, the observed kinetics is single exponential. (c) If emission arises from minimum of two NCs and decay time constants are similar then intensity-lifetime scaling should have shown a value of less than unity (as the intensity of the upper most level (Figure 4.2a) will be nearly doubled without any change in lifetime). However, as the value obtained (~1.22) is above unity, the possibility that the emission is coming from a cluster of NCs is ruled out.

4.2.2. PL flickering.

On the other hand, the PL intensity fluctuation (Figure 4.3a, AII.3, Appendix II) of the majority of single NCs (70% of the studied NCs) is slightly different. These NCs undergo continuous transition between regions of varying intensities. It is difficult to differentiate between a definite ON and OFF state and we assign this as PL flickering. For the convenience of analysis, we have classified the time-trace in three distinct levels (S1, S2 and S3) depending on the intensitiy. PL decay curves corresponding to these levels are shown in Figure 4.3b. Unlike the blinking NCs, these single NCs exhibit a biexponential decay for all three intensity levels and notably the maximum intensity is lower than that of the blinking NCs under the same experimental condition. Considering the similarity with the blinking NCs, here the long component (τ_1) is assigned to single excitonic radiative recombination and the short component (τ_2) to the trion recombination. Importantly, the lifetime components are consistently lower than those of the blinking NCs in their different intensity regions. The amplitude α_2 decreases with increase in intensity but always higher than α_1 irrespective of intensity. FLID (Figure 4.3c) data appears to be linear with a broad distribution suggesting a slightly different recombination dynamics for the flickering NCs.

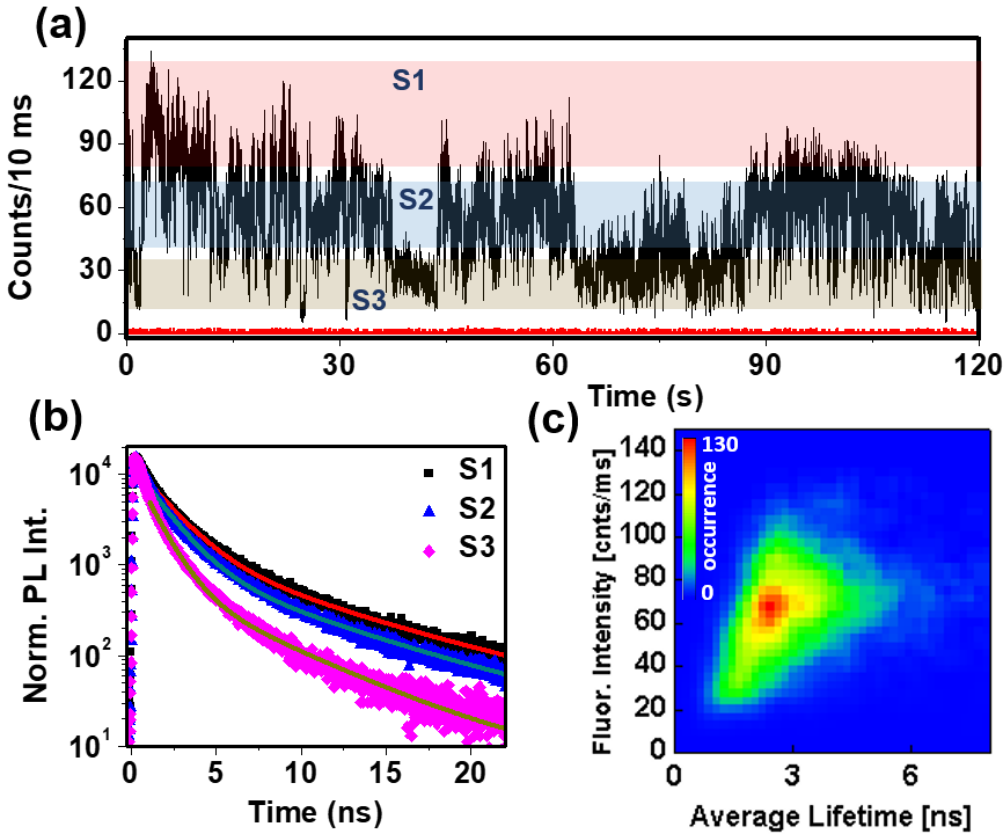

Figure 4.3. (a) PL intensity time trace of a flickering NC with a binning time of 10 ms. (b) PL decay dynamics of different intensity regions marked by red (S1), blue (S2) and grey (S3) shades and (c) FLID of $CsPbBr_3$ single NC when <N> = ~0.09.

Table 4.2. Average lifetime components and their relative amplitudes corresponding to different intensity regions of the flickering time-trace.

Region	τ_1 (α_1)	τ_2 (α_2)
S1	7.3 ± 1.0 (0.17)	1.3 ± 0.2 (0.83)
S2	6.2 ± 0.6 (0.13)	1.1 ± 0.3 (0.87)
S3	5.1 ± 0.9 (0.10)	0.70 ± 0.5 (0.90)

The literature suggests that injection of extra electron in the form of negative bias changes the blinking NCs into flickering ones where the short lifetime component arising from charged exciton recombination dominates over the longer single exciton lifetime.[18] This implies that presence of additional charge trapping sites in the NC leads to faster ON to OFF cycle which falls within the limit of binning time. In our earlier work, we established that PL blinking in $CsPbBr_3$ NCs occurs in microsecond time scale and follows a dispersive kinetics.[38] Hence, in 10 ms binning time many recombination events due to NBC, charged and single exciton contribute and overall intensity of the bin depends on their relative contributions. Such random distribution of intensity in consecutive bins leads to the flickering behavior. Considering lower lifetime and dominant contribution of the trion recombination in the radiative processes (compared to blinking NCs) we speculate higher density of trap states causing faster ON to OFF transitions to be present in these NCs.

4.2.3. Thiol treatment and PL blinking.

To elucidate the nature of the trap states causing observed PL intensity fluctuation we have treated the NCs with alkylthiols as the literature suggests that thiol containing capping ligands improve optoelectronic and photovoltaic properties of the lead based metal chalcogenide QDs and perovskite NCs and films.[46-48] For $CsPbBr_3$ NCs, ~1.4 fold enhancement of PLQY is achieved after treatment with alkyl thiols of different chain lengths (Figure 4.4a, AII.6, Appendix II). Ethanethiol is found to be more effective than any long chained thiols (see Appendix II for details of the treatment). Highly dynamic nature of the parent capping ligands (oleic acid and oleylamine) does not provide perfect protection of the NCs and the unpassivated atoms on the surface give rise to the trap states.[49] Since exciton binding energy for this NC is low (~20-50 meV), it can easily form free carriers at room temperature[29] and despite being defect tolerant these free carriers eventually pass through these short-lived shallow traps leading to fast nonradiative recombination. Ethanethiol with shortest chain can reach the NC surface and protect most effectively as long chain parent ligands create hindrance. Here, the sulfur atoms of ethanethiol form coordinate covalent bond with undercoordinated lead and the thiol protons interact with the exposed bromine on the surface, thereby decreasing the density

of the surface trap states.[46, 49] To further confirm surface passivation by the thiols, we have studied the temperature dependence of PL of the treated and untreated samples. Figure 4.4b (also AII.7, Appendix II) show that decrease in PL with increase in temperature is much less for thiol-treated sample as compared to the untreated one. This observation suggests that the untreated NCs consist of excess shallow traps where phonon mediated transition of the excited carriers and consequent nonradiative relaxation leads to lower PL QY at elevated temperature. Since thiol-treatment leads to the removal of some of these detrimental trap states, we observe a lesser decrease in PL intensity when temperature is raised.

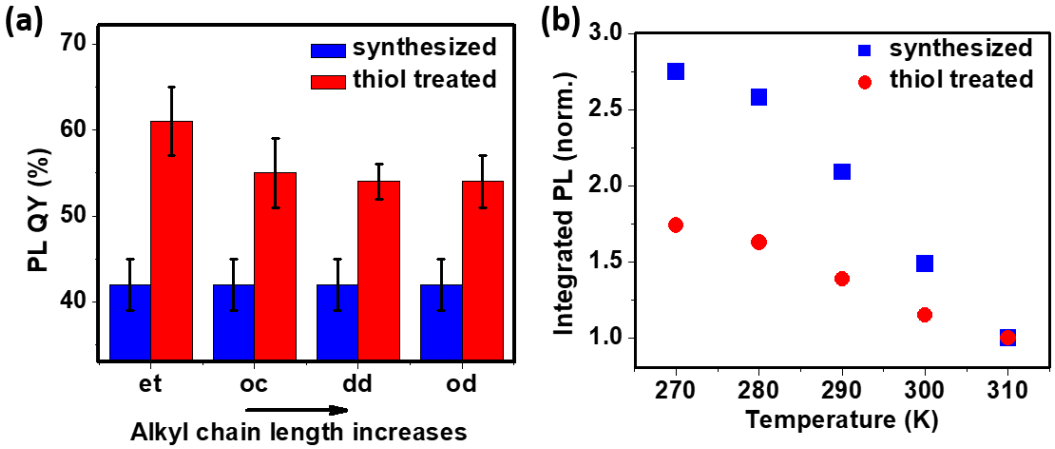

Figure 4.4. (a) Dependence of PL QY on the length of the alkyl chain of thiols (et = ethanethiol, oc = octanethiol, dd = dodecanethiol, od = octadecanethiol). (b) Temperature dependent PL of as-synthesized and ethanethiol treated $CsPbBr_3$ NCs.

We have investigated 42 ethanethiol-treated single $CsPbBr_3$ NCs and the representative PL intensity time trace is shown in Figure 4.5. Nearly 80% of these NCs show blinking feature indicating that thiol-treatment converts the flickering NCs into blinking NCs. Evidently, both the ON-state fraction and maximum intensity are increased (Figure 4.5b). Figure 4.5d shows PL decay curves corresponding to different intensity regions marked and shaded with different color codes. A positive correlation between intensity and lifetime is observed. Except for the T1 region, rest of the PL decay fit properly to a biexponential decay function. Average decay parameters are collected in

Table 4.3. As can be seen, the exciton and trion lifetimes have increased significantly and excitonic recombination dominates over the trion recombination except for the lowest intensity region. FLID follows a curvature relationship and intensity-lifetime scaling (Figure AII.8, Appendix II) produces a value of ~1.4, which indicates that both NBC and trion recombination are responsible for the OFF states.

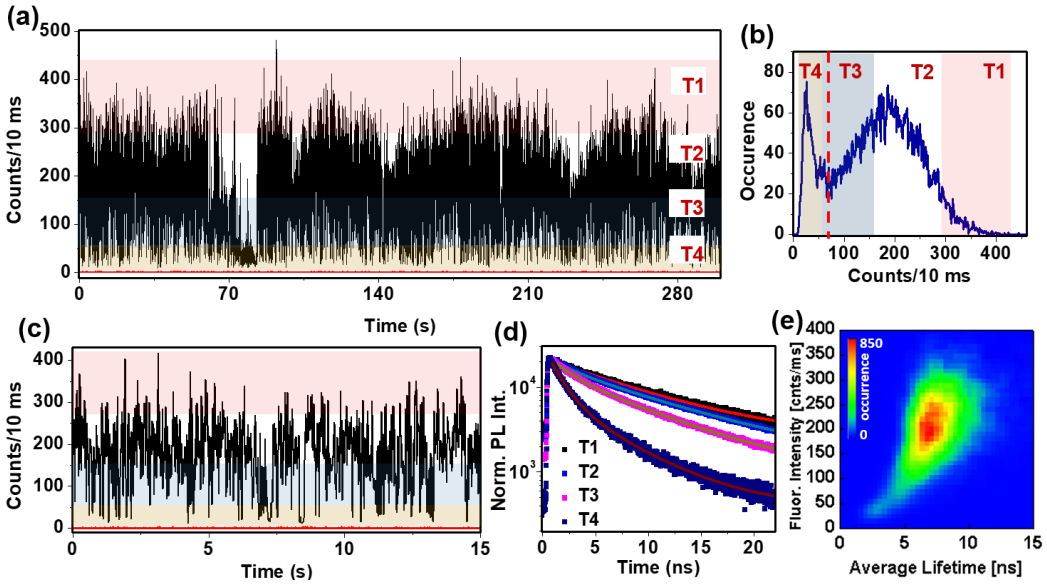

Figure 4.5. (a) PL intensity time-trace of a thiol-treated NC with a binning time of 10 ms. (b) Occurrence of the events, (c) Expanded time-trace of the first 15 seconds, (d) PL decay dynamics of different intensity regions as marked and shaded with colors. FLID of the corresponding time trace. Experiments are performed at same condition as the untreated sample with <N> = ~0.09.

Table 4.3. Average lifetime components and their relative amplitudes corresponding to different intensity regions of ethanethiol-treated blinking time-trace.

Region	τ_1 (α_1)	τ_2 (α_2)
T1	10.9 ± 0.7	
T2	11.4 ± 0.5 (0.79)	2.1 ± 0.3 (0.21)
T3	9.7 ± 0.8 (0.68)	1.8 ± 0.5 (0.32)
T4	6.9 ± 0.9 (0.37)	1.3 ± 0.6 (0.63)

4.2.4. Mechanism of PL fluctuation.

It is thus evident that surface treatment converts flickering NCs into blinking ones and that it has a lesser effect on the blinking NCs. This finding is similar to that observed in the case of $FAPbBr_3$ NCs.[19] In $CsPbBr_3$ NCs, the electron rich defects are likely to be less abundant as under-coordinated lead atoms mainly generate the defects, which are electron deficient by nature and serve as shallow electron trap.[34-36] These traps are generally short lived and presence of excess of them leads to rapid ON – OFF cycle leading to flickering in single NC PL. Linear FLID (Figure 4.3c) indicating shallow trap mediated NBC recombination supports such interpretation.[14] Surface treatment eliminates these trap states leading to a reduction of NBC recombination and retardation of the ON – OFF cycle, which thereby transforms flickering into blinking. Among these many shallow trap states few electronic levels are somewhat deeper and long-lived (≥ 200 ns, Scheme 4.1).[50] Trapping of electrons in these states provides enough time to generate another exciton and hence, a trion. Presumably these considerably long lived traps do not originate from surface rather they come from intrinsic defects as the trion component is found to present in all NCs studied.[19] Presence of deep trap states is neglected here considering highly defect tolerance nature and very high formation energy of the deep defects.[34-37] We assign this charged exciton as positive trion. Radiative lifetime of this trion (~2 ns) matches well with an earlier report.[51] However, shallow electron traps causing NBC recombination cannot be avoided completely as labile nature of the capping ligands always exerts some

of these electronic transition levels. Different recombination processes corresponding to a single $CsPbBr_3$ NC is illustrated in Scheme 4.1.

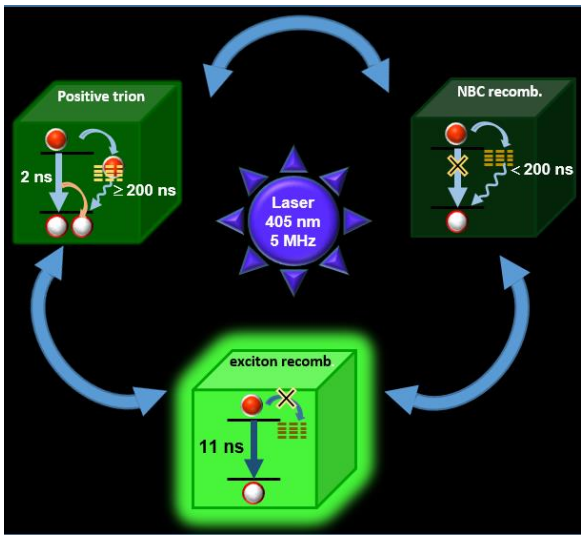

Scheme 4.1. Illustration of the different recombination processes occurring in a single $CsPbBr_3$ NC under laser beam when <N> = ~0.09.

Importantly, we observe a monotonic decrease of the PL lifetime with decrease in intensity of the PL time-trace irrespective of the origin of fluctuation (blinking or flickering). This can be explained considering dynamic nature of the defects (PL quenchers) that are present inside the crystal and on the surface. The nonradiative recombination is dramatic and fluctuates the rate drastically indicating efficient but metastable defect states at work. Lead halide perovskite crystals are ionic with very high charge carrier and significant ion mobility which leads to efficient quenching even when trap state concentration is less.[52, 53] Thus, depending on the carrier mobility, position and diffusion of the intrinsic/surface defects, charge trapping electronic states move in and out of the resonance with the conduction band electron providing a dynamic nature to these states. It is observed that surface defects plays a major role in determining nonradiative recombination of $CsPbBr_3$ NCs and nanoscale movement of the capping ligand is very fast (Diffusion coefficient of tightly bound ligand ~60 $\mu m^2/s$).[49, 54] Hence, fast dynamical

capping of the ligands may also contribute to the fluctuating nonradiative recombination rate.

4.2.5. Statistical analysis of the ON/OFF events.

To shed more light on the nature of the trap states and its effect on the carrier recombination, we have analyzed the blinking statistics by constructing the probability density of the ON and OFF states (Figure 4.6). Since, ON and OFF events are not so well separated, we have considered the threshold at the point where from maximum change in occurrence of the ON and OFF events is observed (red dotted line, Figure 4.5b). The probability density of the OFF events can be fitted to a power law function of the form, $P_{OFF} \propto t^{\alpha OFF}$, with the exponent $\alpha_{OFF} = -1.61$. Whereas, the probability density of the ON state follows a truncated power law behavior, $P_{ON} \propto t^{\alpha ON} \exp(-t/\tau_c)$, with $\alpha_{ON} = -0.69$ and truncation time, τ_c = 670 ms. Power law behavior clearly indicates a dispersive charge trapping and detrapping kinetics,[55] which is due to the distribution of the rates owing to (i) the energetic diffusion of the corresponding charge trapping states or (ii) the trap states undergoing a process of activation-deactivation.[14, 56] For these NCs both the processes are likely to be participating in blinking as both trion and NBC recombination is observed for the same NC. Unlike the conventional chalcogenide based CdSe QDs, the measured ON-state exponent is much larger for these NCs.[57, 58] A smaller value of power law exponents for ON state and larger for OFF state suggests that these NCs tend to longer-ON durations and shorter-OFF duration.

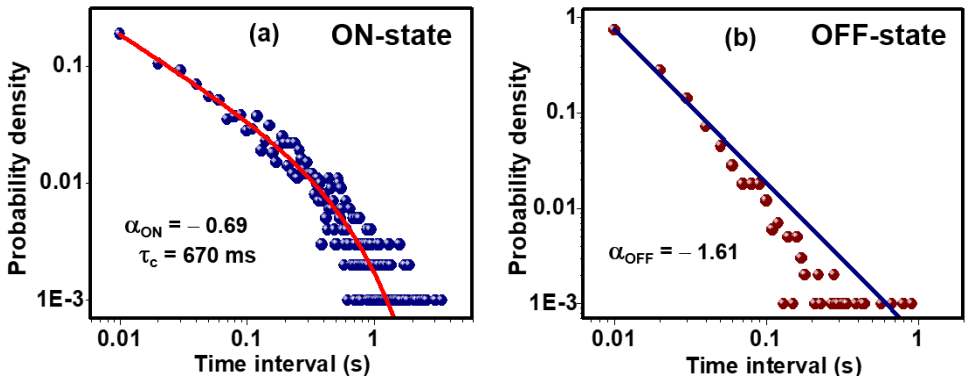

Figure 4.6. Probability density distribution of (a) ON states and (b) OFF states. Power law fitting exponents and truncation time for the ON state are shown inside the panels.

Unlike the untreated ones, these NCs show much improved environment and laser stability. As-synthesized NCs bleach within 3 minutes of laser irradiation whereas, ethanethiol treated NCs show significant brightness even after 5 minutes of measurements (Figure 4.5a, AII.9, Appendix II). As untreated NCs contain some exposed surfaces that are easily accessible to the water molecules from moist air, act as initiation points of degradation for these NCs.[16] Treatment with thiol provides protection to previously exposed surface and prevents rapid degradation of the NCs.

4.3 Conclusion

This single-particle PL study presents a comprehensive picture of the recombination dynamics in $CsPbBr_3$ NC. The results provide an in-depth understanding of the nature of the trap states, their role in PL fluctuation and a guide to manipulate the recombination dynamics in these systems. Specifically, it is shown that two types of PL intermittency, blinking and flickering, are the outcome of trion and NBC recombination processes. Excess surface shallow traps causes faster ON-OFF cycle and leads to PL flickering. Surface treatment which converts flickering into blinking by removing those excess traps has less effect on blinking. Statistical analysis of blinking indicates a dispersive kinetics with longer ON and shorter OFF durations.

4.4 References

(1) Kovalenko, M. V.; Manna, L.; Cabot, A.; Hens, Z.; Talapin, D. V.; Kagan, C. R.; Klimov, V. I.; Rogach, A. L.; Reiss, P.; Milliron, D. J.; Guyot-Sionnnest, P.; Konstantatos, G.; Parak, W. J.; Hyeon, T.; Korgel, B. A.; Murray, C. B.; Heiss, W. *ACS Nano* **2015**, *9*, 1012.

(2) Hu, F.; Lv, B.; Yin, C.; Zhang, C.; Wang, X.; Lounis, B.; Xiao, M. *Phys. Rev. Lett.* **2016**, *116*, 106404.

(3) Beard, M. C.; Luther, J. M.; Semonin, O. E.; Nozik, A. J. *Acc. Chem. Res.* **2013**, *46*, 1252.

(4) Klimov, V. I.; Mikhailovsky, A. A.; McBranch, D. W.; Leatherdale, C. A.; Bawendi, M. G. *Science* **2000**, *287*, 1011.

(5) Park, Y.-S.; Bae, W. K.; Pietryga, J. M.; Klimov, V. I. *ACS Nano* **2014**, *8*, 7288.

(6) Klimov, V. I.; McBranch, D. W. *Phys. Rev. Lett.* **1998**, *80*, 4028.

(7) Neuhauser, R. G.; Shimizu, K. T.; Woo, W. K.; Empedocles, S. A.; Bawendi, M. G. *Phys. Rev. Lett.* **2000**, *85*, 3301.

(8) Padilha, L. A.; Robel, I.; Lee, D. C.; Nagpal, P.; Pietryga, J. M.; Klimov, V. I. *ACS Nano* **2011**, *5*, 5045.

(9) Bae, W. K.; Park, Y.-S.; Lim, J.; Lee, D.; Padilha, L. A.; McDaniel, H.; Robel, I.; Lee, C.; Pietryga, J. M.; Klimov, V. I. *Nat. Commun.* **2013**, *4*, 2661.

(10) Klimov, V. I.; Mikhailovsky, A. A.; Xu, S.; Malko, A.; Hollingsworth, J. A.; Leatherdale, C. A.; Eisler, H.-J.; Bawendi, M. G. *Science* **2000**, *290*, 314.

(11) Michler, P.; Imamoğlu, A.; Mason, M. D.; Carson, P. J.; Strouse, G. F.; Buratto, S. K. *Nature* **2000**, *406*, 968.

(12) Efros, A. L.; Rosen, M. *Phys. Rev. Lett.* **1997**, *78*, 1110.

(13) Nirmal, M.; Dabbousi, B. O.; Bawendi, M. G.; Macklin, J. J.; Trautman, J. K.; Harris, T. D.; Brus, L. E. *Nature* **1996**, *383*, 802.

(14) Frantsuzov, P. A.; Volkán-Kacso, S.; Janko, B. *Phys. Rev. Lett.* **2009**, *103*, 207402.

(15) Yuan, G.; Gómez, D. E.; Kirkwood, N.; Boldt, K.; Mulvaney, P. *ACS Nano* **2018**, *12*, 3397.

(16) Yuan, G.; Ritchie, C.; Ritter, M.; Murphy, S.; Gómez, D. E.; Mulvaney, P. *J. Phys. Chem. C* **2018**, *122*, 13407.

(17) Frantsuzov, P. A.; Marcus, R. A. *Phys. Rev. B* **2005**, *72*, 155321.

(18) Galland, C.; Ghosh, Y.; Steinbruck, A.; Sykora, M.; Hollingsworth, J. A.; Klimov, V. I.; Htoon, H. *Nature* **2011**, *479*, 203.

(19) Yarita, N.; Tahara, H.; Saruyama, M.; Kawawaki, T.; Sato, R.; Teranishi, T.; Kanemitsu, Y. *J. Phys. Chem. Lett.* **2017**, *8*, 6041.

(20) Halder, A.; Pathoor, N.; Chowdhury, A.; Sarkar, S. K. *J. Phys. Chem. C* **2018**, *122*, 15133.

(21) Aboma Merdasa; Tian, Y.; Camacho, R.; Dobrovolsky, A.; Debroye, E.; Unger, E. L.; Hofkens, J.; Sundström, V.; Scheblykin, I. G. *ACS Nano* **2017**, *11*, 5391.

(22) Pathoor, N.; Halder, A.; Mukherjee, A.; Mahato, J.; Sarkar, S. K.; Chowdhury, A. *Angew.Chem.* **2018**, *130*, 11777.

(23) Yuan, H.; Debroye, E.; Caliandro, G.; Janssen, K. P. F.; Loon, J. v.; Kirschhock, C. E. A.; Martens, J. A.; Hofkens, J.; Roeffaers, M. B. J. *ACS Omega* **2016**, *1*, 148.

(24) Swarnkar, A.; Marshall, A. R.; Sanehira, E. M.; Chernomordik, B. D.; Moore, D. T.; Christians, J. A.; Chakrabarti, T.; Luther, J. M. *Science* **2016**, *354*, 92.

(25) Song, J.; Li, J.; Li, X.; Xu, L.; Dong, Y.; Zeng, H. *Adv. Mater.* **2015**, *27*, 7162.

(26) Yakunin, S.; Protesescu, L.; Krieg, F.; Bodnarchuk, M. I.; Nedelcu, G.; Humer, M.; Luca, G. D.; Fiebig, M.; Heiss, W.; Kovalenko, M. V. *Nat. Commun.* **2015**, *6*, 8056.

(27) Ramasamy, P.; Lim, D.-H.; Kim, B.; Lee, S.-H.; Lee, M.-S.; Lee, J.-S. *Chem. Commun.* **2016**, *52*, 2067.

(28) Pan, J.; Quan, L. N.; Zhao, Y.; Peng, W.; Murali, B.; Sarmah, S. P.; Yuan, M.; Sinatra, L.; Alyami, N. M.; Liu, J.; Yassitepe, E.; Yang, Z.; Voznyy, O.; Comin, R.; Hedhili, M. N.; Mohammed, O. F.; Lu, Z. H.; Kim, D. H.; Sargent, E. H.; Bakr, O. M. *Adv. Mater.* **2016**, *28*, 8718.

(29) Protesescu, L.; Yakunin, S.; Bodnarchuk, M. I.; Krieg, F.; Caputo, R.; Hendon, C. H.; Yang, R. X.; Walsh, A.; Kovalenko, M. V. *Nano Lett.* **2015**, *15*, 3692.

(30) Park, Y.-S.; Guo, S.; Makarov, N. S.; Klimov, V. I. *ACS Nano* **2015**, *9*, 10386.

(31) Canneson, D.; Shornikova, E. V.; Yakovlev, D. R.; Rogge, T.; Mitioglu, A. A.; Ballottin, M. V.; Christianen, P. C. M.; Lhuillier, E.; Bayer, M.; Biadala, L. *Nano Lett.* **2017**, *17*, 6177.

(32) Rainò, G.; Nedelcu, G.; Protesescu, L.; Bodnarchuk, M. I.; Kovalenko, M. V.; Mahrt, R. F.; Stöferle, T. *ACS Nano* **2016**, *10*, 2485.

(33) Hu, F.; Zhang, H.; Sun, C.; Yin, C.; Lv, B.; Zhang, C.; Yu, W. W.; Wang, X.; Zhang, Y.; Xiao, M. *ACS Nano* **2015**, *9*, 12410.

(34) Kang, J.; Wang, L.-W. *J. Phys. Chem. Lett.* **2017**, *8*, 489.

(35) Dirin, D. N.; Protesescu, L.; Trummer, D.; Kochetygov, I. V.; Yakunin, S.; Krumeich, F.; Stadie, N. P.; Kovalenko, M. V. *Nano Lett.* **2016**, *16*, 5866.

(36) Mondal, N.; Samanta, A. *Nanoscale* **2017**, *9*, 1878.

(37) Walsh, A.; Scanlon, D. O.; Chen, S.; Gong, X. G.; Wei, S.-H. *Angew. Chem. Int. Ed.* **2015**, *54*, 1791.

(38) Seth, S.; Mondal, N.; Patra, S.; Samanta, A. *J. Phys. Chem. Lett.* **2016**, *7*, 266.

(39) Hu, F.; Yin, C.; Zhang, H.; Sun, C.; Yu, W. W.; Zhang, C.; Wang, X.; Zhang, Y.; Xiao, M. *Nano Lett.* **2016**, *16*, 6425−6430.

(40) Yarita, N.; Tahara, H.; Ihara, T.; Kawawaki, T.; Sato, R.; Saruyama, M.; Teranishi, T.; Kanemitsu, Y. *J. Phys. Chem. Lett.* **2017**, *8*, 1413−1418.

(41) Makarov, N. S.; Guo, S.; Isaienko, O.; Liu, W.; Robel, I.; Klimov, V. I. *Nano Lett.* **2016**, *16*, 2349.

(42) Gibson, N. A.; Koscher, B. A.; Alivisatos, A. P.; Leone, S. R. *J. Phys. Chem. C* **2018**, *122*, 12106−12113.

(43) Swarnkar, A.; Chulliyil, R.; Ravi, V. K.; Irfanullah, M.; Chowdhury, A.; Nag, A. *Angew. Chem.* **2015**, *127*, 15644.

(44) Zhang, A.; Dong, C.; Ren, J. *J. Phys. Chem. C* **2017**, *121*, 13314.

(45) Seth, S.; Samanta, A. *Sci. Rep.* **2016**, *6*, 37693.

(46) Barkhouse, D. A. R.; Pattantyus-Abraham, A. G.; Levina, L.; Sargent, E. H. *ACS Nano* **2008**, *2*, 2356.

(47) Cao, J.; Yin, J.; Yuan, S.; Zhao, Y.; Li, J.; Zheng, N. *Nanoscale* **2015**, *7*, 9443.

(48) Ruan, L.; Shen, W.; Wang, A.; Zhou, Q.; Zhang, H.; Deng, Z. *Nanoscale* **2017**, *9*, 7252.

(49) Roo, J. D.; Ibáñez, M.; Geiregat, P.; Nedelcu, G.; Walravens, W.; Maes, J.; Martins, J. C.; Driessche, I. V.; Kovalenko, M. V.; Hens, Z. *ACS Nano* **2016**, *10*, 2071.

(50) Chirvony, V. S.; González-Carrero, S.; Suárez, I.; Galian, R. E.; Sessolo, M.; Bolink, H. J.; Martínez-Pastor, J. P.; Pérez-Prieto, J. *J. Phys. Chem. C* **2017**, *121*, 13381.

(51) Wang, J.; Ding, T.; Leng, J.; Jin, S.; Wu, K. *J. Phys. Chem. Lett.* **2018**, *9*, 3372.

(52) Yettapu, G. R.; Talukdar, D.; Sarkar, S.; Swarnkar, A.; Nag, A.; Ghosh, P.; Mandal, P. *Nano Lett.* **2016**, *16*, 4838.

(53) Mosconi, E.; Angelis, F. D. *ACS Energy Lett.* **2016**, *1*, 182.

(54) Ahmed, T.; Seth, S.; Samanta, A. *Chem. Mater.* **2018**, *30*, 3633.

(55) Kuno, M.; Fromm, D. P.; Hamann, H. F.; Gallagher, A.; Nesbitt, D. J. *J. Chem. Phys.* **2000**, *112*, 3117.

(56) Tang, J.; Marcus, R. A. *J. Chem. Phys.* **2005**, *123*, 054704.

(57) Peterson, J. J.; Nesbitt, D. J. *Nano Lett.* **2009**, *9*, 338.

(58) Shimizu, K. T.; Neuhauser, R. G.; Leatherdale, C. A.; Empedocles, S. A.; Woo, W. K.; Bawendi, M. G. *Phys. Rev. B* **2001**, *63*, 205316.

Chapter 5

Fluorescent Phase-Pure Zero-Dimensional Perovskite-Related Cs_4PbBr_6 Microdisks: Synthesis and Single-Particle Imaging Study

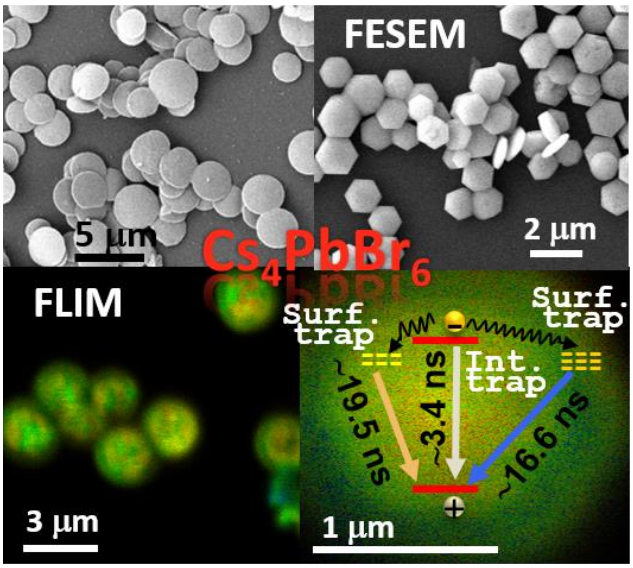

Abstract.

Quantum-confined perovskites are a new class of promising materials in optoelectronic applications. In this context, zero-dimensional perovskite related substance, Cs_4PbBr_6, having high exciton binding energy can be an important candidate, but its photoluminescence (PL) is a topic of recent debate. Herein, we report an ambient condition controlled synthesis of Cs_4PbBr_6 microdisks of different shapes and dimensions, which exhibit fairly strong green PL (quantum yield up to 38%, band gap ~ 2.43 eV) in the solid state. Using confocal fluorescence microscopy imaging of the single particles, we show that the fluorescence of Cs_4PbBr_6 microdisks is inherent to these particles. Fluorescence intensity and lifetime imaging of the microdisks reveals significant spatial heterogeneity with a bright central area and somewhat dimmer edges. This intensity and lifetime distribution is attributed to enhanced trap-mediated nonradiative deactivation at the edges compared to the central region of the microdisks. Our results, which unambiguously establish PL of these Cs_4PbBr_6 and suggest its possible origin, brighten the potential of these materials in photon-emitting applications.

5.1. Introduction

All-inorganic, cesium lead halide perovskites, have become a new milestone in optoelectronic applications involving solar cells, LEDs, lasers and photodetectors, within a very short span of time because of their versatile optical and electronic properties, such as broad and intense absorption, narrow emission, tunable band gap, high photoluminescence quantum yield, low trap state density and high charge carrier mobility.[1-7] $CsPbX_3$ (X = Cl, Br, I), which is the most common material used in such applications, has a cubic crystal phase, where $[PbX_6]^{4-}$ octahedra form a 3-dimensional (3-D) framework by corner-sharing connectivity and Cs^+ cations occupy the octahedral voids.[6] Pb^{2+} and X^- primarily contribute to the low-lying electronic energy states of the valence and conduction bands and the connectivity of the $[PbX_6]^{4-}$ octahedra determines the band gap and hence, the optical properties of the materials.[6,8] When the size of the crystal is lower than the Bohr radius in any direction, it becomes quantum confined in that direction and determines its dimensionality. These structures are better represented by a generalized formulae of Cs_nPbX_{2+n} (n = 1 - 4) for the perovskite materials. By careful selection of the organic capping ligands and reaction conditions, the perovskite structures can be tuned from 3-D nanocubes (n = 1) to 2-D nanoplates (n = 2) to 1-D nanowires (NWs, n = 3) to 0-D dots (n = 4), where $[PbX_6]^{4-}$ octahedra connect themselves to form a layered structure in NPLs, a chain network in NWs and a cluster in dots.[9-15]

Crystals wherein the individual $[PbX_6]^{4-}$ octahedra are not directly connected to each other are termed as 0-D perovskite as the excitons are localized on isolated octahedron.[16-18] Rhombohedral Cs_4PbBr_6 represents such 0-D related structure, where every single $[PbBr_6]^{4-}$ octahedron is separated from each other by CsBr bridges.[17] Because of the confined nature, the exciton binding energy of this material is very high (≥ 170 meV) as compared to the 3-D $CsPbX_3$ nanocrystals (NCs) (~ 40 meV).[6,16,17] Even though extensive studies have been made on higher dimensional lead halide perovskites within a few years, very few reports have so far appeared on its 0-D counterpart.[16-22] This material is commonly prepared following a moderate temperature synthesis protocol,[16,19,20] where $CsPbX_3$ is formed as a side product and hinders characterization of the 0-D perovskite related phase. The optical properties of Cs_4PbBr_6, PL in particular, appear to be highly intriguing and two very different views are currently available.[16-22] Mohammed and

coworkers have shown that Cs_4PbBr_6 is highly luminescent (QY= 45-65%) green emitting (515-520 nm) with a band gap of 2.33 eV both in its powder and nanocrystal forms.[16,17] In millimeter-sized single crystals, PL intensity of Cs_4PbBr_6 is found much higher than that of $CsPbBr_3$ with similar band gap.[18] Some other reports also indicate PL of these materials.[19,20,23] Due to high exciton binding energy and PL QY, this material could be an appealing photon emitter. However, a recent work shows that Cs_4PbX_6 NCs (9-37 nm) do not exhibit any PL in the visible region due to high band gap (>3.2 eV).[21] Another work demonstrates ligand-mediated transformation of green emitting $CsPbBr_3$ to nonfluorescent Cs_4PbX_6 NCs without commenting much on the PL of the NCs.[22] Hence, two different types of Cs_4PbX_6 perovskites with different band gap and luminescence property seem to emerge from the recent literature. A very recent report hypothesizes that PL of 0-D perovskite related Cs_4PbX_6 single crystal arises from the mid band gap states formed due to the halogen vacancy.[24]

Here, we report a simple ambient condition synthetic strategy for the preparation of phase-pure Cs_4PbBr_6 microdisks (MDs) using a surfactant mediated anti-solvent precipitation method that allows tuning of the shape and size of the MDs just by varying the surfactant concentration. We prove the intrinsic luminescent nature of the Cs_4PbBr_6 MDs by PL intensity and lifetime imaging of these individual MDs and reveal its spatially resolved PL decay dynamics using time-resolved confocal fluorescence microscopy, a powerful tool for structure-dependent optical characterization of materials.[25]

5.2. Results

5.2.1. Synthesis and morphology tuning

The Cs_4PbBr_6 MDs were synthesized following an anti-solvent precipitation method[14] by adding toluene (anti-solvent) into a vigorously stirring dimethyl formamide (DMF) solution of CsBr, $PbBr_2$ (1:1) and cetyltrimethylammonium bromide (CTAB) (see Appendix III for details), where CTAB acts as a capping ligand and growth directing template. Addition of toluene induces CTAB-mediated formation of micelle inside which crystallization of the MDs takes place due to supersaturation. The amount of added anti-solvent controls the growth kinetics, size distribution and optical properties of the MDs.

An optimum CTAB (0.1 mM) concentration is found to result in the formation of well-shaped hexagonal disks. Figure 5.1a and d show the transmission electron microscopy (TEM) and field emission scanning electron microscopy (FESEM) images of these MDs, having a diameter of 1 - 2 μm and thickness of 100 - 300 nm (Figure AIII.1, Appendix III). High resolution TEM (HRTEM) image shows (Figure 5.1b, Figure AIII.2, Appendix III) that the MDs are bound by (110) and (300) planes in the in-plane and side-plane facets as evident from the lattice fringes of the two respective planes. Selected area electron diffraction (SAED) pattern (Figure 5.1c) demonstrates the single-crystalline nature of the MDs with diffraction spots corresponding to (110) and (300) planes. Elemental ratio of Cs:Pb:Br of individual MDs as obtained from energy dispersive X-ray (EDX) spectroscopy (Figure 5.1e) is found to be 4.2:1:6.3 confirming the Cs_4PbBr_6 composition. Measurements on several such MDs show the consistency of the result. Presence of nitrogen and little excess of Br confirms that the MDs are capped with CTAB surfactants. The elemental mapping (Figure 5.1e) shows that individual constituent elements are uniformly distributed throughout the disk. Furthermore, powder X-ray diffraction (PXRD) pattern establishes that the obtained MDs are phase-pure rhombohedral Cs_4PbBr_6 perovskite. The SAED and PXRD pattern shows that the MDs are free from any traceable impurity of other compositions such as $CsPbBr_3$.[16,20]

Morphology of these Cs_4PbBr_6 MDs can be tuned easily by varying the concentration of CTAB in the precursor solution. Large spherical disks of 2 to 4 μm diameter and 30 to 60 nm thickness are formed (Figure 5.1f and AIII.3, Appendix III) in the presence of a lower amount of CTAB (0.05 mM). SAED pattern of the spherical MDs are found similar to those of the hexagonal ones indicating similar single-crystalline nature (Figure AIII.3b, Appendix III). PXRD, EDX and elemental mapping confirm the Cs_4PbBr_6 composition of these MDs (Figure 5.1g and AIII.3, Appendix III).

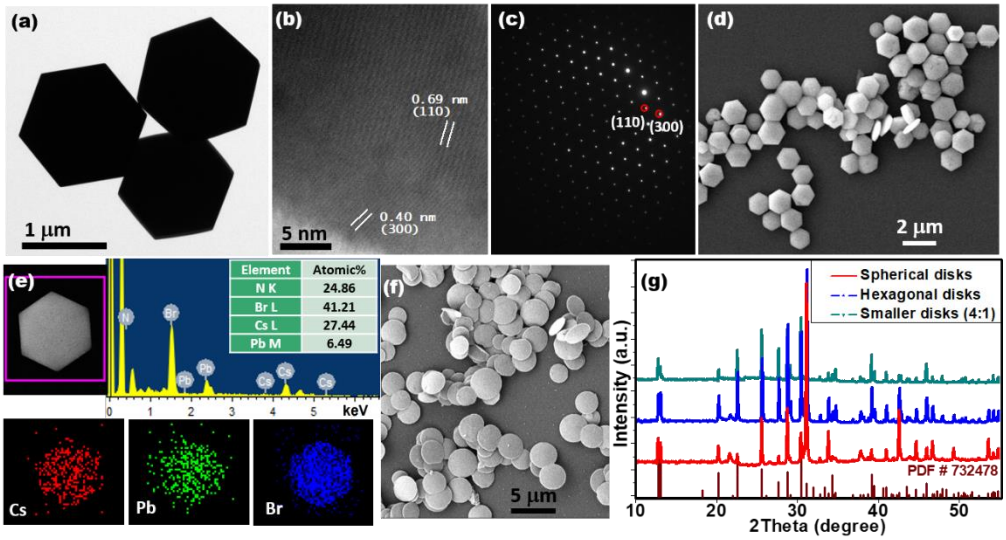

Figure 5.1. (a) TEM image of the Cs_4PbBr_6 microdisks. (b) HRTEM image showing two different planes with their lattice fringes corresponding to (110) and (300) facets. (c) SAED pattern of a single MD showing different planes by encircled spots. (d) FESEM image of the hexagonal MDs. (e) EDX spectrum and elemental mapping show Cs_4PbBr_6 composition and distribution of the elements throughout the disk. (f) FESEM image of the spherical MDs. (g) Powder XRD pattern of different morphologies with the standard reference of rhombohedral Cs_4PbBr_6. JCPDS no. 73-2478.

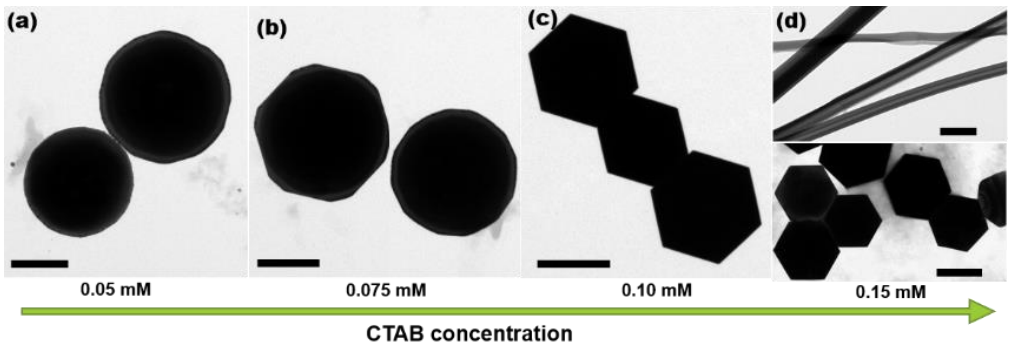

Figure 5.2. CTAB concentration dependent morphology evolution of Cs_4PbBr_6 perovskite MDs, (a) 0.05 mM, (b) 0.075 mM, (c) 0.1 mM and (d) ≥1.5 mM. Scale bar is 1 µm in all TEM images. Two images in the d panel are taken from the different places of the same sample.

Figure 5.2 depicts a series of TEM images of the particles formed for different CTAB concentrations. The shape and size of the MDs indicate two growth directions. As the MDs are bound by (110) and (300) crystal planes in the in-plane and side-plane facets (Figure 5.1b) and the disks have a larger diameter (μm) than the thickness (nm), it is evident that CTAB molecules preferentially bind to the (110) plane as compared to the (300) plane and restrict its growth. For a higher concentration (0.1 mM), CTAB binds to both planes giving a proper hexagonal structure with sharp edges (Figure 5.2c). Even though the $PbBr_6^{4-}$ octahedra in Cs_4PbBr_6 are isolated, the intervening Cs^+ ions bind to the adjacent octahedral units to form a hexagonal structure.[17,21] For a lower concentration of CTAB (0.05 mM), the ligands bind mostly to the (110) plane and hence, growth along other direction becomes spontaneous and faster resulting in a spherical MD of larger size (2-4 μm) and lesser thickness (30-60 nm) (Figure 5.2a and AIII.3, Appendix III). For intermediate CTAB concentration (0.075 mM), formation of polygonal disks (angle >6) tending towards the spherical one (Figure 5.2b) is in agreement with the above interpretation. Formation of wires of micrometer size along with hexagonal MDs (Figure 5.2d) is observed upon increasing the CTAB concentration to saturation level (≥1.5 mM) in the precursor solution. These microwires could be a new material of $CsPb_2Br_5$ composition (Figure AIII.6, Appendix III) that calls for a detailed structural and optical characterization that will be taken up separately. Unlike the higher dimensional perovskites, our MDs are quite robust against degradation for several months when stored at ambient condition of ~ 30 % relative humidity.

Instead of using a precursor solution with 1:1 molar ratio of CsBr and $PbBr_2$ (results discussed above) for the synthesis of Cs_4PbBr_6 MDs, we have also experimented with a few other CsBr/$PbBr_2$ precursor ratios (2:1 and 4:1). Obtained particles and their characteristics are presented in Appendix III.

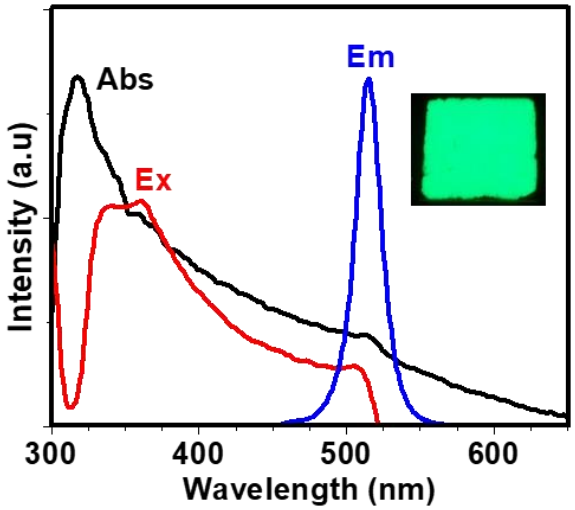

Figure 5.3. Absorption, PL excitation (λ_{em} = 515 nm) and PL spectra (λ_{exc} = 405 nm) of hexagonal Cs_4PbBr_6 MDs. Inset shows the digital image of a thin film sample under 365 nm UV lamp illumination.

5.2.2. Optical properties and PL imaging

The as-synthesized Cs_4PbBr_6 MDs are highly luminescent green-emitting material. Figure 5.3 depicts steady state UV-vis absorption, excitation and PL spectra of the hexagonal MDs. The peak of the narrow PL spectrum appears at 515 nm (2.41 eV) with an fwhm of 21 nm. The absorption spectrum exhibits a hump around 512 nm (2.42 eV) followed by a strong peak at 318 nm. The PL excitation spectrum which shows a peak at 507 nm (2.44 eV) matches well with the absorption hump indicating band edge type absorption of photons. Even though two spectra differ in the short wavelength region (which is quite common for most samples), they match well with earlier reports on Cs_4PbBr_6 powder and NCs.[16,17] Based on the absorption and PL excitation data the band gap is estimated to be ~2.43 eV. The PL peak appears at 515 nm, typical for a semiconductor material of band gap of ~2.4 eV. PL QY of this material is measured to be as high as 38%, which however, can vary depending on the amount of anti-solvent used in the synthesis. Larger amount of anti-solvent destabilizes the precursor solution leading to uncontrolled micelle formation, yielding MDs with a wider distribution of size and low PL QY (Figure AIII.7, Appendix III). As best quality of MDs are obtained with 4:1 precursor solution to anti-solvent ratio, we consider this as the optimum. Optical properties

of the spherical MDs are quite similar to those of the hexagonal ones except a small (~3 nm) red-shift in their absorption, excitation and PL spectra (Figure AIII.8, Appendix III) and little less PL QY (up to 30%). This could be due to the larger size of the spherical MDs. These PL QY values are quite high considering that even highly luminescent perovskite NCs exhibit a much reduced PL QY value in their thin film form.[26]

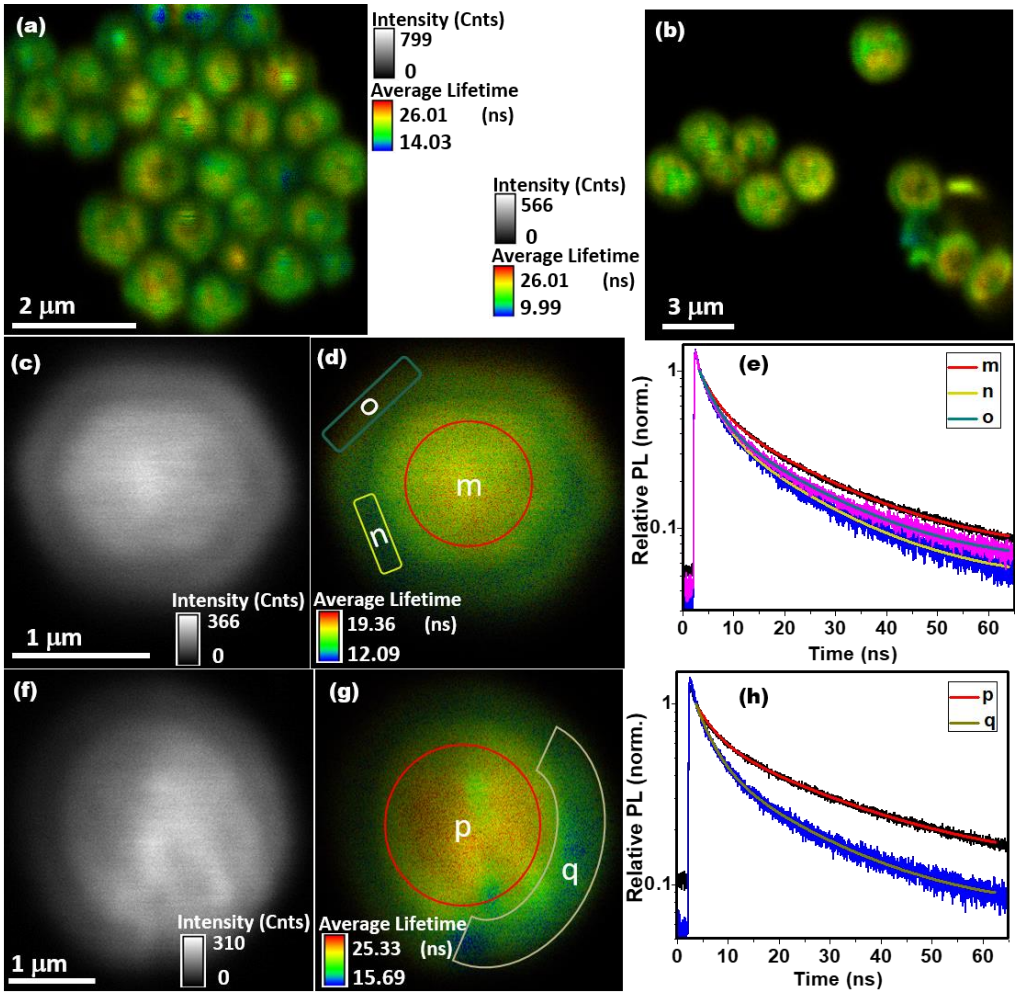

Figure 5.4. Fluorescence intensity and lifetime images of Cs_4PbBr_6 MDs showing the spatial variation. FLIM images of (a) hexagonal and (b) spherical MDs. (c, f) PL intensity, (d, g) FLIM images and (e, h) local time-resolved PL decay curves of marked places of a single hexagonal and spherical MDs respectively. Excitation source was 485 nm pulsed laser operated at 60 nW optical power and 10 MHz repetition rate.

5.3. Discussion

The PL of the 0-D Cs_4PbBr_6 perovskite is a controversial topic.[21,27] Though majority of the reports confirm PL of the material,[16-20,23] its origin is doubted very recently and PL is attributed to the presence of trace amount of highly fluorescent $CsPbBr_3$ NCs in the samples that cannot be detected by PXRD measurements.[21,28] Until now, all photophysical measurements on the 0-D Cs_4PbBr_6 perovskite were performed in the ensemble level, which often do not provide clear evidence of the identity of actual emitter. In order to resolve this issue we focus on fluorescence imaging of Cs_4PbBr_6 MDs down to the single particle level using steady state and time-resolved confocal fluorescence microscopy techniques. Figure 5.4 demonstrates FLIM (a, b, d, g) and fluorescence intensity (c, f) images of the as-synthesized Cs_4PbBr_6 MDs. Additional images are provided in the Appendix III (Figure AIII.9 and AIII.10, Appendix III). The images of the individual particles show that the fluorescence photons are emitted from the entire exposed area of the particles suggesting that PL is not due to small quantity of impurity localized in some specific places of the MDs. The presence of a larger quantity of impurity can of course show a similar kind of PL image, but in that case the impurity should have been detected easily in PXRD or SAED measurements (which however show purely Cs_4PbBr_6 crystal signature).[24] Hence, we confirm that green emission is intrinsic to the Cs_4PbBr_6 MDs and it does not originate from any undesired species.

As a mixture of Cs_4PbBr_6 MDs and $CsPb_2Br_5$ microwires are formed at high CTAB concentrations (Figure AIII.6, Appendix III) and the latter is non-luminescent,[29] one expects to observe only the MDs on fluorescence imaging of the mixed samples. However, if any small quantity of highly luminescent $CsPbBr_3$ is also formed as side product in the process and is distributed among all particles, then both Cs_4PbBr_6 MDs and $CsPb_2Br_5$ microwires should be visible. The observation of only the MDs (Figure 5.5a) clearly proves that $CsPbBr_3$ is not formed and the luminescence of the MDs are inherent to Cs_4PbBr_6 only.

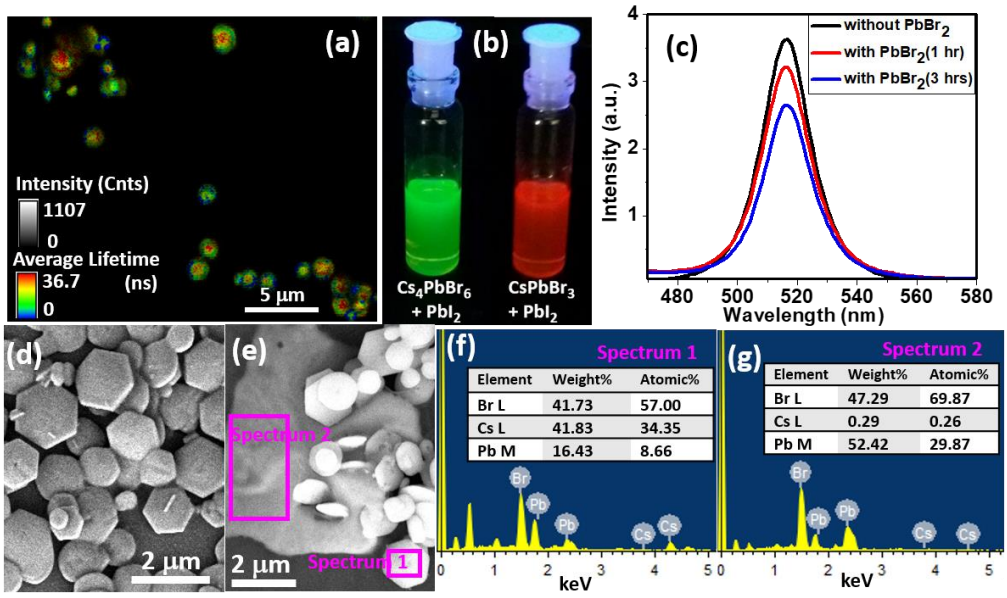

Figure 5.5. (a) Fluorescence image of the coexisting MDs and microwire sample. (b) Digital images of photo-illuminated (365 nm) Cs_4PbBr_6 and $CsPbBr_3$ perovskite solutions after addition of PbI_2. (c) Change in emission spectrum (λ_{exc} = 405 nm) with time of a toluene dispersion of Cs_4PbBr_6 MDs. (d,e) FESEM images and (f,g) EDX spectra of different regions (marked) of $PbBr_2$ solution (in DMF) added sample of Cs_4PbBr_6.

To further substantiate our claim we have performed halide exchange experiment on $CsPbBr_3$ and Cs_4PbBr_6 considering that this exchange is facile at room temperature for $CsPbBr_3$ but not for Cs_4PbBr_6 perovskite material.[14,17,30] We have used lead iodide dissolved in DMF as the source of iodine. Addition of PbI_2 leads to immediate change of PL of the $CsPbBr_3$ solution from green to red due to formation of $CsPbI_3$,[14,30] but the PL of the Cs_4PbBr_6 solution remains unaffected (Figure 5.5b).[17] Had there been a trace amount of $CsPbBr_3$ present as impurity in Cs_4PbBr_6 and was responsible for the PL of latter, a similar green to red PL change was expected on addition of PbI_2. Thus we prove that our method produces phase-pure Cs_4PbBr_6 crystals and the green PL is intrinsic to this material.

Furthermore, we have checked the phase and dimensionality transformation of Cs_4PbBr_6 by adding DMF solution of $PbBr_2$ into the MDs dispersion.[21] It is evident from FESEM images and EDX spectra (Figure 5.5) that the individual particles retain their

shapes, sizes and composition in the presence of $PbBr_2$. EDX spectrum of the chosen MD confirms the Cs_4PbBr_6 composition, whereas the bulk like substance is found to be $PbBr_2$ (Figure 5.5e, f). If any trace amount of $CsPbBr_3$ impurity in Cs_4PbBr_6 MDs was the origin of PL, an enhancement in PL intensity and change in elemental composition would have been observed in the case of transformation of Cs_4PbBr_6 into $CsPbBr_3$, which, however, is not the case. In fact, a small and slow decrease in PL intensity with time is observed (Figure 5.5c), which we attribute to polar DMF-assisted defect generation. Thus, we affirm that no coexisting $CsPbBr_3$ is the source of PL of the Cs_4PbBr_6 MDs, and these MDs are inherently luminescent and structurally different from the nonluminescent Cs_4PbBr_6 nanocrystals.

FLIM study along with PL intensity images (Figure 5.4) provide deep insight into the excitonic recombination dynamics of the MDs. Spatial distribution of PL intensity on the MDs is clearly not uniform. The intensity at the central region is much higher (~ 2.5 fold) as compared to the edges. This spatial variation of PL intensity is a reflection of the variation of local nonradiative recombination rates suggesting more surface defects towards the edges. Spatially distributed false color coding of the FLIM images reveals significant lifetime heterogeneity on the MDs, which is greater for the spherical one (Figure 5.4). In order to obtain a quantitative estimate of lifetime distribution we have constructed local PL decay curves of the marked areas on magnified single particle images (Figure 5.4d-e, g-h). These decay curves are best represented by a biexponential function (Chapter 2) and the results are collected in Table 5.1. These images and the data presented in Table 5.1 show that the central position of the MDs (area-m) has higher average lifetime as compared to the edges (area-n). Since the hexagonal MDs have substantial thickness, the emission from area-o can be assumed to originate from the side plane of the disk. The PL lifetime of this region is found to be intermediate between thosefrom the other two places (area-m, n). Fluorescence intensity and lifetime imaging of > 20 single MDs of each type shows a similar trend (few are shown in Appendix III). Individual lifetime components are averaged and shown along with their mean deviations in Table AIII.1, Appendix III.

Table 5.1. Local PL decay parameters of different regions of the two MDs shown in Figure 5.4.[#]

Sample	Positions	$\tau_1(\alpha_1)$ (ns)	τ_2 (α_2) (ns)	$\langle\tau\rangle$ (ns)
Hexagonal disk	area-m	3.44 (0.47)	19.49 (0.53)	11.95
	area-n	3.31 (0.57)	17.23 (0.43)	9.26
	area-o	3.29 (0.54)	18.00 (0.46)	10.03
Spherical disk	area-p	3.70 (0.40)	25.31 (0.60)	16.61
	area-q	3.43 (0.57)	19.46 (0.43)	10.37

Here, τ_i's and α_i's are the lifetimes and associated exponents. $\langle\tau\rangle$ is the amplitude-averaged lifetime.

As in Cs_4PbBr_6 crystal the $PbBr_6$ octahedral units are spatially isolated, they endow a large band gap (≥ 3.8 eV) and cannot show green PL.[21,24] However, we have convincingly shown that the observed green PL is intrinsic to the Cs_4PbBr_6 MDs. This apparent contradiction can only be resolved if the PL is due to the recombination from the mid-band gap states arising from the crystal defects (quite common for the perovskite materials).[31-33] This is indeed confirmed in a recent report on Cs_4PbBr_6 single crystal.[24] Considering this we speculate that the observed PL intensity and lifetime distribution on the MDs is a result of charge carrier recombination from the trap states located on the interior and surface of the MDs. Of the two lifetime components, the shorter one (~3.4 ns) does not vary much with change in position or disk unlike the longer component (Table 5.1 and Appendix III). Considering high exciton binding energy of these materials[16,17,24] and consistency of the value over the MDs, we ascribe the short lifetime component to the trapped exciton recombination inside the crystal and the long one to surface energy state mediated recombination (Figure 5.6). A relatively lower value of the long component towards the dim edges is presumably the reflection of a higher density of surface trap-

states as compared to the bright region, which is mostly populated by the interior trap-states (Figure 5.6). A close look at the exponents (α_i) associated with the lifetime components (τ_i) (Table 5.1 and Appendix III) also shows a progressive increase in deep-trap mediated nonradiative deactivation rather than trap assisted radiative recombination as one moves towards the edges. In these materials, the trap states presumably arise from Br^- vacancy, which generally leads to formation of trap states near the conduction band.[33] Therefore, we attribute the observed trap-states to the electron-traps in the present case.

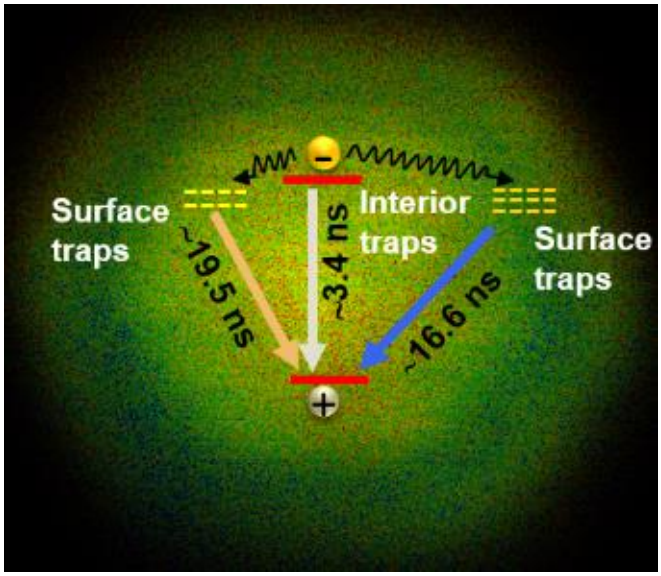

Figure 5.6. Schematic illustration of the spatially resolved PL decay components across the MD. The lifetimes shown in the Scheme are averaged values for twenty different hexagonal MDs.

The above PL decay dynamics (Figure 5.6) is further corroborated by analyzing the moisture-degraded MDs using FESEM and FLIM measurements. Exposure of the spherical MDs at ambient condition to ~60-65% humidity for 2 to 3 weeks leads to etching of the surface (Figure AIII.11a, Appendix III) and opens additional nonradiative decay channels resulting in a substantial enhancement of PL lifetime heterogeneity across the disk (Figure AIII.11b, Appendix III). The lifetime data of these samples (Table AIII.2, Appendix III) is consistent with our interpretation.

5.4 Conclusion

We report the first surfactant mediated synthesis of phase-pure Cs_4PbBr_6 MDs. The method provides a simple and convenient route to tuning the morphology of Cs_4PbBr_6 MDs, including synthesis of a new class of perovskite related $CsPb_2Br_5$ microwires. Fluorescence imaging studies down to the single particle level confirm the intrinsic PL of the MDs. PL imaging of the individual MDs reveals a spatial distribution of intensity and lifetime. The more fluorescent central region of the MDs shows slower PL decay compared to the edges due to lower density of the nonradiative trap states. Unlike the higher dimensional perovskites, this material shows resistance to anion exchange, and phase and dimensionality transformation due to strong interaction among the constituting elements. The present study, which provides a clear understanding of the structural and photophysical properties of the 0-D perovskite related Cs_4PbBr_6 material involving local charge recombination dynamics is likely to help realization of the true potential of these substances in practical applications.

References

(1) Swarnkar, A.; Marshall, A. R.; Sanehira, E. M.; Chernomordik, B. D.; Moore, D. T.; Christians, J. A.; Chakrabarti, T.; Luther, J. M. *Science* **2016**, *354*, 92.

(2) Song, J.; Li, J.; Li, X.; Xu, L.; Dong, Y.; Zeng, H. *Adv. Mater.* **2015**, *27*, 7162.

(3) Yakunin, S.; Protesescu, L.; Krieg, F.; Bodnarchuk, M. I.; Nedelcu, G.; Humer, M.; Luca, G. D.; Fiebig, M.; Heiss, W.; Kovalenko, M. V. *Nat. Commun.* **2015**, *6*, 8056.

(4) Zhang, Q.; Su, R.; Liu, X.; Xing, J.; Sum, T. C.; Xiong, Q. *Adv. Funct. Mater.* **2016**, *26*, 6238.

(5) Ramasamy, P.; Lim, D.-H.; Kim, B.; Lee, S.-H.; Leeb, M.-S.; Lee, J.-S. *Chem. Commun.* **2016**, *52*, 2067.

(6) Protesescu, L.; Yakunin, S.; Bodnarchuk, M. I.; Krieg, F.; Caputo, R.; Hendon, C. H.; Yang, R. X.; Walsh, A.; Kovalenko, M. V. *Nano Lett.* **2015**, *15*, 3692.

(7) Yettapu, G. R.; Talukdar, D.; Sarkar, S.; Swarnkar, A.; Nag, A.; Ghosh, P.; Mandal, P. *Nano Lett.* **2016**, *16*, 4838.

(8) Saparov, B.; Mitzi, D. B. *Chem. Rev.* **2016**, *116*, 4558−4596.

(9) Akkerman, Q. A.; Motti, S. G.; Kandada, A. R. S.; Mosconi, E.; D'Innocenzo, V.; Bertoni, G.; Marras, S.; Kamino, B. A.; Miranda, L.; Angelis, F. D.; Petrozza, A.; Prato, M.; Manna, L. *J. Am. Chem. Soc.* **2016**, *138*, 1010.

(10) Bekenstein, Y.; Koscher, B. A.; Eaton, S. W.; Yang, P.; Alivisatos, A. P. *J. Am. Chem. Soc.* **2015**, *137*, 16008.

(11) Weidman, M. C.; Seitz, M.; Stranks, S. D.; Tisdale, W. A. *ACS Nano* **2016**, *10*, 7830.

(12) Imran, M.; Stasio, F. D.; Dang, Z.; Canale, C.; Khan, A. H.; Shamsi, J.; Brescia, R.; Prato, M.; Manna, L. *Chem. Mater.* **2016**, *28*, 6450.

(13) Amgar, D.; Stern, A.; Rotem, D.; Porath, D.; Etgar, L. *Nano Lett.* **2017**, *17*, 1007−1013.

(14) Seth, S.; Samanta, A. *Sci. Rep.* **2016**, *6*, 37693.

(15) Sun, S.; Yuan, D.; Xu, Y.; Wang, A.; Deng, Z. *ACS Nano* **2016**, *10*, 3648.

(16) Saidaminov, M. I.; Almutlaq, J.; Sarmah, S.; Dursun, I.; Zhumekenov, A. A.; Begum, R.; Pan, J.; Cho, N.; Mohammed, O. F.; Bakr, O. M. *ACS Energy Lett.* **2016**, *1*, 840.

(17) Zhang, Y.; Saidaminov, M. I.; Dursun, I.; Yang, H.; Murali, B.; Alarousu, E.; Yengel, E.; Alshankiti, B. A.; Bakr, O. M.; Mohammed, O. F. *J. Phys. Chem. Lett.* **2017**, *8*, 961.

(18) Cha, J.-H.; Han, J. H.; Yin, W.; Park, C.; Park, Y.; Ahn, T. K.; Cho, J. H.; Jung, D.-Y. *J. Phys. Chem. Lett.* **2017**, *8*, 565.

(19) Chen, D.; Wan, Z.; Chen, X.; Yuan, Y.; Zhong, J. *J. Mater. Chem. C* **2016**, *4*, 10646.

(20) Huang, K.; Li, D.; Yang, L.; Liu, S.; Yang, F. *Journal of Alloys and Compounds* **2017**, *710*, 244.

(21) Akkerman, Q. A.; Park, S.; Radicchi, E.; Nunzi, F.; Mosconi, E.; Angelis, F. D.; Brescia, R.; Rastogi, P.; Prato, M.; Manna, L. *Nano Lett.* **2017**, *17*, 1924.

(22) Liu, Z.; Bekenstein, Y.; Ye, X.; Nguyen, S. C.; Swabeck, J.; Zhang, D.; Lee, S.-T.; Yang, P.; Ma, W.; Alivisatos, A. P. *J. Am. Chem. Soc.* **2017**, *139*, 5309.

(23) Rakita, Y.; Kedem, N.; Gupta, S.; Sadhanala, A.; Kalchenko, V.; Böhm, M. L.; Kulbak, M.; Friend, R. H.; Cahen, D.; Hodes, G. *Cryst. Growth Des.* **2016**, *16*, 5717−5725.

(24) Bastiani, M. D.; Dursun, I.; Zhang, Y.; Alshankiti, B. A.; Miao, X.; Yin, J.; Yengel, E.; Alarousu, E.; Turedi, B.; Almutlaq, J. M.; Saidaminov, M. I.; Mitra, S.; Gereige, I.; Alsaggaf, A.; Zhu, Y.; Han, Y.; Roqan, I. S.; Bredas, J.-L.; Mohammed, O. F.; Bakr, O. M. *Chem. Mater.* **2017**, DOI: 10.1021/acs.chemmater.7b02415.

(25) deQuilettes, D. W.; Vorpahl, S. M.; Stranks, S. D.; Nagaoka, H.; Eperon, G. E.; Ziffer, M. E.; Snaith, H. J.; Ginger, D. S. *Science* **2015**, *348*, 683.

(26) Kim, Y.; Yassitepe, E.; Voznyy, O.; Comin, R.; Walters, G.; Gong, X.; Kanjanaboos, P.; Nogueira, A. F.; Sargent, E. H. *ACS Appl. Mater. Interfaces* **2015**, *7*, 25007.

(27) Nikl, M.; Mihokova, E.; Nitsch, K.; Somma, F.; Giampaolo, C.; Pazzi, G. P.; Fabeni, P.; Zazubovich, S. *Chem. Phys. Lett.* **1999**, *306*, 280.

(28) Li, X.; Cao, F.; Yu, D.; Chen, J.; Sun, Z.; Shen, Y.; Zhu, Y.; Wang, L.; Wei, Y.; Wu, Y.; Zeng, H. *Small* **2017**, 1603996.

(29) Li, G.; Wang, H.; Zhu, Z.; Chang, Y.; Zhang, T.; Song, Z.; Jiang, Y. *Chem. Commun.* **2016**, *52*, 11296.

(30) Nedelcu, G.; Protesescu, L.; Yakunin, S.; Bodnarchuk, M. I.; Grotevent, M. J.; Kovalenko, M. V. *Nano Lett.* **2015**, *15*, 5635.

(31) Seth, S.; Mondal, N.; Patra, S.; Samanta, A. *J. Phys. Chem. Lett.* **2016**, *7*, 266.

(32) Ball, J. M.; Petrozza, A. *Nat. Energy* **2016**, *16149*.

(33) Kang, J.; Wang, L.-W. *J. Phys. Chem. Lett.* **2017**, *8*, 489−493.

Chapter 6

Concluding Remarks

A summary of the results obtained during the course of this thesis work is presented here. The scope of further studies based on the present findings and current literature on the topics is also outlined.

6.1. Overview

This thesis encompasses work on two different crystalline materials of the perovskite community ($CsPbX_3$ and Cs_4PbBr_6) having enormous potential in photovoltaic and optoelectronic applications. These materials with reduced dimensionality possessing quantum confinement and rich surface chemistry are potential light harvester or emitter. However, the performance of these materials is largely controlled by the charge trapping crystal defects. The main objective of this thesis is to understand how the activity of the defects in these substances influences the excited-state charge carrier dynamics in individual particles and for this purpose, we have used three different spectroscopic techniques based on single-particle photoluminescence (PL) of the systems.

As defects give rise to fluctuation of PL in single particles, commonly termed as blinking, one can extract important information on the dynamics of all radiative and nonradiative processes, which follow the photo-excitation of the system, by monitoring blinking of PL. However, depending on the defect concentration and charge trapping efficiency in a particle, blinking can have a time distribution from few microseconds to several seconds and no single experimental technique can cover the entire time window. Hence, we have used multiple techniques. The faster time window (microseconds to few milliseconds) is probed employing fluorescence correlation spectroscopy (FCS) technique on freely diffusing $CsPbBr_3$ and $CsPbBr_2I$ nanocrystals (NCs). PL blinking at longer timescale (millisecond to second) is investigated from the PL intensity-time trace of immobilized $CsPbBr_3$ NCs. For the study of zero-dimensional perovskite-related substance, Cs_4PbBr_6, whose PL is a subject matter of debate, we have utilized fluorescence lifetime imaging microscopy (FLIM) technique. In addition to the time-resolved confocal fluorescence microscope setup, which is used for single particle study, we have used other techniques such as TEM, FESEM, PXRD for structural characterization, UV-visible spectrophotometer, steady state spectroflurimeter and time-correlated single photon counting fluorimeter for basic optical characterization of the materials.

$CsPbBr_3$ NCs are the most stable and luminescent among all the halide variants and well explored in devices. However, PL QY and device effciency of the NCs often vary in different reports suggesting the influence of defects in carrier recombination dynamics.

We have explored the PL behavior of $CsPbBr_3$ NCs as a function of the excitation power employing FCS technique which reveals fluorescence blinking in the microsecond time scale. To understand the effect of alloying with another halide, we have performed a comparative study with $CsPbBr_2I$ NCs. The dispersive nature of the blinking kinetics of both the NCs suggests the existence of a distribution of trap states in these NCs. A faster blinking at higher excitation power is attributed to an enhancement of the contribution of nonradiative Auger recombination process. Photon induced PL enhancement or phtoactivation in these NCs are observed when higher photon flux is used or phtoirradiation is continued for a long time. The photoactivation phenomenon, which is found to be more prominent in the case of $CsPbBr_2I$, appears to be due to structural reorganization as well as filling of the trap states. The observation provides insight into the radiative and nonradiative deactivation pathways of these promising substances.

Having understood the blinking dynamics at faster timescale, we probed a longer time window (millisecond to second) to obtain an in-depth understanding of the carrier recombination dynamics of $CsPbBr_3$ NCs, a comprehensive picture of all possible recombination processes and to provide remedy for the undesired recombination. This study reveals two distinct types of PL fluctuations of the NCs, which we have assigned to flickering and blinking. We found the flickering to be due to excess surface trap on the NCs and show that post-synthetic surface treatment can convert the flickering NCs into the blinking ones with significant enhancement of PL and stability. Intensity correlated lifetime analysis of the PL time-trace reveals both trap-mediated nonradiative band edge carrier recombination and positive trion recombination in single NCs. Dynamical and statistical analysis suggests a diffusive nature of the trap states, which is responsible for the PL intermittency in these systems.

Hence, from the two sets of experiments described above we are able to reveal a complete single particle carrier dynamics of $CsPbBr_3$ NCs. The findings throw light on the nature of the trap states, show the manifestation of these trap states in PL fluctuation and provide an effective way to control the dynamics in these systems.

Quantum-confined semiconductors are promising materials in optoelectronic applications because of their high radiative recombination rate and potential towards nonlinear applications. In this context, zero-dimensional perovskite related substance, Cs_4PbBr_6, having high exciton binding energy can be an important candidate, but its PL is

a topic of recent debate. We have developed a new method for the synthesis of Cs_4PbBr_6 microdisks of different shapes and dimensions, which exhibit fairly strong green PL (QY up to 38%, band gap ~ 2.43 eV) in the solid state. Using confocal fluorescence microscopy imaging of the single particles, we show that the fluorescence of Cs_4PbBr_6 microdisks is inherent to these particles. Fluorescence intensity and lifetime imaging of the microdisks reveals significant spatial heterogeneity with a bright central area and dimmer edges. This intensity and lifetime distribution is attributed to enhanced trap-mediated nonradiative deactivation at the edges compared to the central region of the microdisks. Unlike the higher dimensional perovskites, this material shows resistance to anion exchange, and phase and dimensionality transformation due to strong interaction among the constituting elements. Our results, which unambiguously establish PL of these Cs_4PbBr_6 and suggest its possible origin, brighten the potential of these materials in photon-emitting applications.

6.2. Future scope

Studies presented in the first two working chapters (Chapter 3 and 4) of the thesis demonstrate the methods that one can follow to understand the carrier dynamics of any NC in the single particle level. Herein, as our studies are mostly focused on $CsPbBr_3$ NCs, scope of extending these works to other halide cousins still remains. In this context, it is to be remembered that energy levels of the most abundant defects due to halide vacancies in these NCs vary with the identity of the constituent halide with respect to the band alignment. This suggests that efficiency and time of trapping is dependent on the NCs and hence, the carrier dynamics is expected to be influenced. Therefore, it will be interesting to see the blinking patterns for other $CsPbX_3$ NCs. A detailed analysis may reveal many exciting properties of this class of NCs, which may be helpful in better realization of the true potential of the materials.

The carrier dynamics of a semiconductor often varies with the excitation frequency and photon fluences due to additional linear and nonlinear recombination processes such as multi-exciton generation, Auger recombination, hot carrier trapping, etc. In our FCS study (chapter 3), though we varied the excitation power we did not apply it for the blinking study performed on immobilized NCs (chapter 4). Excitation with higher

energy photons leads to hot carrier generation and relaxation of these carriers may introduce additional recombination channels. Understanding of these processes is very crucial for fabricating efficient devices. Hence, studying hot carrier dynamics of single particles by varying excitation wavelength will be an important direction towards materials development.

The operating conditions of devices made of these NCs are different from the spectroscopic measurement conditions. As for example, the charge transport layers are generally integrated with the semiconductor NCs in the devices. Investigating PL blinking in these NCs with such charge transport layers is necessary for estimating charge transfer efficiency. One should also note that during operation, devices produce heat or gets exposed to high energy photons for a long time. These harsh conditions generate new defects in the semiconductor layer and eventually decreases efficiency. Performing PL blinking studies in such conditions will be an important area of research which may reveal the nature of the traps and methods to control their activity.

Generally, the nonblinking semiconductor NCs are desirable for several photonic applications. However, surface or intrinsic defects make it hard to realize such photon emitter. Several methodologies have been developed for achieving non-blinking metal chalcogenide quantum dots. However, for $CsPbX_3$ NCs, this interesting area is largely under-explored. Reports available till date indicate nonblinking nature of the $CsPbI_3$ NCs. Recently, several strategies have been developed that produce near-unity PL QY suggesting defect-free $CsPbX_3$ NCs. Investigating these NCs in single particle level will be an active area of research that may guide to the preparation of nonblinking NCs.

Zero-dimensional perovskite related Cs_4PbBr_6 crystals are another important class of materials, which did not receive much attention despite its better quantum confinement and higher exciton binding energy compared to the $CsPbX_3$ NCs. Probably, the controversy over its PL was an issue, which however, have been resolved successfully by us. Even though, we have proved its intrinsic emissive nature, origin of this emission is not known with certainty. Few studies have speculated that halide vacancies are the origin of this green emission, but confirmatory experiments are still lacking. More convincing

experiments and theoretical calculations can only reveal the actual origin of the observed green emission of these substances.

Appendix

Appendix I

Synthesis of $CsPbX_3$ NCs: $CsPbX_3$ NCs were prepared using 0.10175 g Cs_2CO_3, 0.3125 mL OA and 5 mL ODE were mixed in a 50 mL double necked round bottom (RB) flux and kept in vacuum for 1 hour at 120 °C, later temperature was raised to 160 °C for complete solubilisation of the solid material which leads to formation of a clear solution of Cesium oleate (Cs-oleate). Since Cs-oleate gets precipitated at room temperature, so it has been kept at 100 °C under N_2 atmosphere before injection. For the synthesis of $CsPbBr_3$ 0.069 g $PbBr_2$ and 5 mL ODE in 50 mL 2-necked RB flask were dried for 1 hour at 120 °C then previously dried OA and OLA 0.5 mL each were injected into the RB at 120 °C under N2 atmosphere. Temperature was raised to 180 °C after complete solubilisation of the PbBr2 salt and 0.4 mL Cs-oleate solution was injected followed by rapid cooling of the reaction mixture using ice-water bath after 3-4s. $CsPbBr_2I$ was synthesized in a similar manner replacing $PbBr_2$ with the mixture of 0.046 g $PbBr_2$ and 0.029 g PbI_2. The crude solution was then centrifuged and nanocrystals were redispersed in toluene or ODE by discarding the supernatant for long term colloidal stable solution.

Analytical expressions of different fitting models to the fluorescence correlation signals:

A1. Equation for simple 3 D diffusion fit

$$G(\tau) = \frac{1}{N}\left(1+\frac{\tau}{\tau_D}\right)^{-1}\left(1+\frac{\tau}{\kappa^2\tau_D}\right)^{-\frac{1}{2}}$$

Where, N is the average number of molecules diffusing through the observation volume, τ_D is the diffusion time, $\kappa = (\omega_z/\omega_{xy})$ is the structure parameter of the observation volume, where ω_z and ω_{xy} are longitudinal and transverse radius, respectively. κ was calibrated using Rhodamine 6G in water of known diffusion coefficient ($430 \pm 40\ \mu m^2 s^{-1}$)

A2. Equation for simple 3D diffusion with single exponential fit

$$G(\tau)=\left[1+\frac{T}{1-T}\exp\left(-\frac{\tau}{\tau_T}\right)\right]\frac{1}{N}\left(1+\frac{\tau}{\tau_D}\right)^{-1}\left(1+\frac{\tau}{\kappa^2\tau_D}\right)^{-\frac{1}{2}}$$

T is the fraction of molecules in their off state, τ_T is the off-state relaxation time and N is the average number of molecules undergoing reversible fluorescence on and off state in the observation volume.

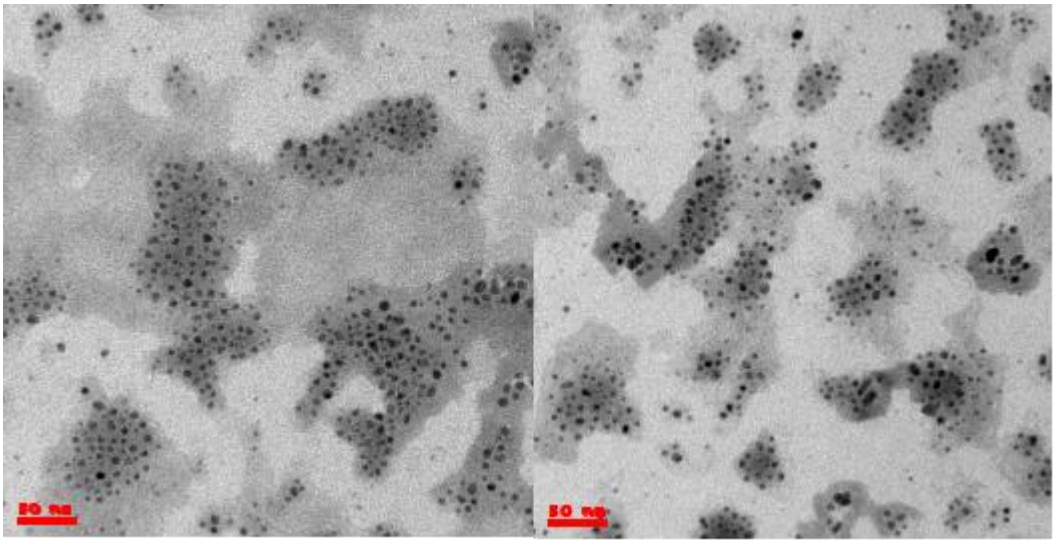

Figure AI.1. TEM images of (a) $CsPbBr_3$ and (b) $CsPbBr_2I$ NCs. Edge length estimated for $CsPbBr_3$ is 10 ± 2 nm and for $CsPbBr_2I$ is 12 ± 3 nm.

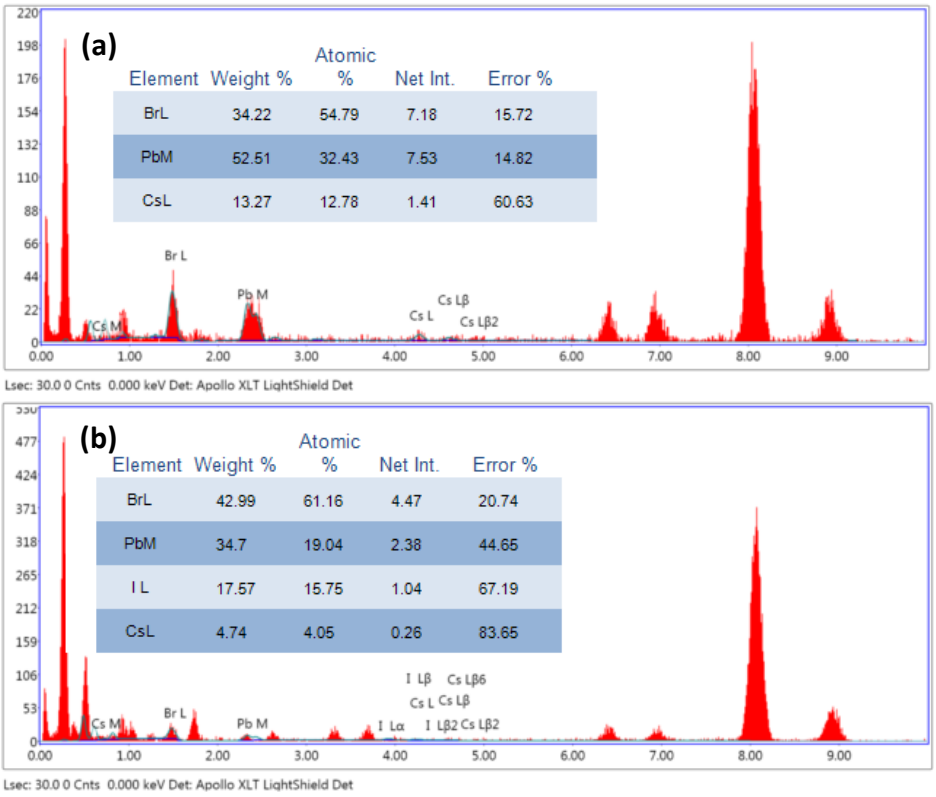

Figure AI.2. EDX spectra of (a) $CsPbBr_3$ and (b) $CsPbBr_2I$ NCs

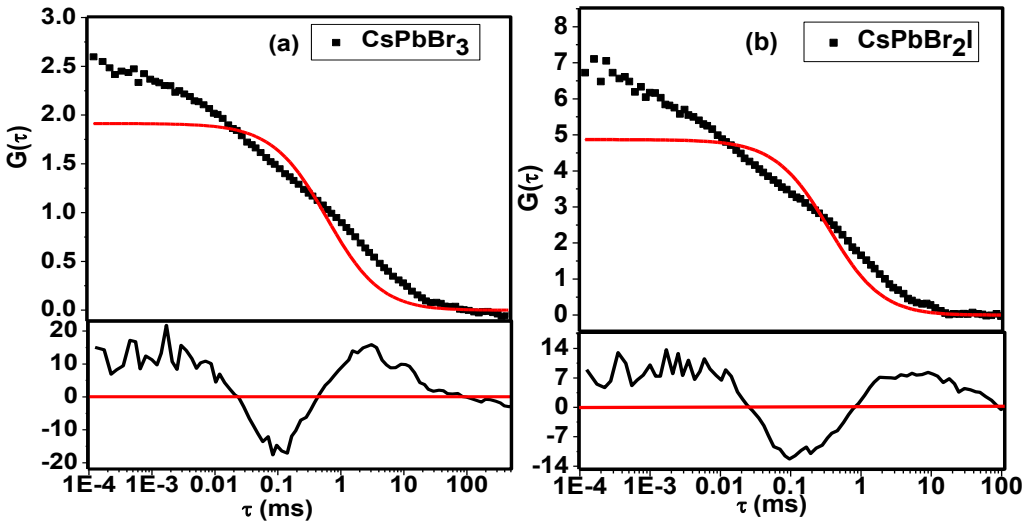

Figure AI.3. Simple 3D diffusion fit to the correlation curve of (a) $CsPbBr_3$ and (b) $CsPbBr_2I$ in ODE with the residuals shown at the bottom of the correlation curves at 5 μW excitation power.

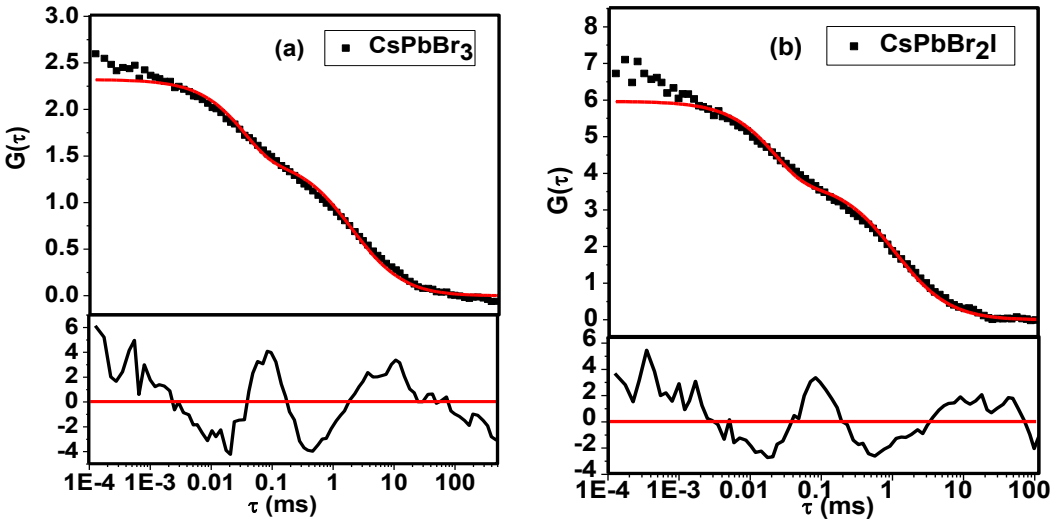

Figure AI.4. Simple 3D diffusion with single exponential fit to the correlation curve of (a) $CsPbBr_3$ and (b) $CsPbBr_2I$ in ODE with the residuals shown at the bottom of the correlation curves at 5 μW excitation power.

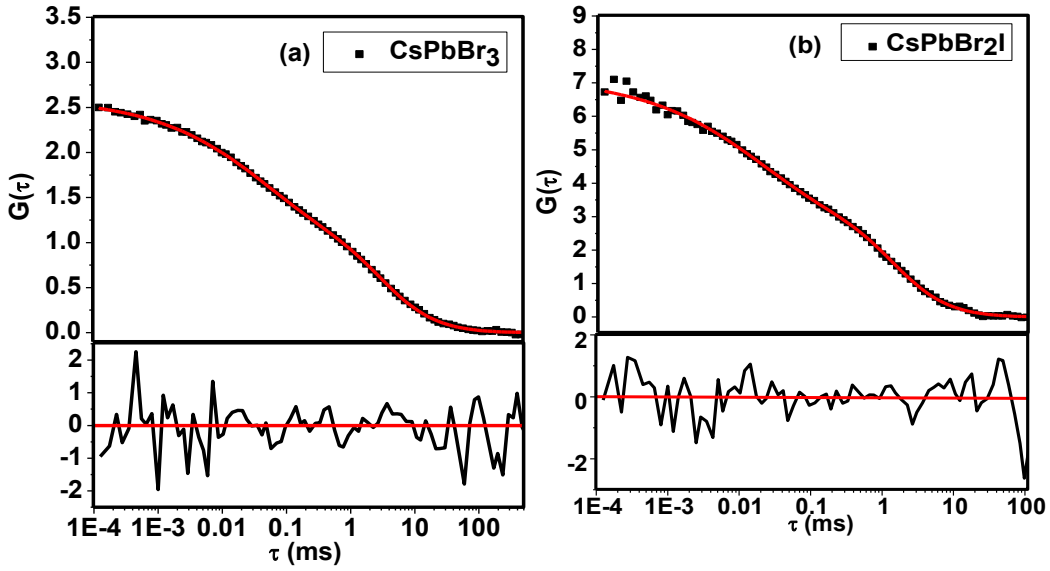

Figure AI.5. 3D diffusion with stretched exponential fit to the correlation curve of (a) $CsPbBr_3$ and (b) $CsPbBr_2I$ with the residuals shown at the bottom of the correlation curves at 5 μW excitation power.

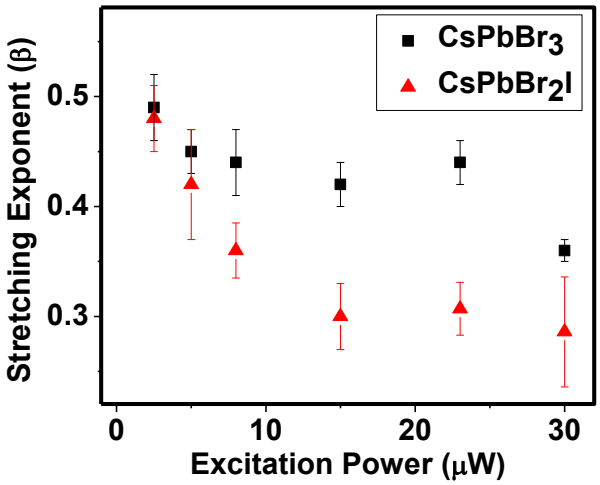

Figure AI.6. Plot of stretching exponent (β) versus excitation power.

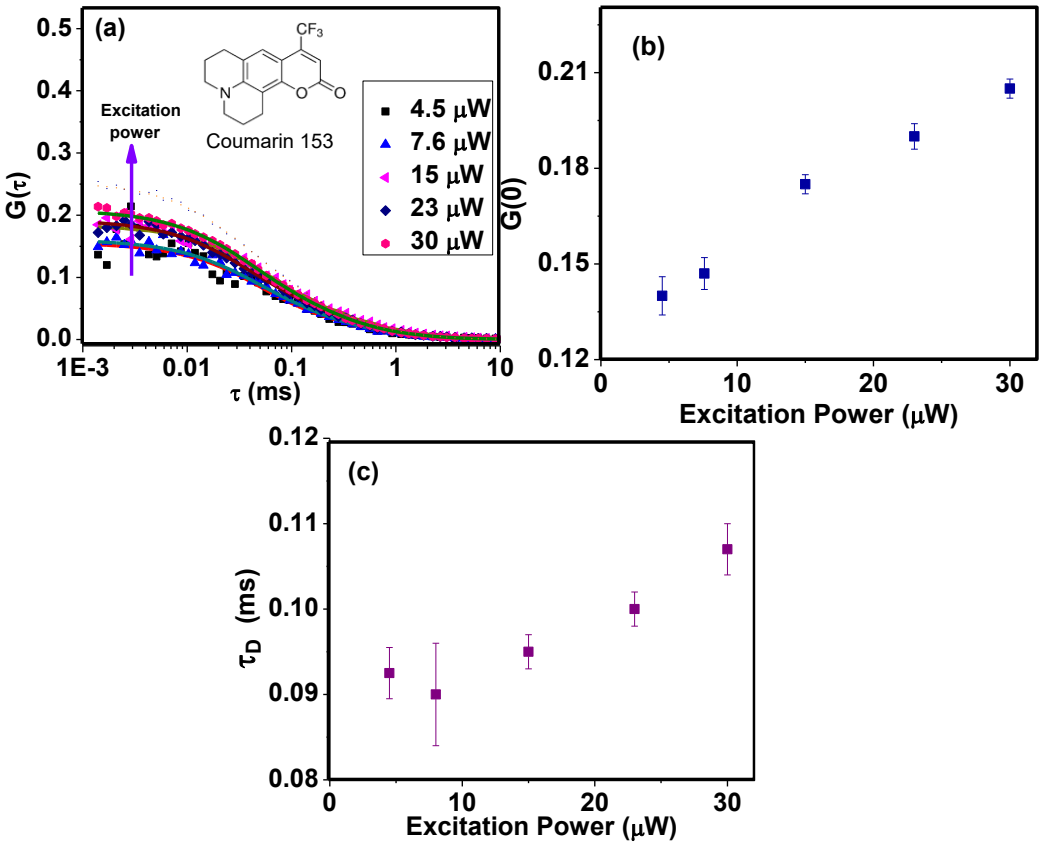

Figure AI.7. Plot of (a) correlation curves (b) G(0) value and (c) diffusion time (τ_D) as a function of excitation power of C153 in ODE. Structure of C153 is given in the inset of (a). Increase in G(0) value with excitation power is because of photobleaching.

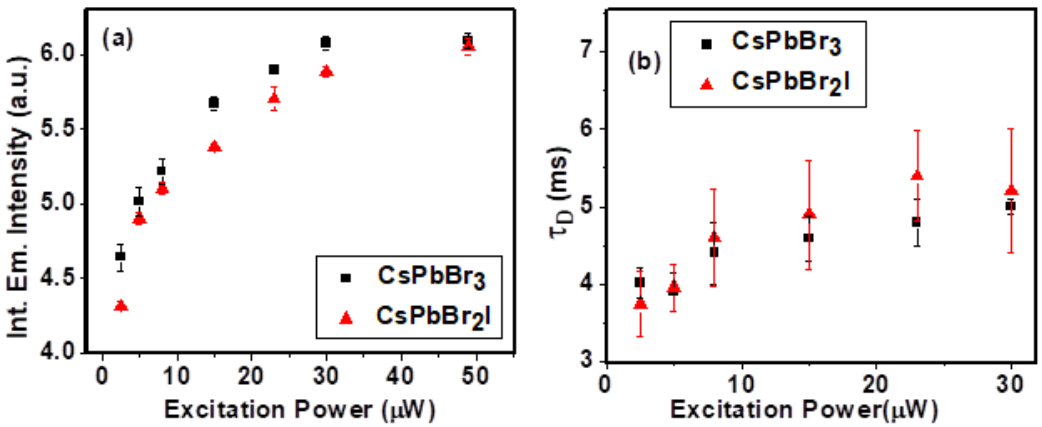

Figure AI.8. Plot of (a) Integrated emission intensity obtained from the count rate histogram of FCS measurements and (b) diffusion time (τ_D) versus excitation power.

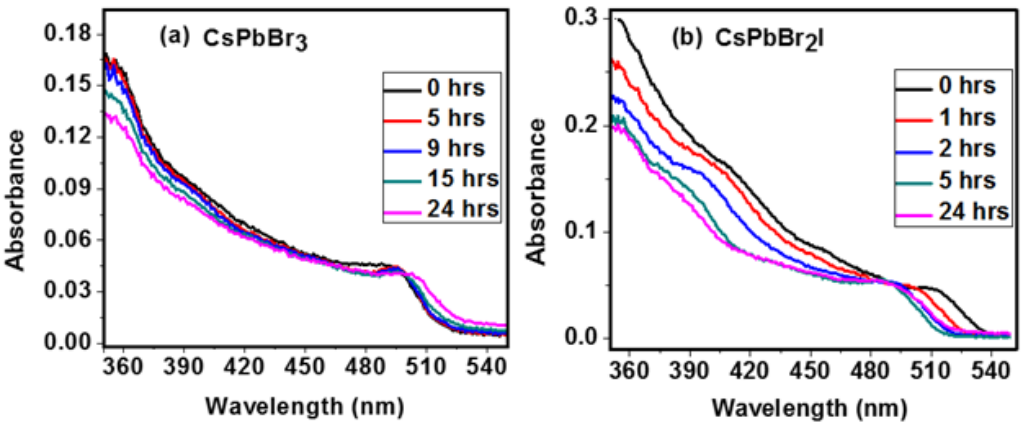

Figure AI.9. Absorption spectra for (a) $CsPbBr_3$ and (b) $CsPbBr_2I$ in ODE at different light irradiation times.

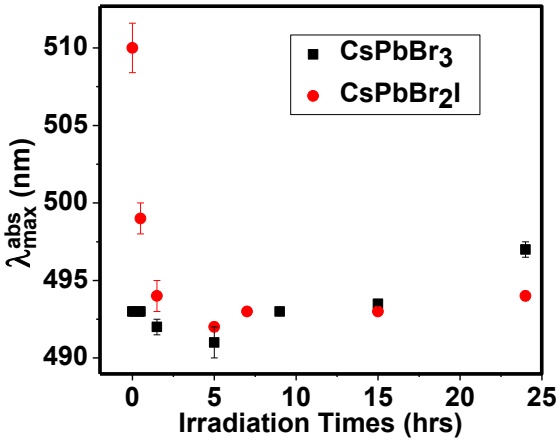

Figure AI.10. Plot of first excitonic peak wavelength ($\lambda_{\max}^{exciton}$) as a function of light irradiation time.

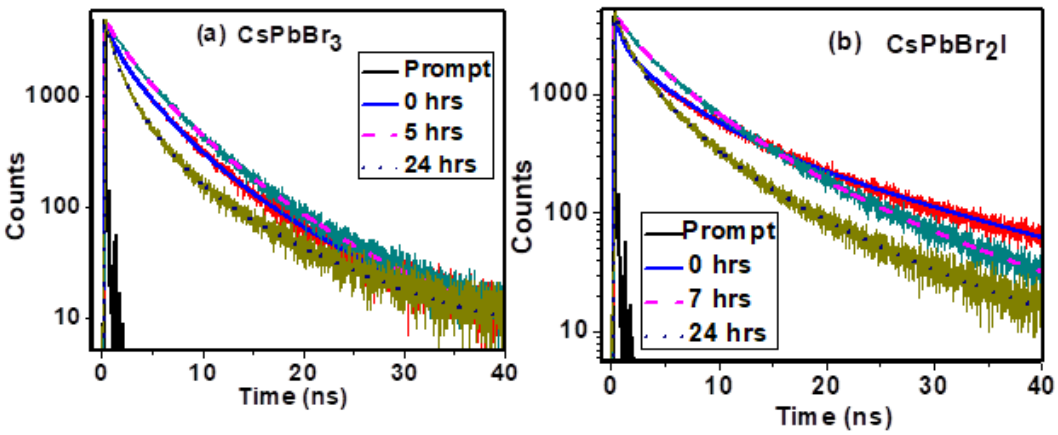

Figure AI.11. Fluorescence decay ($\lambda_{ex} = 405nm$) profiles of (a) $CsPbBr_3$ and (b) $CsPbBr_2I$ in ODE after different irradiation times. Black solid line is the instrument response function and emission monitored at the peak wavelength.

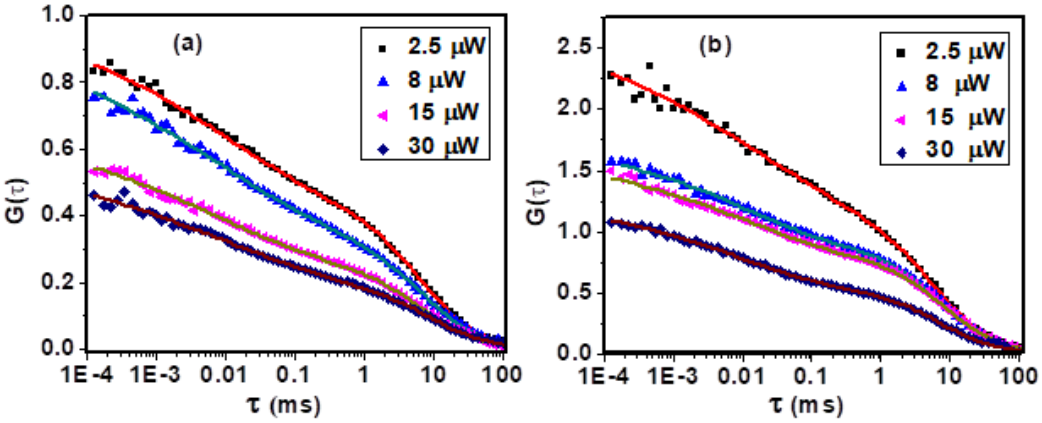

Figure AI.12: Amplitude of fluorescence correlation of (a) $CsPbBr_3$ (b) $CsPbBr_2I$ in ODE as a function of excitation power after light irradiation for 7 hrs.

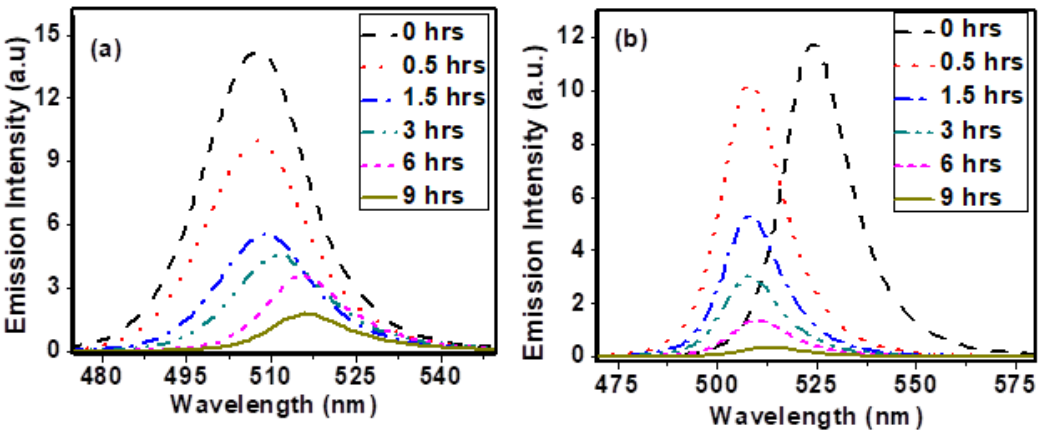

Figure AI.13. Emission spectra of (a) $CsPbBr_3$ and (b) $CsPbBr_2I$ in toluene recorded following irradiation of samples for different periods.

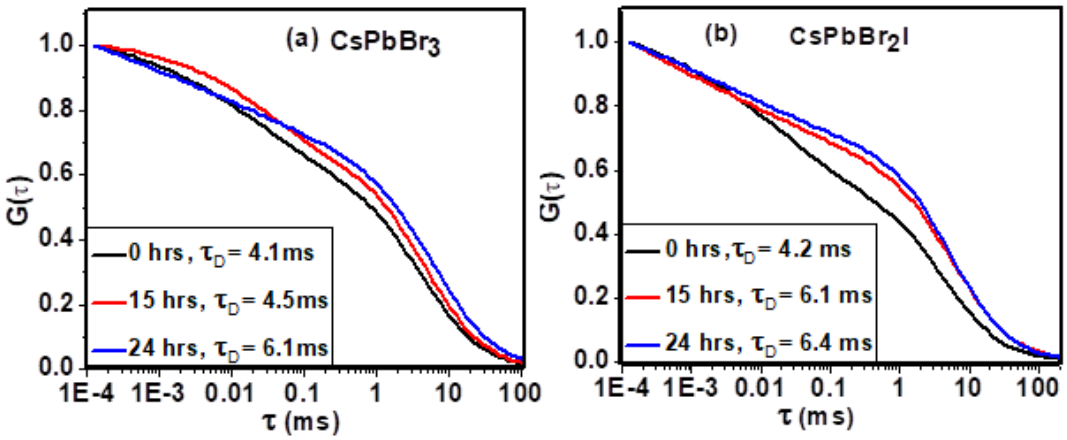

Figure AI.14. Normalized correlation curves for (a) $CsPbBr_3$ and (b) $CsPbBr_2I$ in ODE after illumination of the samples for different periods indicated. The FCS data was collected for excitation power = 5μW.

Appendix

Table AI.1. Time resolved fluorescence parameters of $CsPbBr_3$ and $CsPbBr_2I$ in ODE after different illumination times.

	Irradiation time (hrs)	**τ_1 (ns)**	**α_1**	**τ_2 (ns)**	**α_2**	**τ_3 (ns)**	**α_3**	**$\langle\tau\rangle^a$ (ns)**
$CsPbBr_3$	0	3.18 ± 0.07	0.47	8.83 ± 0.07	0.12	0.64 ± 0.01	0.40	2.85 ± 0.05
	1.5	3.80 ± 0.06	0.56	9.23 ± 0.05	0.10	1.21 ± 0.10	0.34	3.46 ± 0.07
	5	3.88 ± 0.09	0.53	8.18 ± 0.1	0.14	1.57 ± 0.09	0.32	3.70 ± 0.09
	9	4.01 ± 0.07	0.52	9.73 ± 0.1	0.10	1.38 ± 0.05	0.37	3.57 ± 0.06
	15	3.71 ± 0.10	0.47	10.34 ± 0.1	0.08	1.18 ± 0.02	0.45	3.10 ± 0.06
	24	2.44 ± 0.07	0.41	8.40 ± 0.07	0.07	0.77 ± 0.01	0.51	1.98 ± 0.04
$CsPbBr_2I$	0	4.46 ± 0.08	0.37	15.21 ± 0.08	0.15	0.73 ± 0.01	0.48	4.28 ± 0.05
	1.5	4.95 ± 0.08	0.46	15.21 ± 0.10	0.12	1.09 ± 0.01	0.42	4.56 ± 0.04
	5	5.54 ± 0.10	0.51	15.01 ± 0.20	0.08	1.66 ± 0.10	0.41	4.72 ± 0.11
	7	5.37 ± 0.10	0.53	13.31 ± 0.10	0.08	1.67 ± 0.05	0.37	4.79 ± 0.07
	13	5.13 ± 0.09	0.50	12.16 ± 0.20	0.09	1.83 ± 0.04	0.46	4.24 ± 0.13
	24	3.43 ± 0.10	0.43	9.80 ± 0.10	0.10	0.98 ± 0.01	0.46	2.90 ± 0.06

$\langle\tau\rangle^a$ is defined as, $\langle\tau\rangle = (\alpha_1\tau_1+\alpha_2\tau_2+\alpha_3\tau_3)/\alpha_1+\alpha_2+\alpha_3$, here α_1, α_2, and α_3 are the corresponding amplitudes of the lifetime component.

Appendix II

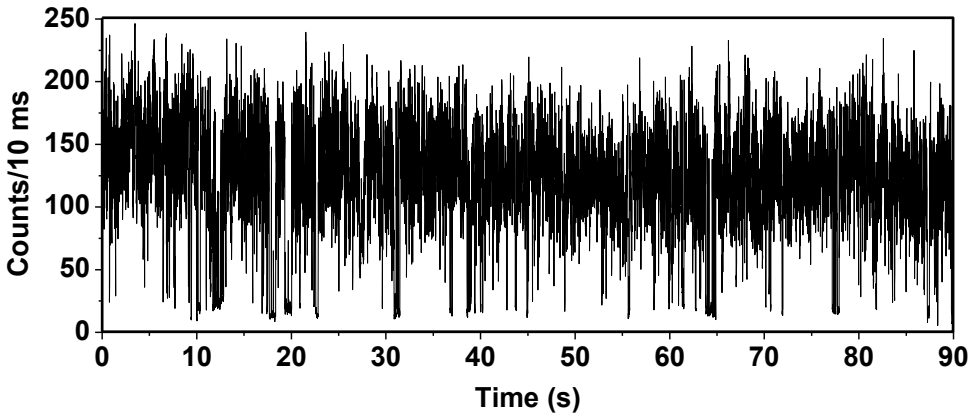

Figure AII.1. Blinking time-trace of single $CsPbBr_3$ NCs.

Intensity-lifetime scaling

Intensity-lifetime scaling or the ratio of radiative rates between two different intensity levels (η)

$$\eta = \frac{\tau_{ON}}{I_{ON}} \times \frac{I_{OFF}}{\tau_{OFF}}$$

Where τ and I are the PL lifetime and intensity of the corresponding ON or OFF states.

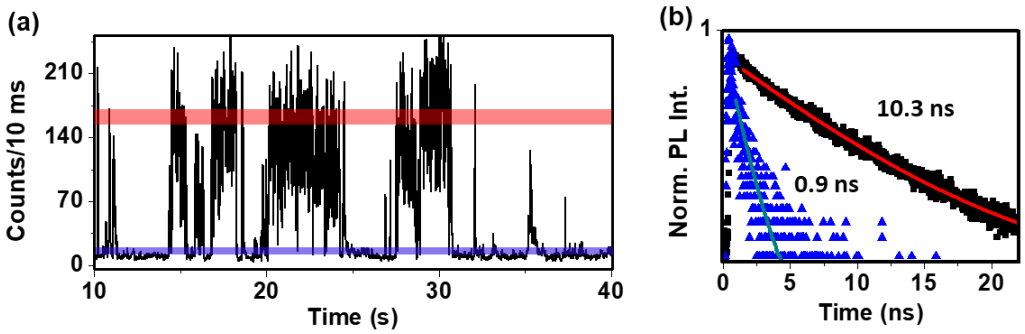

Figure AII.2. (a) PL blinking time-trace in 30 s window. (b) PL lifetime decay of the two shaded regions corresponding to the intensities of 160 counts/10 ms (red region) and 17 counts/10 ms (blue region). Resultant η value is approximately 1.22

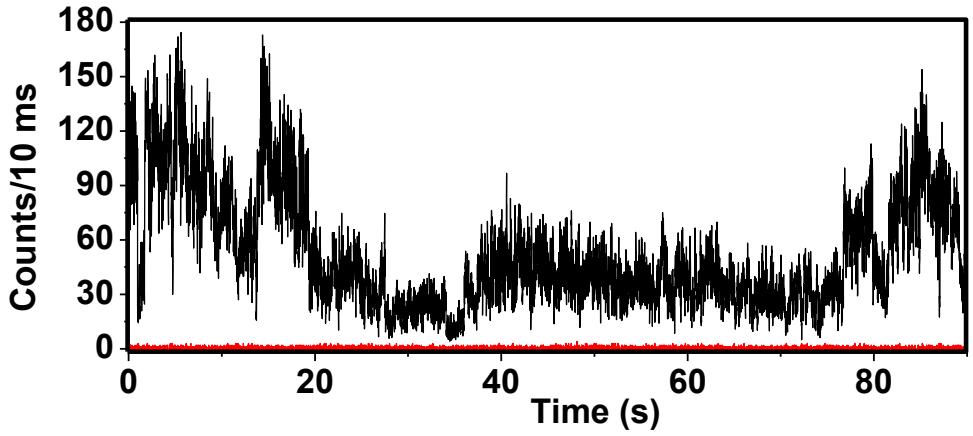

Figure AII.3. Time-trace for single CsPbBr3 NC showing flickering nature.

Post synthetic surface treatment.

$CsPbBr_3$ NCs that are synthesized following room temperature anti solvent precipitation method does not contain much lead nanoparticles. These lead nanoparticles are one of the main factor deteriorating the optical properties of the NCs synthesized following hot injection method. Use of little excess of oleic acid (OA) as compared to oleylamine (OLA) in the room temperature method leads to NCs of poor surface quality as excess OA protonates amines and removes from the surface.

Effect of acids. We have tried different capping ligands for the capping of the NC surface such as aliphatic acids, amine and thiols of different chain lengths. Acids straight away quenches the PL of the NCs (Figure S4) with slowest rate in case of OA as these removes ligands from the surface (evident from the TEM image).

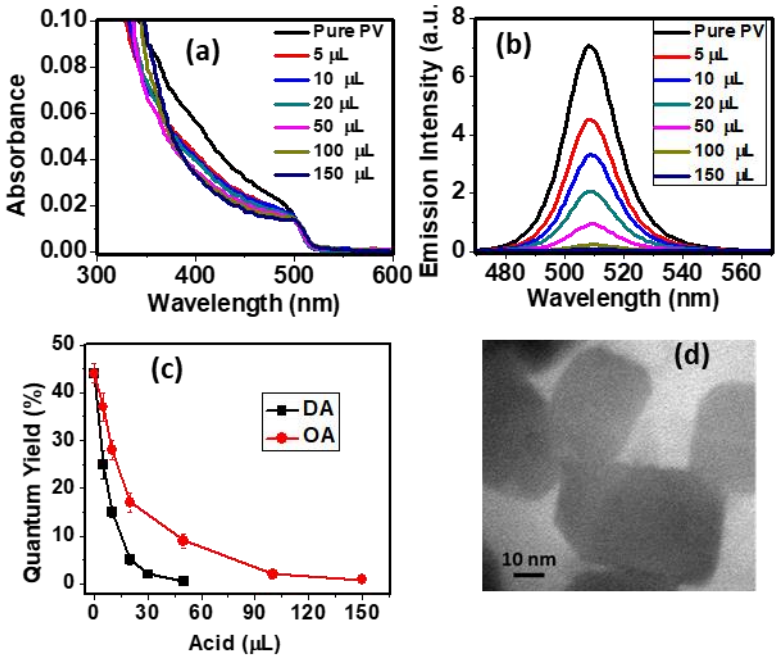

Figure AII.4. Post synthetic surface treatment of $CsPbBr_3$ NCs using OA. Acid was diluted (1/10 volume proportion) in toluene prior use. Absorption (a) and emission (b) spectral change with addition of acid. PL QY change for OA and decanoic acid (DA) (c), and TEM image after the treatment (d).

Effect of amines. Aliphatic amines of different chain length have slight different effect than acids. With addition of amines PL QY of the NCs has increased but with increase in amount it has started degrading as evident from Figure S5. NCs cannot retain its size and morphology. Even though less amount of amines do increase the PL properties, long term storage gets affected as a quick precipitation and quenching of PL of the NCs in the colloidal solution are observed.

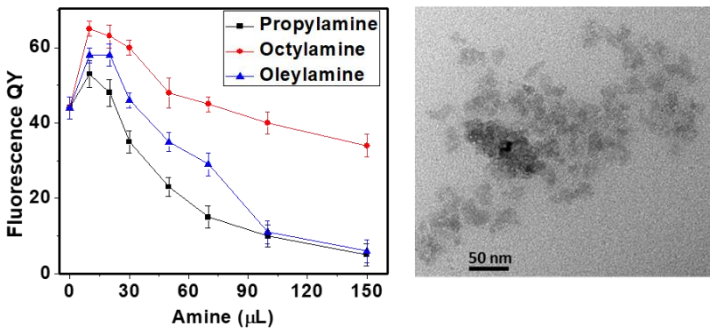

Figure AII.5. Post synthetic surface treatment and their effect on the PL of $CsPbBr_3$ NCs using aliphatic amines of different chain lengths. TEM image after treatment with excess amines

Effect of thiols. Thiols are known to be a very good capping ligand for lead based metal-chalcogenide quantum dots due to the soft-soft interaction between lead and sulfur group. alkylthiols treatment retains the shape and size integrity of the NCs as evident from the unaltered absorption spectrum and TEM image (Figure S6). However excess addition and treatment for longtime does quench the PL and to some extent and precipitate out some of the NCs. Here excess thiols protonates amines and eliminates from the surface. We have used four different thiols of different alkyl chain lengths namely, ethanethiol, octanethiol, dodecanethiol and octadecanethiol. All the thiols are effective in improving optical properties with a predominate contribution from ethanethiol.

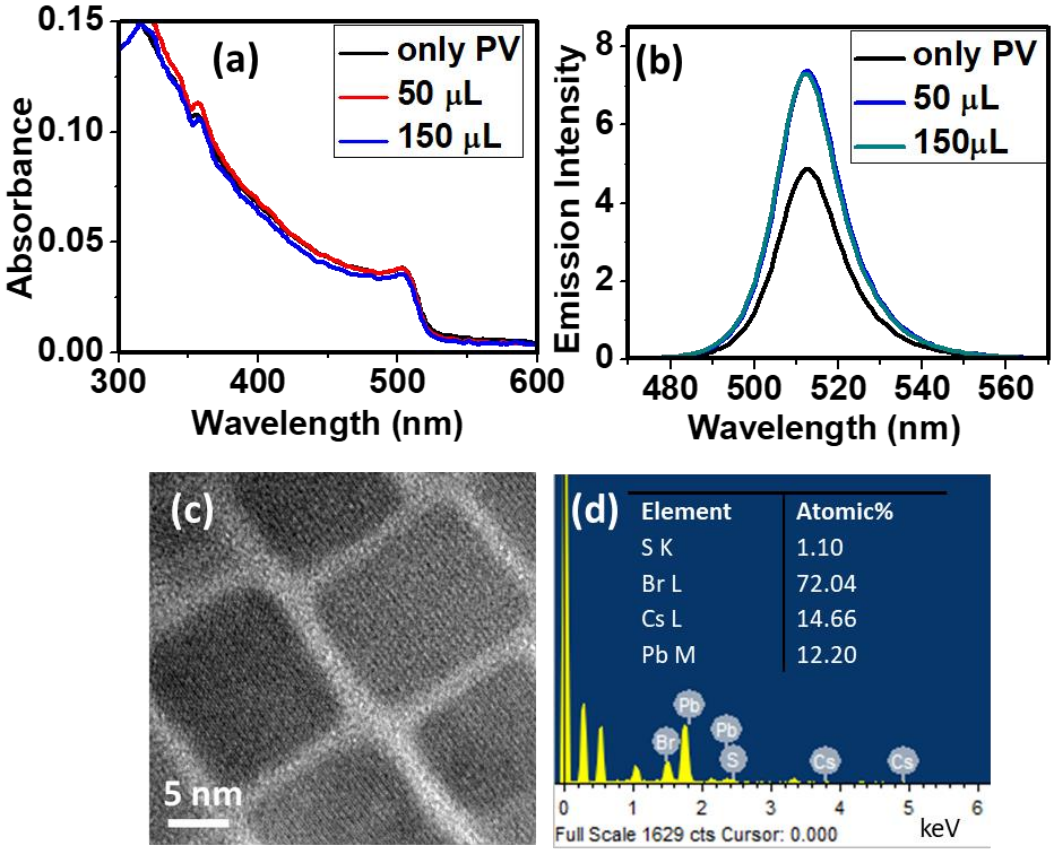

Figure AII.6. Post synthetic surface treatment using ethanethiol. (a) Absorption spectra, (b) emission spectra, (c) TEM image and (d) elemental composition after the treatment. Presence of sulfur in the elemental composition confirms capping of the NCs with ethanethiol.

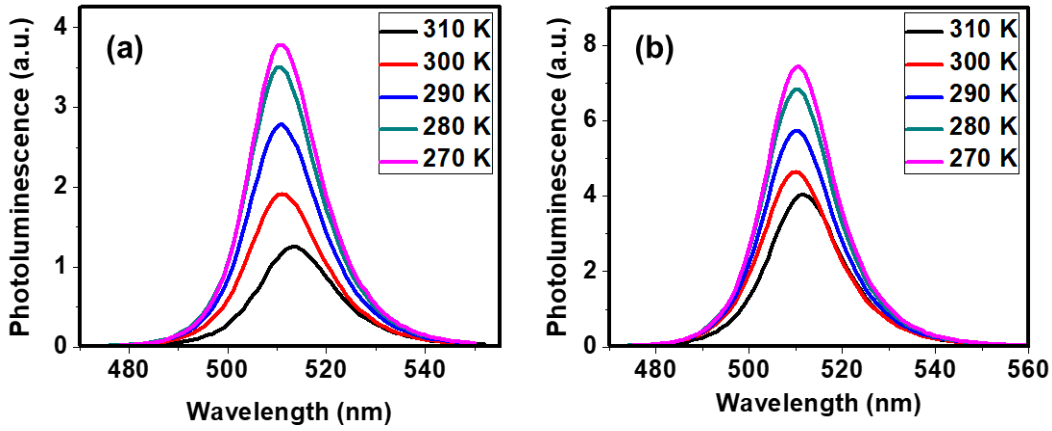

Figure AII.7. Temperature dependent PL studies of as-synthesized and ethanethiol treated $CsPbBr_3$ NCs.

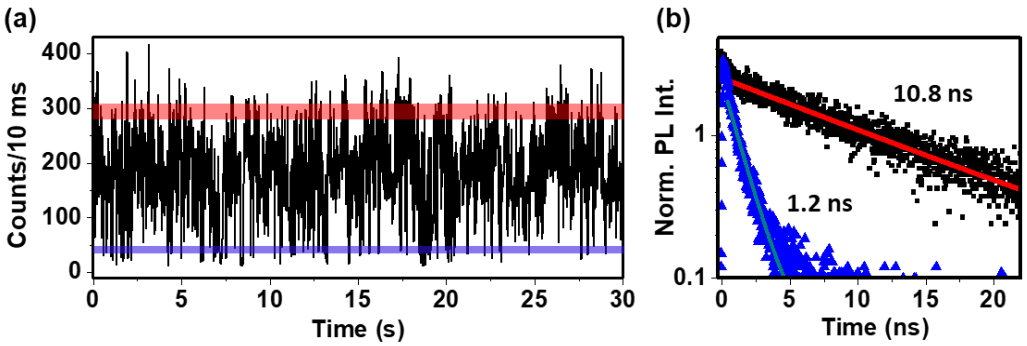

Figure AII.8. (a) PL blinking time-trace in 30 s window for ethanethiol treated NCs. (b) PL lifetime decay of the two shaded regions corresponding to the intensities of 290 counts/10 ms (red region) and 45 counts/10 ms (blue region). Resultant η value is approximately 1.4.

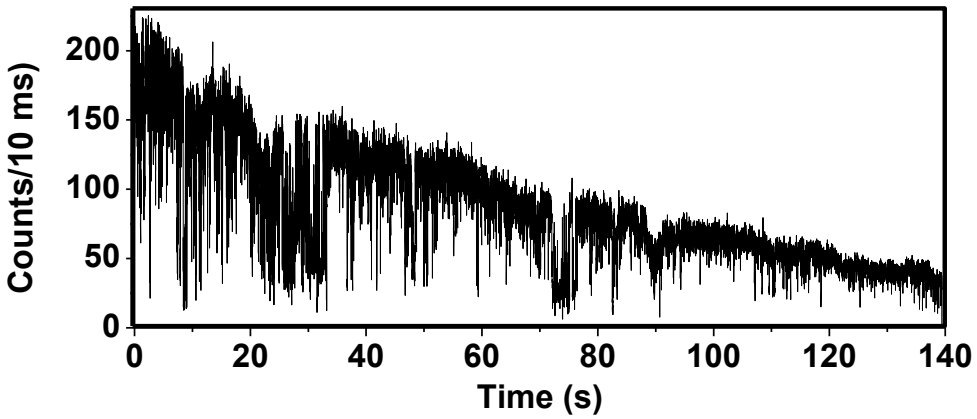

Figure AII.9. Steady decrease in PL intensity with time of an untreated blinking NC. Majority of the NCs degrade within three minutes of measurement time.

Appendix III

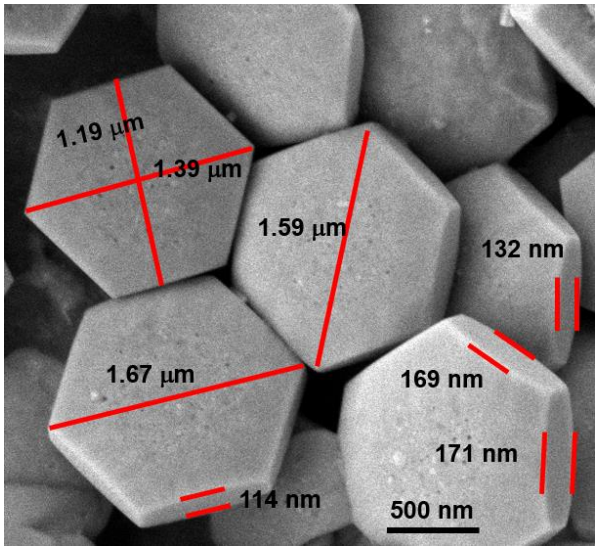

Figure AIII.1: FESEM image of hexagonal microdisks showing size and thickness distribution.

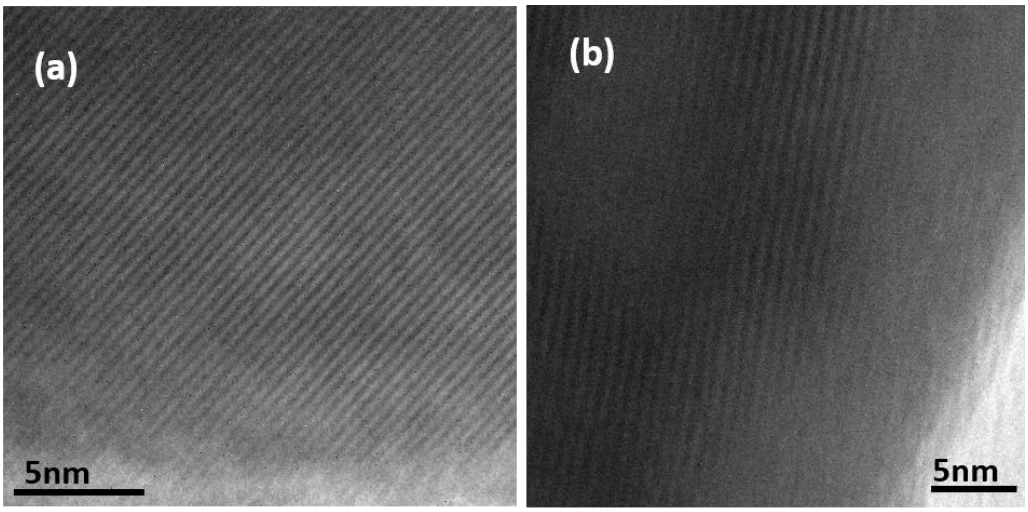

Figure AIII.2. (a and b) HRTEM images of the hexagonal MDs.

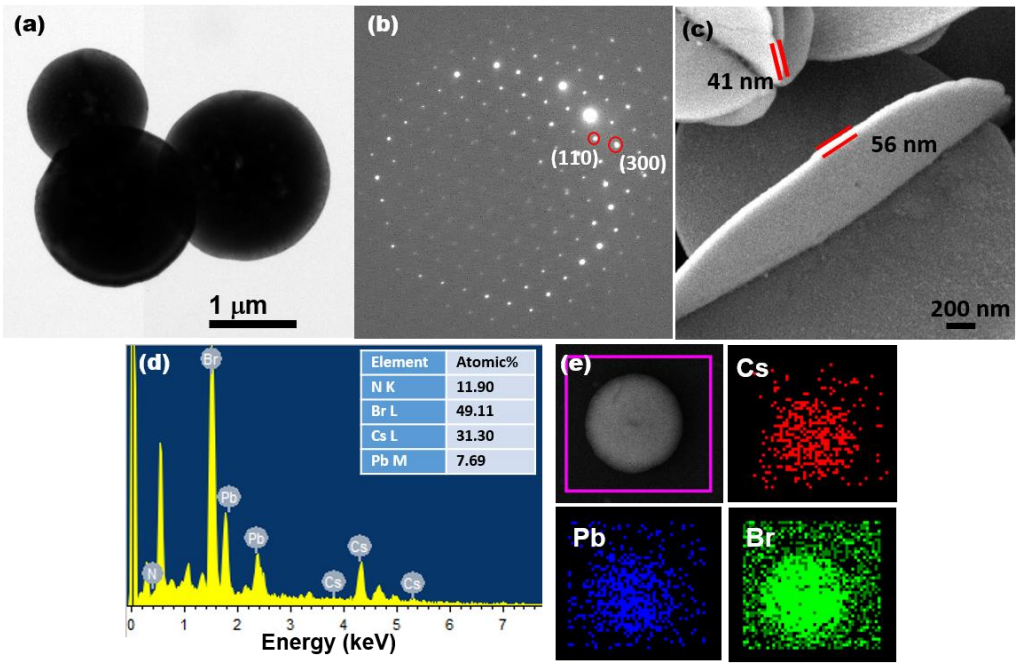

Figure AIII.3. (a) TEM image of the spherical MDs. (b) SAED pattern shows single-crystal nature of the disks. Spots corresponding to (110) and (300) crystal planes are encircled. (c) FESEM image of disks showing edge thickness. (d) EDX spectrum confirms Cs_4PbBr_6 composition. (e) Elemental mapping of constituent elements shows their even distribution in the MDs.

Synthesis with 2:1 and 4:1 $CsBr/PbBr_2$ precursor ratios.

Following the similar synthetic method as discussed in the main manuscript we have checked with 2:1 and 4:1 $CsBr/PbBr_2$ precursor ratios also with 0.05 mM CTAB in DMF solution. Though 2:1 ratio produces hexagonal disks (< 1 μm), the size of hexagons were not uniform and cubic and plate kind of structures are also seen (Figure S3). Reaction with 4:1 ratio takes longer time (>2 hrs) and forms a white suspension. The particles in the suspension are found to be quite heterogeneous in both shape and size and contains mostly cubes and diamonds as obtained in some other report (Figure S4).[1] Because of poor solubility much of CsBr precipitates out of the solution immediately on addition of anti-solvent and remaining amount reacts with $PbBr_2$ to yield the product particles. Here

unreacted CsBr and obtained particles form the white suspension. PXRD and EDX spectra of both the samples confirm that the obtained particles are also of Cs_4PbBr_6 composition (Figure 1f (main manuscript), S3 and S4). Hence, 1:1 molar ratio of $CsBr/PbBr_2$ is essential for the synthesis of well-defined Cs_4PbBr_6 MDs. A similar conclusion was drawn by Saidaminov et al. though they could not synthesize Cs_4PbBr_6 with higher ratio.[2]

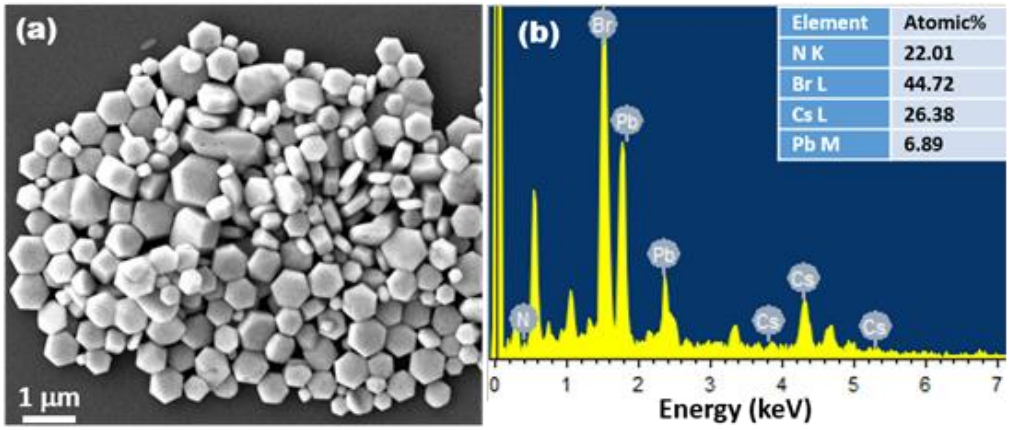

Figure AIII.4. (a) FESEM image and (b) EDX pattern of the disks obtained when 2:1 precursor ratio was used.

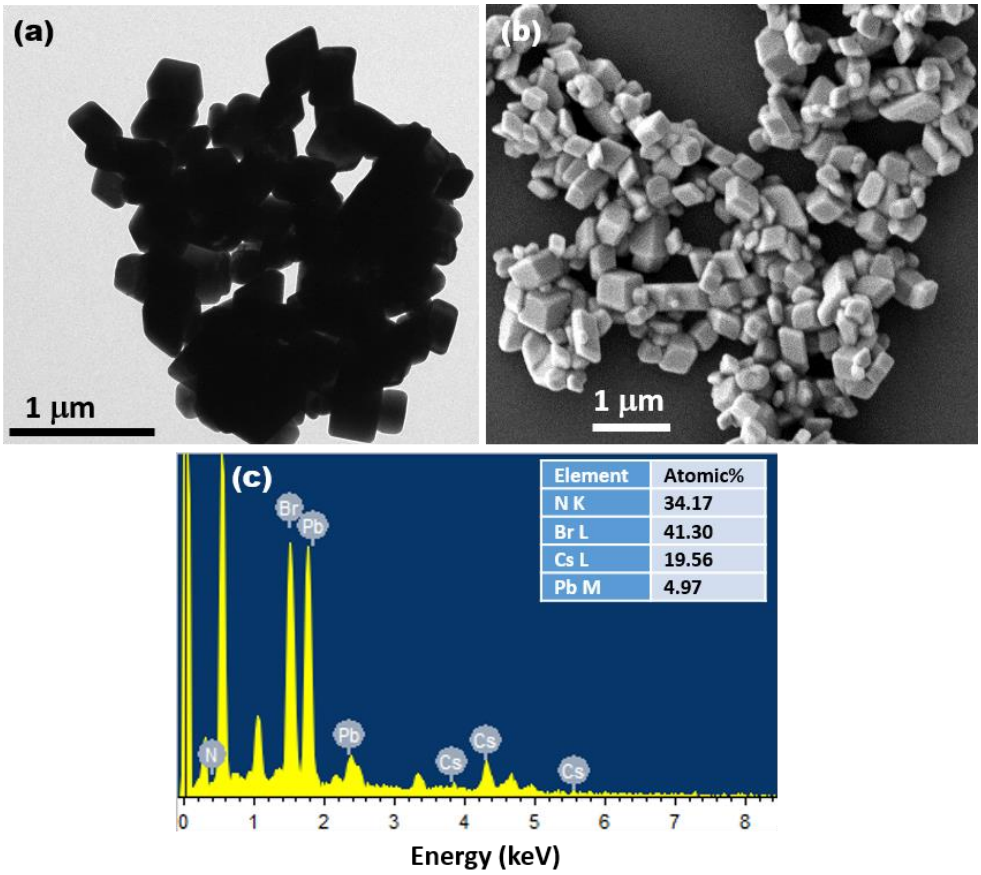

Figure AIII.5. (a) TEM (b) FESEM images and (c) EDX pattern of the disks obtained when 4:1 precursor ratio was used.

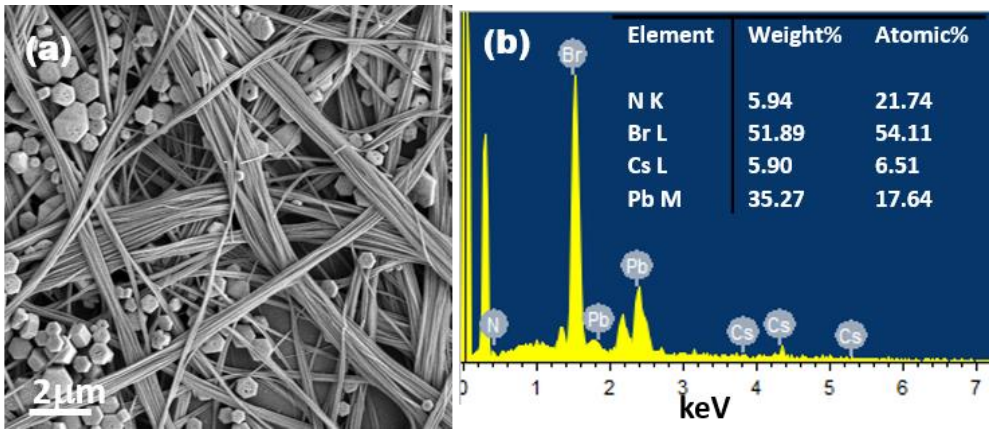

Figure AIII.6. (a) FESEM image of the particles obtained for the CTAB saturated solution. (b) EDX spectrum and elemental ratio of only microwires suggesting a $CsPb_2Br_5$ composition.

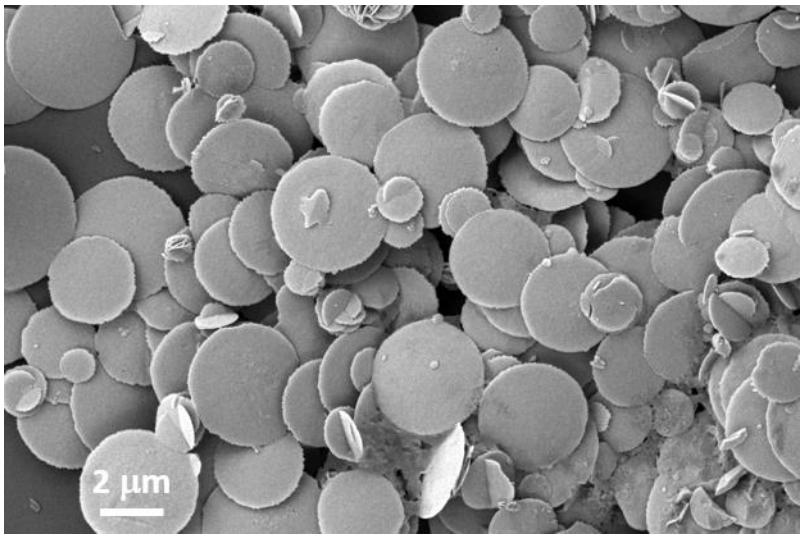

Figure AIII.7. FESEM image when nucleation and growth is rapid in presence of larger amount of anti-solvent.

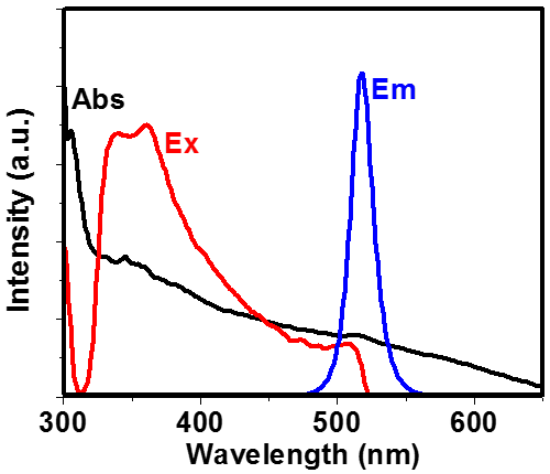

Figure AIII.8. Absorption, excitation and emission spectra of spherical Cs_4PbBr_6 MDs.

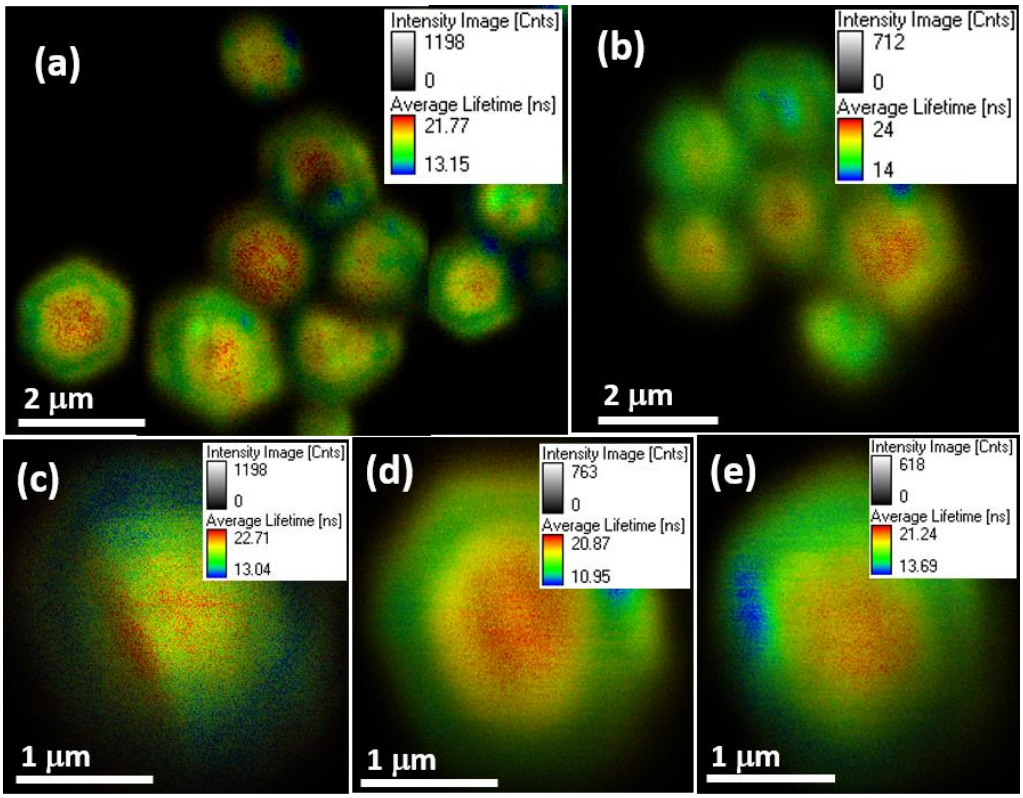

Figure AIII.9. FLIM images of the (a, b) collective and (c, d, e) single hexagonal Cs_4PbBr_6 MDs

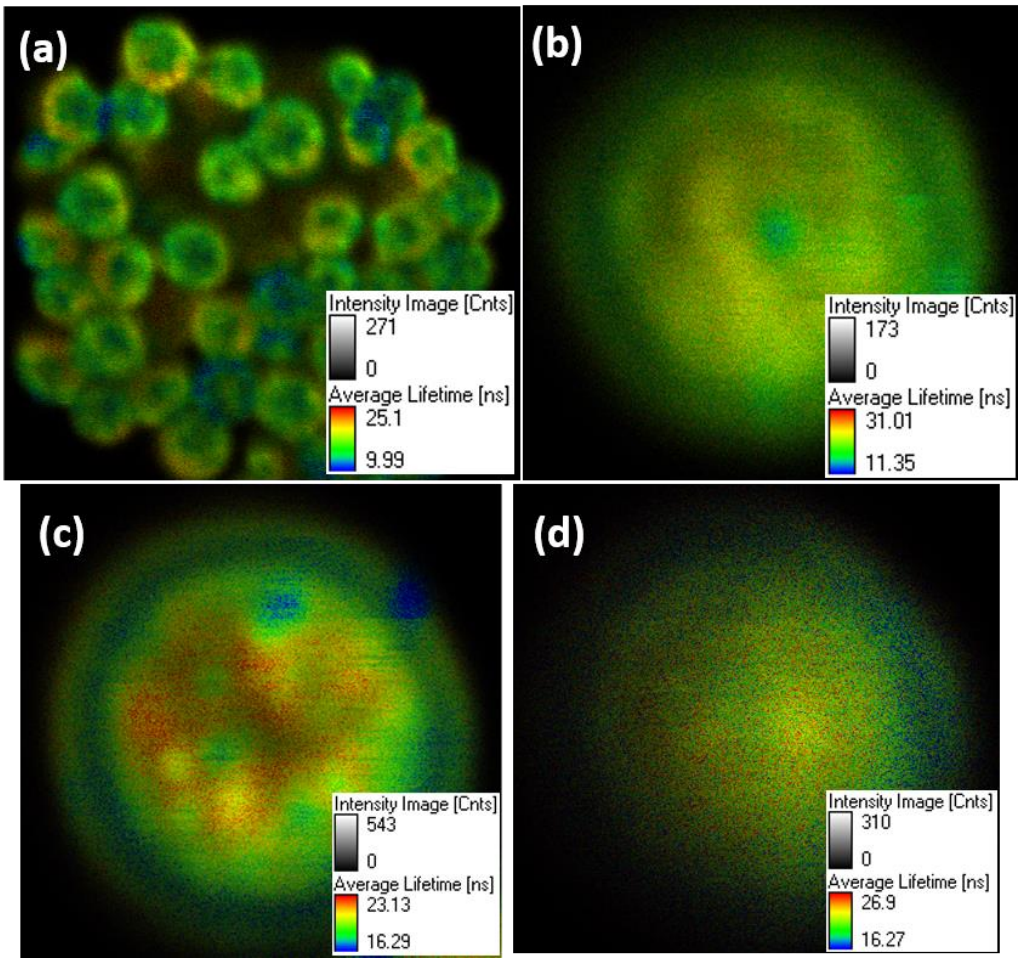

Figure AIII.10. FLIM images of (a) collective and (b, c, d) single spherical Cs_4PbBr_6 MDs.

Table AIII.1. Average lifetime components along with their mean deviations of dark and bright areas on 20 individual MDs of each morphology.

sample	positions	τ_1 (α_1) (ns)	τ_2 (α_2) (ns)
Hexagonal disk	bright	3.42 ± 0.14 (0.47 ± 0.02)	19.58 ± 1.02 (0.53 ± 0.02)
	dark	3.26 ± 0.11 (0.57 ± 0.02)	16.64 ± 0.74 (0.43 ± 0.02)
Spherical disk	bright	3.71 ± 0.20 (0.43 ± 0.03)	22.23 ± 0.78 (0.57 ±0.03)
	dark	3.20 ± 0.10(0.54 ± 0.02)	18.69 ± 0.52 (0.46 ± 0.02)

Imaging and PL decay dynamics of degraded samples.

Exposure of the MDs at high relative humidity leads to etching of the material. Degradation is found to be more near the central region where the average lifetime is the least. Even though lifetime heterogeneity across the disk has enhanced after degradation shorter component does not alter much (excitonic recombination) as compared to the longer component (tarp-assisted recombination. In the degraded regions on the MD (area-y, Figure S11), value of the longer lifetime component is shortest (Table S2) as etching increases the population of unpassivated bonds in those places resulting in generation of more of deep level trap states. Since nonradiative recombination centers are more on the degraded MDs, overall lifetime is found to be less as compared to the unaffected disks. Evidently PL QY of the degraded MDs reduced to ~10%.

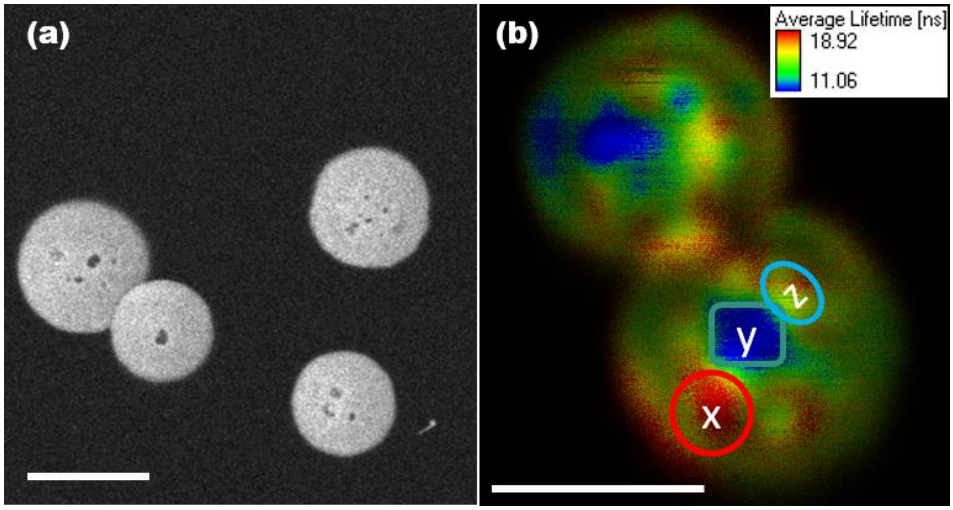

Figure AIII.11. (a) FESEM and (b) FLIM images of the degraded spherical MDs. Scale bar in both case is 2 μm.

Table AIII.2. Local PL decay parameters of different regions of the degraded MDs. Here, τ_1, τ_2 are the lifetime components and α_1, α_2 are the corresponding exponents. τ_{avg} is the average lifetime.

Sample	**Positions**	**τ_1 (α_1) (ns)**	**τ_2 (α_2) (ns)**	**τ_{avg} (ns)**
Degraded spherical disk	area-x	3.40 (0.45)	22.52 (0.55)	13.92
	area-y	3.82 (0.58)	11.42 (0.42)	7.01
	area-z	3.73 (0.48)	15.80 (0.52)	10.00

References.

(1) Huang, K.; Li, D.; Yang, L.; Liu, S.; Yang, F. *Journal of Alloys and Compounds* **2017,** *710***,** 244-252.

(2) Saidaminov, M. I.; Almutlaq, J.; Sarmah, S.; Dursun, I.; Zhumekenov, A. A.; Begum, R.; Pan, J.; Cho, N.; Mohammed, O. F.; Bakr, O. M. *ACS Energy Lett.* **2016**, *1*, 840-845.

Single-Particle Photoluminescence and Carrier Dynamics of Cesium Lead Halide Perovskites and Related Materials

by Sudipta Seth

Single-Particle Photoluminescence and Carrier Dynamics of Cesium Lead Halide Perovskites and Related Materials

ORIGINALITY REPORT

5%	2%	4%	1%
SIMILARITY INDEX	INTERNET SOURCES	PUBLICATIONS	STUDENT PAPERS

PRIMARY SOURCES

1	Sudipta Seth, Tasnim Ahmed, Anunay Samanta. " Photoluminescence Flickering and Blinking of Single CsPbBr Perovskite Nanocrystals: Revealing Explicit Carrier Recombination Dynamics ", The Journal of Physical Chemistry Letters, 2018 Publication	1%
2	pubs.acs.org Internet Source	<1%
3	Submitted to University of Hyderabad, Hyderabad Student Paper	<1%
4	Submitted to Indian Institute of Science Education and Research (IISER) Bhopal Student Paper	<1%
5	Sudipta Seth, Anunay Samanta. " Fluorescent Phase-Pure Zero-Dimensional Perovskite-Related Cs PbBr Microdisks: Synthesis and Single-Particle Imaging Study ", The Journal of	<1%

Publication

27	ddd.uab.cat Internet Source	<1%
28	Submitted to Indian Institute of Science, Bangalore Student Paper	<1%
29	Sk Saddam Hossain, Anunay Samanta. "Solute Rotation and Translation Dynamics in an Ionic Deep Eutectic Solvent Based on Choline Chloride", The Journal of Physical Chemistry B, 2017 Publication	<1%
30	Ramavath Babu, Surya Prakash Singh. " Solvent-Assisted Tuning of the Size and Shape of CsPbBr Nanocrystals via Redispersion Process at Ambient Condition ", Langmuir, 2018 Publication	<1%

Exclude quotes	On	Exclude matches	< 14 words
Exclude bibliography	On		

Single-Particle Photoluminescence and Carrier Dynamics of Cesium Lead Halide Perovskites and Related Materials

ORIGINALITY REPORT

51%	19%	50%	2%
SIMILARITY INDEX	INTERNET SOURCES	PUBLICATIONS	STUDENT PAPERS

PRIMARY SOURCES

1	Sudipta Seth, Anunay Samanta. " Fluorescent Phase-Pure Zero-Dimensional Perovskite-Related Cs PbBr Microdisks: Synthesis and Single-Particle Imaging Study ", The Journal of Physical Chemistry Letters, 2017 Publication	16%
2	Sudipta Seth, Navendu Mondal, Satyajit Patra, Anunay Samanta. " Fluorescence Blinking and Photoactivation of All-Inorganic Perovskite Nanocrystals CsPbBr and CsPbBr I ", The Journal of Physical Chemistry Letters, 2016 Publication	12%
3	pubs.acs.org Internet Source	11%
4	Sudipta Seth, Tasnim Ahmed, Anunay Samanta. " Photoluminescence Flickering and Blinking of Single CsPbBr Perovskite Nanocrystals: Revealing Explicit Carrier Recombination Dynamics ", The Journal of Physical Chemistry Letters, 2018	5%

26	repository.unikom.ac.id Internet Source	<1%
27	Hui Hu. "Molecular tagging velocimetry and thermometry and its application to the wake of a heated circular cylinder", Measurement Science and Technology, 06/01/2006 Publication	<1%
28	ddd.uab.cat Internet Source	<1%
29	Submitted to Indian Institute of Science, Bangalore Student Paper	<1%
30	Sk Saddam Hossain, Anunay Samanta. "Solute Rotation and Translation Dynamics in an Ionic Deep Eutectic Solvent Based on Choline Chloride", The Journal of Physical Chemistry B, 2017 Publication	<1%

Exclude quotes	Off	Exclude matches	< 14 words
Exclude bibliography	On		